

May 2023

Impact of the Pre-a Motif on Truncated Hemoglobin N Activity

Alexander Shayne Drena
University of Wisconsin-Milwaukee

Follow this and additional works at: <https://dc.uwm.edu/etd>



Part of the [Biochemistry Commons](#), and the [Inorganic Chemistry Commons](#)

Recommended Citation

Drena, Alexander Shayne, "Impact of the Pre-a Motif on Truncated Hemoglobin N Activity" (2023). *Theses and Dissertations*. 3137.

<https://dc.uwm.edu/etd/3137>

This Dissertation is brought to you for free and open access by UWM Digital Commons. It has been accepted for inclusion in Theses and Dissertations by an authorized administrator of UWM Digital Commons. For more information, please contact scholarlycommunicationteam-group@uwm.edu.

IMPACT OF THE PRE-A MOTIF ON TRUNCATED HEMOGLOBIN N ACTIVITY

by

Alexander Shayne Drena

A Dissertation Submitted in
Partial Fulfillment of the
Requirements for the Degree of

Doctor of Philosophy

in Chemistry

at

The University of Wisconsin-Milwaukee

May 2023

ABSTRACT

IMPACT OF THE PRE-A MOTIF ON TRUNCATED HEMOGLOBIN N ACTIVITY

by

Alexander Shayne Drena

The University of Wisconsin-Milwaukee, 2023
Under the Supervision of Professor A. Andrew Pacheco

Tuberculosis (TB) remains the leading cause of death by an infectious agent and therefore a global health crisis, according to the most recent report by the World Health Organization. This is due, in part, to *Mycobacterium tuberculosis*' impressive defensive mechanisms against immune response, as well as the rise of Multi-Drug Resistant strains that have recently developed. Towards the turn of the century, a small heme protein called truncated hemoglobin N (trHbN) was discovered to protect the bacteria against reactive nitrogen species by converting nitric oxide (NO) to nitrate at rates far exceeding those of myoglobin and closer to those of the well-known NO dioxygenase flavohemoglobin. Ferrous oxygenated trHbN (oxy-trHbN) first converts NO to nitrate, which leaves the protein in a ferric state (met-trHbN). Met-trHbN is re-reduced to give a 5-coordinate ferrous species (red-trHbN), which is then re-oxygenated to oxy-trHbN. Recently, a unique 12-amino acid motif at the trHbN N-terminus was identified, the so-called pre-A tail, that appears to enhance the organism's ability to convert NO to nitrate. The results presented herein show that the pre-A tail of trHbN affects every step of the putative NO dioxygenation catalytic cycle, but it affects the rate of met-trHbN re-reduction most profoundly. In a variant that lacks the pre-A tail (trHbN_{delN}), met-trHbN_{delN} was reduced about 40 times more slowly than met-trHbN_{WT} by the non-specific reductant Ru^{II}. By comparison, the reactions of oxy-trHbN or red-trHbN with NO were only 2x –

4x slower in the trHbN_{delIN} variant than in the wild type (the reaction of red-trHbN with NO is a good surrogate for the reaction of red-trHbN with O₂). Importantly, the effect of the pre-A tail is completely lost in variants that lack distal site residues Tyr33 and Gln 58. These residues help to hold O₂ firmly on the heme in oxy-trHbN, and a water molecule on the heme of met-trHbN. They also anchor a non-coordinated water molecule in the distal site of red-trHbN that blocks access by incoming diatomic gases. In a variant that lacks Tyr33 and Gln 58 (trHbN_{DM}), met-trHbN_{DM} is reduced 5x more rapidly by Ru^{II} than is met-trHbN_{WT} because the distal site is now either vacant or occupied by weakly bound water, so rate-limiting water loss upon heme reduction is accelerated. A variant that lacks Tyr33, Gln 58, and the pre-A tail (met-trHbN_{TM}), is reduced by Ru^{II} at the same rate as is met-trHbN_{DM}, showing that tail loss does not affect the reduction rate if the distal site amino acids are absent. This is strong evidence that the pre-A tail's primary function is to facilitate release of the distal water molecule from met-trHbN, a function that is less important in met-trHbN_{DM} and met-trHbN_{TM} than it is in trHbN_{WT}.

© Copyright by Alexander Shayne Drena, 2023
All Rights Reserved

Dedication

Thank you to family, friends, and coworkers who have all helped me greatly during this process. A special thank you to my wife, Victoria, who has been tremendously supportive along the way.

I hope I've been able to return the favor. Another special thank you to my advisor, Prof. Andy Pacheco, who has been not just a mentor, but a friend. To a continued partnership in chemistry and climbing.

TABLE OF CONTENTS

Contents

LIST OF FIGURES.....	viii
LIST OF SCHEMES.....	xii
LIST OF TABLES.....	xiii
LIST OF ABBREVIATIONS.....	xiv
ACKNOWLEDGEMENTS	xvi
Chapter 1 Introduction	1
1.1. Project overview	1
1.2. Nitric oxide.....	2
1.3. Globins as nitric oxide dioxygenases	5
1.4. Truncated hemoglobin N	11
1.5. Thesis Objectives.....	17
1.6. References.....	18
Chapter 2 Flash photolysis studies.....	24
2.1. Overview.....	24
2.2. Materials and methods.....	27
2.2.1. General methods.....	27
2.2.2. Synthesis of PaPy ₃ H	28
2.2.2.1. Bis(2-pyridylmethyl)amine (2,2'-dipicolylamine, DPA).	28
2.2.2.2. N-(2-(bis(2-pyridylmethyl)amino)ethyl)-phthalimide.	28
2.2.2.3. (2-aminoethyl)bis(2-pyridylmethyl)amine (DPEA).	29
2.2.2.4. N,N-bis(2-pyridylmethyl)amine-N-ethyl-2-pyridine-2-carboxamide (PaPy ₃ H).....	29
2.2.3. Synthesis of [Mn(PaPy ₃)(NO)]ClO ₄ (1)	30
2.2.3.1. [Mn(PaPy ₃)(H ₂ O)]ClO ₄	30
2.2.3.2. In situ nitric oxide synthesis.	30
2.2.3.3. [Mn(PaPy ₃)(NO)]ClO ₄	32
2.3. Results and discussion	32
2.3.1. PaPy ₃ H synthesis	32
2.3.2. Synthesis of complex 1.....	34
2.4. Summary.....	36
2.5. References.....	37
Chapter 3 Reaction of oxy-trHbN and red-trHbN variants with photogenerated NO	39
3.1. Overview.....	39
3.2. Materials and methods.....	41
3.2.1. General methods.....	41
3.2.2. trHbN expression and purification	41

3.2.3. Time-resolved flash photolysis	43
3.3. Results	44
3.4. Discussion	48
3.5. Summary	52
3.6. References	52
<i>Chapter 4 Stopped-Flow analysis of met-trHbN reduction</i>	<i>54</i>
4.1. Overview of ferriglobin reduction chemistry	54
4.1.1. Myoglobin oxidation	55
4.1.2. Reduction of metmyoglobin	56
4.2. Materials and methods	62
4.3. Results	62
4.4. Discussion	70
4.6. Summary	75
4.7. References	76
<i>Chapter 5 Preparation of pre-A tail variants of trHbN</i>	<i>79</i>
5.1. Overview	79
5.2. Materials and methods	79
5.2.1. General methods	79
5.2.2. Expression and purification of trHbN variants	80
5.3. Results and Discussion	84
5.4. References	87
<i>Chapter 6 Possible strategies for designing trHbN-based anti-mycobacterial therapeutics</i>	<i>88</i>
6.1. Overview	88
6.2. N- and C- terminal modulation of conformational dynamics in proteins	88
6.3. Towards treating trHbN as a therapeutic target	90
6.4. References	95
<i>Chapter 7 Conclusions and suggestions for further study</i>	<i>98</i>
7.1. References	101

LIST OF FIGURES

- Figure 1.1. Various pathways utilizing NO biologically and environmentally. These include oxidation to nitrogen dioxide and peroxyxynitrite by environmental dioxygen and superoxide, nitrosylation of the amino acids Cys and Tyr and hemes, and oxidation to nitrite and nitrate by various enzymes. 3
- Figure 1.2. Crystal structures of (a) sperm whale myoglobin (PDB entry 1MBO), (b) flavohemoglobin from *Alcaligenes eutrophus* (PDB entry 1CQX), and (c) truncated hemoglobin N from *Mycobacterium tuberculosis* (PDB entry 1IDR). 7
- Figure 1.3. Sequence alignment of (a) truncated hemoglobin N from *M. tuberculosis*, (b) the globin domain of flavohemoglobin from *E. coli*, and (c) Sperm whale myoglobin. Residues within the blue and red boxes represent the Phe at the CD1 position and proximal heme-binding His residue respectively that are both conserved within the globin domain. Bolded in green are the conserved TyrB10 residues found within trHbN and flavoHb. Bolded in blue and purple are the residues found at the E7 position in each globin, while bolded in red are the residues found at the E11 position in trHbN and flavoHb. 9
- Figure 1.4. (a) Crystal structure of oxy-trHbN_{WT} (Protein Data Bank entry 1IDR). The heme is shown as sticks, the bound dioxygen as spheres, and the two permanent tunnels as wire mesh. The 12-amino acid N-terminal tail, referred to as the “pre-A tail”, is seen at the bottom. In the crystal structure the pre-A tail appears α -helical; however, an NMR study showed that it is more of a random coil in solution.⁶³ (b) Active site of oxy-trHbN_{WT}, showing the two amino acid residues, Tyr33 and Gln58, that play a crucial role in stabilizing O₂ at the heme center. The structure was illustrated using PyMol. 12
- Figure 2.1. Schematic diagram showing the apparatus and procedure used for the synthesis of NO *in situ*. (a) Solutions of 5 mL of 1 M FeSO₄ in 1 M H₂SO₄ and 5 mL of 1 M NaNO₂ in A and B, respectively, are degassed using the freeze-pump-thaw 30

method. The solutions are then mixed *in vacuo* with the system isolated via valve 1, and the resulting gas is transferred to container C, which has been submerged in liquid N₂ with valve 2 open slightly to allow passage, while passing through a dry ice/ethanol cold trap to remove excess water. (b) Valve 2 can be opened slightly to allow NO gas contained in container C to be transferred *in vacuo* to container D, which has been submerged in liquid N₂ with valve 3 open slightly to allow gas passage through a KOH column to remove any acid nitrogen oxides. (c) Valve 3 can be opened slightly to allow NO gas contained in container D to be transferred *in vacuo* to container E, which has been submerged in liquid N₂ with valve 4 open slightly to allow passage and equipped with a magnetic stir bar and a degassed solution of [Mn(PaPy₃)(H₂O)]⁺ in acetonitrile.

Figure 2.2.	Absorption spectrum of [Mn(PaPy ₃)(NO)] ⁺ in acetonitrile and upon irradiation with white light.	34
Figure 3.1.	Molar extinction coefficient spectra for oxy-trHbN _{TM} (black), met-trHbN _{TM} (red), and red-trHbN _{TM} (blue).	40
Figure 3.2.	Schematic of the apparatus used for the flash photolysis experiments outlined in this chapter. Laser pulses generated by the tunable laser are transmitted via the fiber optic cable shown in blue to irradiate a sample cuvette shown as a red box. A spectrophotometer beam shown as the black dashed line is transmitted perpendicular to the laser pulse.	41
Figure 3.3.	Blue trace: spectral changes at 424 nm that follow irradiation by a 455 nm, 10 ns laser pulse of a solution initially containing 24.5 μM oxy-trHbN _{TM} , 30 μM of photoactive species 1 , and 0.5 mM EDTA, in a 50 mM Tris buffer, pH 8.1. Red trace: least-squares fit to a single exponential decay (see main text for details).	42
Figure 3.4.	Blue circles: dependence of the apparent rate constants on trHbN _{TM} concentrations for (a) reaction of oxy-trHbN _{TM} with NO, and (b) nitrosylation of red-trHbN _{TM} . Red lines: linear least-squares fits of the data (y-intercepts fixed at zero).	44

Figure 3.5.	Dependence of the apparent rate constants on trHbN _{deIN} concentrations for nitrosylation of red-trHbN _{deIN} . Blue circles: data from this work; green squares: data from Koebke et al ¹ ; red line: linear least-squares fits of the data from this work (not including the two data points at highest red-trHbN _{deIN} concentration).	46
Figure 4.1.	(a) blue, green, light blue, and yellow traces: UV/Vis spectral changes observed at selected times after a solution containing approximately 9 μ M trHbN _{wt} was mixed in a 1:1 ratio with one containing 2 mM hexaammineruthenium(II) (Ru ^{II}); 50 mM tris buffer, pH 8.1. (b) absorbance vs time slices taken at 407 nm and 426 nm from the spectra depicted in (a). Dashed red traces: least-squares best fits to the model of Scheme 4.1.	62
Figure 4.2.	Blue, green, aqua, and yellow traces: spectral components S ₀ – S ₃ obtained by fitting the Fig. 4.1a spectra to the Scheme 4.2 model. Dashed red traces: least-squares Beer's law fits of the spectral components with the independently obtained extinction coefficient spectra of met-trHbN _{WT} , red-trHbN _{WT} , and oxy-trHbN _{WT} .	63
Figure 4.3.	Concentrations of met-trHbN _{WT} , red-trHbN _{WT} , and oxy-trHbN _{WT} as a function of time, calculated from the Fig. 4.1 and 4.2 fits using the Scheme 4.3 equations.	64
Figure 4.4.	Arrhenius plots showing how the rate constants k_2 (a) and k_3 (b) obtained from the Fig. 4.1 fits vary with temperature.	65
Figure 4.5.	Concentrations of red-trHbN _{WT} , red-trHbN _{deIN} , red-trHbN _{DM} , and red-trHbN _{TM} as a function of time after mixing 8 - 10 μ M of the corresponding met-trHbN variant in a 1:1 ratio with one containing 2 mM Ru ^{II} ; 50 mM tris buffer, pH 8.1, temperature fixed at 25.0 °C.	66
Figure 4.6.	S ₀ components obtained for each variant in the Fig. 4.5 experiments. The dashed red traces are the least-squares Beer's law fits of the spectral components with the independently obtained extinction coefficient spectra of met-trHbN, red-trHbN, and oxy-trHbN for each variant.	67
Figure 5.1	Full DNA fragment for the expression of trHbN _{HT} . Shown in blue are the complimentary segments for the forward and	79

reverse primer sequences, with restriction sites for HindIII and BamHI restriction endonucleases shown in bold. Shown in red is the ribosomal binding site and shown in black is the codon optimized sequence for trHbN_{HT}.

- Figure 5.2 Agarose gel (2% w/v) of pUC19 and gene fragments for trHbN_{BTA} and trHbN_{DC} variants with a 1 kb DNA ladder on the left. The numbered lanes contain the following: (1) pUC19 fragment after restriction digest, (2) and (3) gene fragments for trHbN_{BTA} and trHbN_{DC} respectively after restriction digest, (4) and (5) PCR products after ligation of digested pUC19 and trHbN_{BTA} and trHbN_{DC} fragments respectively using M13 primers. 79
- Figure 5.3 SDS-PAGE gel of trHbN_{WT} (1), trHbN_{Cys} (2), and trHbN_{DC} (3) with a prestained protein ladder on the left. 81
- Figure 5.4 Truncated sequence comparison between trHbN (a) wild type (WT), and the variants (b) single Cys (SC), (c) hexa-His tag (HT), (d) half tail (HALF), (e) base to acid (BTA), (f) double Cys (DC). 83

LIST OF SCHEMES

Scheme 1.1.	Steps required for a NO dioxygenase catalytic cycle at a heme center. Step 1 is the dioxygenation step; in step 2, the ferriheme is reduced back to the ferrous state, and in step 3 O ₂ re-binds to the heme. Note that when the heme is trHbN, the oxygenated ferrous heme will be referred to throughout this article as oxy-trHbN, while the ferric heme will be referred to as met-trHbN and the oxygen-free ferrous heme as red-trHbN.	3
Scheme 1.2.	Proposed mechanisms for the conversion of NO to NO ₃ ⁻ by O ₂ ⁻ by heterolytic cleavage (a), homolytic cleavage (b), and isomerization (c).	4
Scheme 2.1.	(a) Structure of the {Mn – NO} ⁶ compound [Mn(PaPy ₃)(NO)] ⁺ (species 1). (b) Structure of the {Mn – NO} ⁶ compound [Mn(PaPy ₂ Q)(NO)] ⁺ (species 2).	24
Scheme 2.2.	Outline for synthesis of the pentadentate ligand PaPy ₃ H.	26
Scheme 2.3.	(a) Synthesis of [Mn(PaPy ₃)(NO)] ⁺ from PaPy ₃ H and [Mn(H ₂ O) ₆] ²⁺ . (b) Photolysis of [Mn(PaPy ₃)(NO)] ⁺ to yield one equivalent of NO in solution.	33
Scheme 4.1.	The two mechanistic steps typically involved in ferric heme reduction, as ascertained from studies with myoglobin and other model proteins. ^{10, 16-19} Both the 6-coordinate Fe(III) and 5-coordinate Fe(II) states are high-spin, whereas the 6-coordinate Fe(II) intermediate is low-spin. ¹⁶	55
Scheme 4.2.	Equations 3 – 6 were integrated numerically with initial conditions: $y_0(0) = 1$; $y_1(0) = y_2(0) = y_3(0) = 0$.	63
Scheme 4.3.	Equations used to obtain the Fig. 4.3 plots of met-trHbN _{WT} , red-trHbN _{WT} , and oxy-trHbN _{WT} concentrations as a function of time. [met-trHbN] _n , [red-trHbN] _n , and [oxy-trHbN] _n ($n = 0 - 3$) are the concentrations of each species that contribute to S ₀ – S ₃ , respectively, as listed in Table 4.1, while $y_0(t) - y_3(t)$ are the values generated in the empirical Scheme 4.2 fit (see main text for details).	63

LIST OF TABLES

Table 3.1.	Second-order rate constants obtained for the reactions of NO with WT, DeIN, DM, and TM variants of oxy-trHbN and red-trHbN. Values in parentheses are for comparison to earlier literature values.	44
Table 4.1.	Concentrations of met-trHbN _{WT} , red-trHbN _{WT} , and oxy-trHbN _{WT} that contribute to the S ₀ – S ₃ , components obtained in the Fig. 4.1 fits, as calculated from the S ₀ – S ₃ Beer's law fits (Fig. 4.2).	64
Table 4.2.	Comparison of the $k_1 - k_3$ rate constant values for trHbN _{wt} , trHbN _{deIN} , trHbN _{DM} , and trHbN _{TM} , obtained by fitting experimental data with the Scheme 4.2 model. In each case, the temperature was fixed at 25 °C, and hexaammineruthenium(II) concentrations were 1 mM after stopped-flow dilution.	67

LIST OF ABBREVIATIONS

Where possible all abbreviations used are those recommended in “ACS Guide to Scholarly Communication” Section 5.3.8.

5ALA	5-aminolevulinic acid
BTA	Variant of truncated hemoglobin N in which all basic Arg and Lys residues within the Pre-A tail were converted to Glu
DeIN	Variant of truncated hemoglobin N in which the Pre-A motif was deleted
DC	Variant of truncated hemoglobin N with a R6C/D17C mutation
DM	Variant of truncated hemoglobin N with a Y33F/Q58V mutation
DPA	Bis(2-pyridylmethyl)amine
DPEA	(2-aminoethyl)bis(2-pyridylmethyl)amine
<i>E. coli</i>	<i>Escherichia coli</i>
ET	Electron transfer
Et ₂ O	Diethyl ether
EtOH	Ethanol
FdR	NADH-ferredoxin/flavodoxin
Fig	Figure
FlavoHb	Flavo-hemoglobin
<i>G. intestinalis</i>	<i>Giardia intestinalis</i>
HALF	Variant of truncated hemoglobin N in which the first six amino acid residues were truncated at the N-terminus
Hb	Hemoglobin
HT	Variant of truncated hemoglobin N with a hex-His segment added at the N-terminus
InhA	Enoyl acyl carrier protein
KatG	Catalase peroxidase protein from <i>M. tuberculosis</i>
<i>M.</i>	<i>Mycobacterium</i>
Mb	Myoglobin
MD	Molecular Dynamics
metMb	Myoglobin in a ferric state
met-trHbN	Truncated hemoglobin N in a ferric state
MV _{red}	Methyl viologen monoradical
oxyMb	Myoglobin in a reduced state with dioxygen bound
oxy-trHbN	Truncated hemoglobin N in a reduced state with dioxygen bound
PaPy ₂ QH	<i>N,N</i> -bis(2-pyridylmethyl)amine- <i>N</i> -ethyl-2-quinoline-2-carboxamide
PaPy ₃ H	<i>N,N</i> -bis(2-pyridylmethyl)amine- <i>N</i> -ethyl-2-pyridine-2-carboxamide
PCR	Polymerase chain reaction
PDB	Protein Database
red-trHbN	Truncated hemoglobin N in a reduced, 5-coordinate state
Ru ^{II} /Ru ^{III}	Hexammineruthenium (II/III) chloride

SC	Variant of truncated hemoglobin N with a S5C mutation.
SDS-PAGE	Sodium dodecyl sulfate–polyacrylamide gel electrophoresis
swMb	Sperm whale myoglobin
TB	Tuberculosis
TM	Variant of truncated hemoglobin N with a Y33F/Q58V/DelN mutation
trHbN	Truncated hemoglobin N from <i>M. tuberculosis</i>
UGDH	UDP- α -D-glucose-6-dehydrogenase
WT	Wild type

ACKNOWLEDGEMENTS

I'd like to thank Dr. Trevor Hagemann for his help throughout the synthesis of the NO precursor complex outlined in this thesis, as well as the development of synthetic routes utilized in the current work. I'd like to thank Dr. Karl Koebke for his previous work and early communication which allowed this project to take place, and Christian Hoydic for his preliminary work on the NO precursor complex. I'd like to thank Prof. Jarett Wilcoxon for the use of his stopped-flow that made up a good portion of the thesis work. I'd like to thank my labmates and coworkers who have helped throughout my time here, especially Dr. Shahid, Steve Reinhardt, Dr. Trevor Melkonian, and David Koltermann. I'd also like to thank my committee members, Prof. Nicholas Silvaggi, Prof. Alan Schwabacher, Prof. Jorg Woehl, and Prof. Joseph Aldstadt. I'd like to give a special thanks to my advisor and mentor Prof. Andy Pacheco for his guidance and expertise that truly made this thesis possible. Lastly, I'd like to thank my wife and labmate, Victoria Mandella, for her help not only in the lab, but support outside it as well.

Financial support provided by grants from UWM's Research Growth Initiative (RGI-101X377) and from the National Science Foundation (CHE-2032265) is also gratefully acknowledged.

Chapter 1 Introduction

1.1. Project overview

Mycobacterium tuberculosis is the well-known causative agent of tuberculosis (TB), a disease that has plagued mankind for millennia. Heroic efforts have been undertaken for centuries to combat TB, but it remains the leading cause of death by infection worldwide, and recent multi-drug resistant strains of *M. tuberculosis* mean alternative methods of treatment are increasingly urgent.¹ Though much has been studied about the bacteria and disease over the past hundred or so years, it was only at the turn of the century that a small heme-containing protein known as truncated hemoglobin N (trHbN) was identified and started garnering interest as an agent capable of protecting *M. tuberculosis* against reactive nitrogen species generated by the human immune system.²⁻⁴ Nitric oxide is well known to play a critical role as a toxic agent against mycobacterial infection, and upregulation of nitric oxide synthase systems is observed within macrophages after infection, though the effectiveness of these systems is still under evaluation.⁵ This thesis presents a mechanistic study of trHbN, with the long-term goal of identifying ways in which the protein could be therapeutically inactivated, thus making *M. tuberculosis* more susceptible to NO toxicity. By way of introduction, this chapter presents reviews of nitric oxide chemistry and its antimicrobial roles (Section 1.2), globins and their ability to destroy nitric oxide (Section 1.3), and trHbN as an exceptionally efficient nitric oxide destroyer (Section 1.4). Section 1.5 then provides a more detailed summary of the topics to be covered in each thesis chapter.

1.2. Nitric oxide

The biological chemistry of nitric oxide (NO) has grown to be a fascinating field. As a highly reactive radical, NO had long been viewed as a toxic molecule. Nitrogen dioxide (NO₂), formed from the spontaneous oxidation of NO by O₂, is a well-known cause of morbidity as well as a known air pollutant.⁶ In fact, the Clean Air Act lists NO₂ as one of the six criteria air pollutants, contributing to acid rain, smog, and nutrient pollution in coastal waters.⁷ Only recently has NO been shown to not only be a molecule of benefit, but critical to many life processes. Discovery of NO as the endothelium-derived relaxation factor culminated in the 1998 Nobel Prize in Physiology or Medicine to Robert F. Furchgott, Louis J. Ignarro, and Ferid Murad “for their discoveries concerning nitric oxide as a signaling molecule in the cardiovascular system”.⁸ However, the story of NO metabolism is one that is still unfolding.

Though NO oxidizes to NO₂ under atmospheric conditions in the presence of O₂, biology provides a multitude of pathways for NO interconversion. In fact, NO sits at an interesting crossroads within the biological nitrogen cycle, as shown in Fig. 1.1. Nitric oxide reductases are known to reduce NO to N₂O,⁹ NO acts as an intermediate and substrate in many dissimilatory nitrate/nitrite reductases,¹⁰ and NO is the main product within the L-arginine dependent NO synthase metabolic pathway.¹¹ The nitrate-nitrite-NO pathway has been of particular interest as a therapeutic target for a variety of cardiovascular diseases.¹² Of particular interest for the topic of this thesis are a wide variety of globins which catalyze the dioxygenation of NO to NO₃⁻, acting as NO sinks to prevent formation of further reactive nitrogen species (Scheme 1.1).

Under non-biological conditions, superoxide reacts with NO to yield NO_3^- via a peroxynitrite intermediate (ONOO^- , Scheme 1.2 eq. 1).¹³ The mechanism by which this occurs, whether by heterolytic or homolytic cleavage or isomerization, has been a topic of debate; the

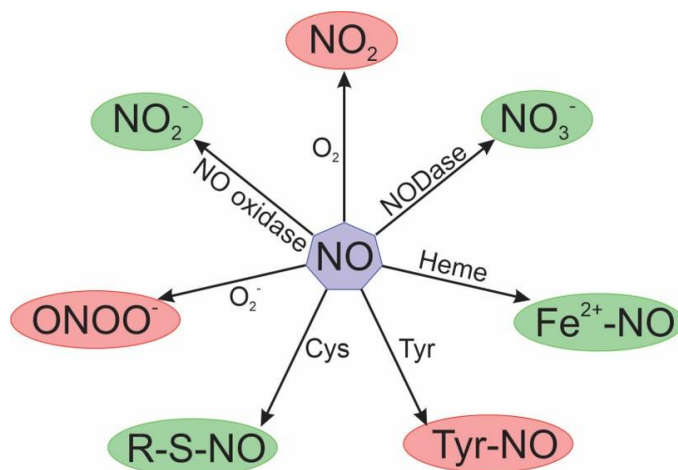
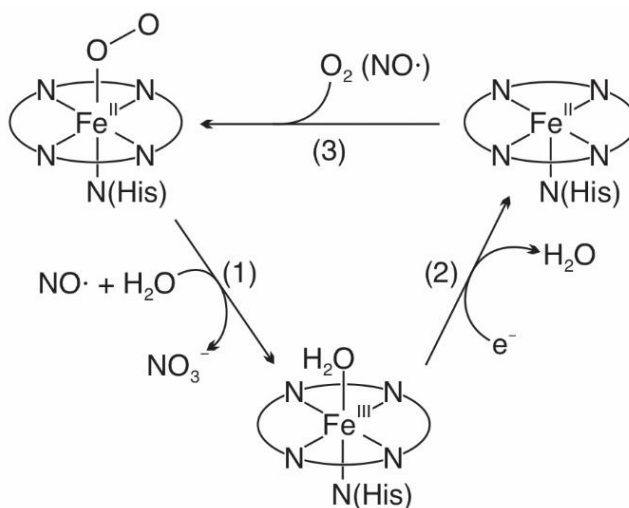
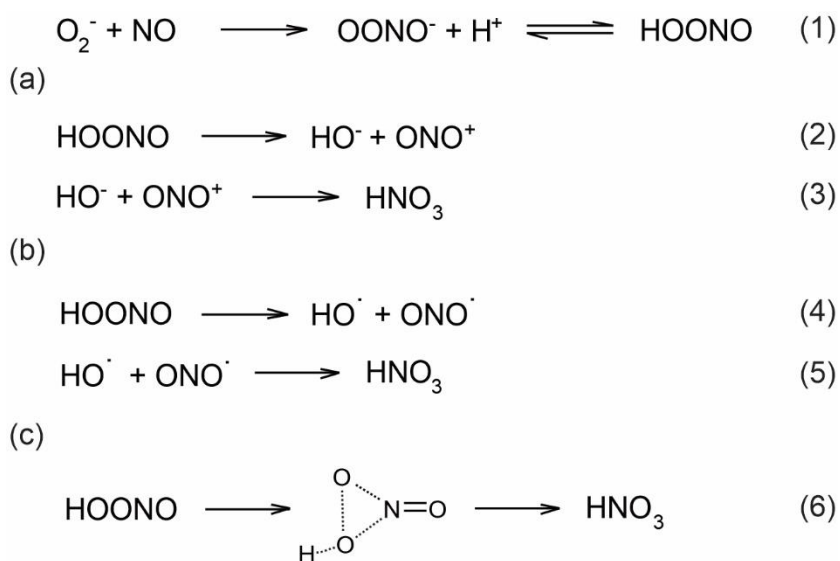


Figure 1.1. Various pathways utilizing NO biologically and environmentally. These include oxidation to nitrogen dioxide and peroxynitrite by environmental dioxygen and superoxide, nitrosylation of the amino acids Cys and Tyr and hemes, and oxidation to nitrite and nitrate by various enzymes.



Scheme 1.1. Steps required for a NO dioxygenase catalytic cycle at a heme center. Step 1 is the dioxygenation step; in step 2, the ferriheme is reduced back to the ferrous state, and in step 3 O_2 re-binds to the heme. Note that when the heme is trHbN, the oxygenated ferrous heme will be referred to throughout this article as oxy-trHbN, while the ferric heme will be referred to as met-trHbN and the oxygen-free ferrous heme as red-trHbN.

options are outlined in Scheme 1.2.¹⁴ Regardless of the mechanism, peroxyntirite is a very powerful oxidant that wreaks havoc on cells.¹⁵ Superoxide itself is also an extremely powerful oxidant, and as a result organisms have developed systems to counteract superoxide toxicity such as the robust and rather efficient superoxide dismutase superfamily. This means that enzymes which metabolize NO to NO₃⁻ must have proper activation and control over highly reactive intermediates, and globins are well-tuned to be able to do both.



Scheme 1.2. Proposed mechanisms for the conversion of NO to NO₃⁻ by O₂⁻ by heterolytic cleavage (a), homolytic cleavage (b), and isomerization (c).

Though there is structural variation amongst the globins capable of catalyzing the dioxygenation of NO to NO₃⁻, much has been learned about how these proteins catalyze such a difficult reaction from a number of detailed computational and experimental studies on a handful of representative systems.¹⁶⁻²¹ Similarly to the reaction between O₂⁻ and NO, the exact mechanism for heme-mediated NO dioxygenation has been a topic of debate for a few decades. The overwhelming consensus is that the first step is the reaction between NO and oxygen-bound heme to form Fe(III)-(OONO⁻),²² though the evidence for such an intermediate

has been debated.^{23, 24} There then exists much debate as to how peroxynitrite rearranges to yield NO_3^- . MetMb (ferric myoglobin) has long been known to catalyze the rearrangement of peroxynitrite to NO_3^- with strong supporting evidence that the process proceeds via homolytic cleavage to yield a caged NO_2 radical and ferryl-oxo species (Scheme 1.2a).²⁴⁻²⁶ Many have focused on a similar mechanism for the dioxygenation of NO by Mb and other similar proteins including flavoHb and trHbN.^{16-19, 25, 27} NO_2 produced during this pathway has the ability to nitrate Tyr residues that are often utilized in the distal architecture of such proteins, and this is indeed seen during the ONOO^- isomerization by metMb; however, the decrease in nitration observed during NO dioxygenation by oxy-Mb suggests there could be an alternative mechanism.²⁵ This could be through a concerted rearrangement that has been proposed for the isomerization of ONOOH (Scheme 1.2c).²⁸ The lack of detectable NO_2 during NO dioxygenation catalyzed by Mb also supports the Scheme 1.2c alternative.²¹ However, many computational studies consistently predict as the predominant theory for dioxygenation of NO at heme centers the homolytic cleavage of the peroxo- bond in a peroxynitrite intermediate, followed by rapid recombination to yield the nitrate- complex which then is released and the cycle turned over.^{16-18, 29} Regardless of mechanism, the protein structure plays a pivotal role in determining the effectiveness of globins at catalyzing NO dioxygenation, so this is the topic of the next section.

1.3. Globins as nitric oxide dioxygenases

Globins are some of the most well-studied proteins in science, with the O_2 -transport and storage proteins hemoglobin (Hb) and myoglobin (Mb) taking center stage.³⁰ The history is rich, as highlighted by the fact that the 1962 Nobel Prize in Chemistry was awarded to Max F. Perutz

and John C. Kendrew “for their studies of the structure of globular proteins”, having successfully studied crystals of Mb and Hb by X-ray diffraction.³¹ In general, globins are characterized by a series of α -helices that fold over one another to create a hydrophobic pocket surrounded by a hydrophilic surface, leading to the term “globin-fold”. This fold creates a perfect scaffold for a heme cofactor consisting of a porphyrin ring surrounding an iron atom at its core, with the exact architecture varying between globins, depending on function (Fig. 1.2). Though there has long been a connection between globins and NO, their biological function as NO scavengers is only a recent proposition.¹⁹ Both myoglobin and hemoglobin were known to react with NO to yield nitrate as far back as 1981,³² but the concept of a biologically relevant NO dioxygenase was not realized until Gardner’s discovery in 1998 that flavohemoglobin (flavoHb) protected *E. coli* from NO toxicity.³³

FlavoHb is a chimera-like protein comprising joined globin and reductase domains (Fig. 1.2b), while myoglobin and hemoglobin lack integrated reductase domains with which to promote redox activity. This provides the hint that while myoglobin and hemoglobin function primarily as O₂-transport proteins, flavoHb serves a more active role catalytically. The discovery of a similar protein found in yeast suggests that these coupled globin-reductase proteins share a long history dating back approximately 1.8 billion years.³⁴ In fact, globins are one of the most ancient families of proteins, occurring in all forms of life.^{30, 35} Studies on the evolution of hemoproteins highlight that the globin genetic ancestor was most likely involved in redox cycling in some capacity before O₂ was readily available.³⁶ During the Great Oxidation Event, the O₂ that was being produced by organisms, being a powerful oxidizer, was toxic for most

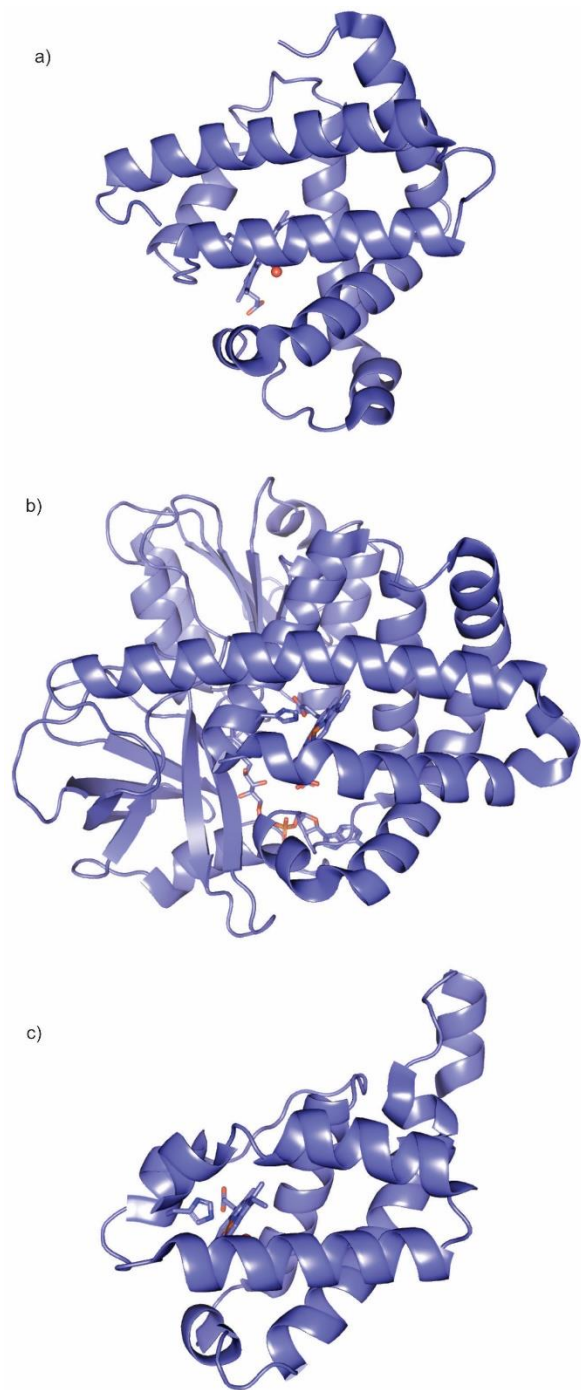


Figure 1.2. Crystal structures of (a) sperm whale myoglobin (PDB entry 1MBO), (b) flavohemoglobin from *Alcaligenes eutrophus* (PDB entry 1CQX), and (c) truncated hemoglobin N from *Mycobacterium tuberculosis* (PDB entry 1IDR).

biological life. As a result, the early evolution of hemoglobin and similar proteins centered on providing protection against O₂ toxicity.³⁷ Many globins still perform primary or secondary roles in redox catalysis; for example, neuroglobin has been shown to provide a number of non-transport roles such as nitrite reduction or as a terminal oxidase.³⁸ The overwhelming need in most aerobic organisms, however, is for large amounts of O₂ that acts as the terminal electron acceptor in aerobic respiration.³⁹ Thus, as organisms became more advanced, globin structures evolved to become more specialized. In particular, O₂ affinity is now fine-tuned to either hold O₂ tightly for use in chemistry or release it readily for storage and transport.⁴⁰ This is evident in the large variation between globins in on and off rates for ligand binding.¹⁹ One can follow the evolution of one amino acid in particular, at the E7 position, to see how O₂ affinity has evolved over time (Fig. 1.3). Early bacteria and yeast utilize a Gln for its tight hydrogen-bonding network, whereas plant hemoglobins replace Gln for a His, and a variety of vertebrates and invertebrates use all sorts of polar or nonpolar residues based on individual need for O₂ regulation, such as the His seen in sperm whale myoglobin.⁴¹

In the case of flavoHb, and other efficient NO dioxygenases, the need for O₂ lies in its catalytic activity. This begins before NO even enters the heme pocket. FlavoHb's active site is well-tuned to latch on to O₂ (step 3, Scheme 1.1) due to a tight hydrogen-bonding network facilitated by a Tyr at the B10 position and a Gln at the E7 position (Fig. 1.3). This ensures that O₂ stays bound, ready to react with NO, and may also help to activate the bound oxygen for reaction.^{42, 43} Another distinctive feature of flavoHb relative to O₂ is that the proximal side of the heme cofactor in *E. coli* flavoHb displays a triad of well-conserved residues that partially deprotonate the N_{d1} of the proximal histidine ligand, making it electron rich, and thus pushing

```

(a) -----MGLLSRLRKREPISYDKIGGHEAIEVVVEDFYVRVLADDQ-LSAFFSG
(b) -MLDA-----QTIATVKATIP--LLVETG-----PKLTAHFYDRMFTHNPELKEIFNM
(c) MVLSEGEWQLVLHVWAKVEAD-----VAGHG-----QDILIRLFKSHPETLEKFDR

(a) TNM-----SRLKGKQVEFFAAALGGP-----EPYT---GAPMKQVHQGRGITMH
(b) SNQRNGDQ-----R---EALFN-AIAAYASNIENLPALLPAVEKIAQKHTSFQIKPE
(c) FKHLKTEAEMKASEDLKKHGVTVLT-ALGAILKKKGH---HEAELKPLAQSHATKHKIPI

(a) -HFSLVAGHLADALTAAGVPSETITEILGVIAP----LAVDVTSGESTTAPV-
(b) QY-NIVGEHLLATLDEMFSPQEVLDAWGK---AYGVLANVFINREAEI----
(c) KYLEFISEAIIHVLH-SRHPGDFGADAQGAMNKALELFRKDIAAKYKELGYQG

```

Figure 1.3. Sequence alignment of (a) truncated hemoglobin N from *M. tuberculosis*, (b) the globin domain of flavohemoglobin from *E. coli*, and (c) Sperm whale myoglobin. Residues within the blue and red boxes represent the Phe at the CD1 position and proximal heme-binding His residue respectively that are both conserved within the globin domain. Bolded in green are the conserved TyrB10 residues found within trHbN and flavoHb. Bolded in blue and purple are the residues found at the E7 position in each globin, while bolded in red are the residues found at the E11 position in trHbN and flavoHb.

electron density into the Fe.⁴⁴ Evidence for the imidazolate character of the proximal ligand comes from resonance Raman studies, which show Fe-His stretching frequencies at 244 cm⁻¹ in *E. coli* flavoHb and at 235/257 cm⁻¹ (two bands) in *Giardia intestinalis* flavoHb.^{42, 43} These frequencies are much higher than those observed in Mb and Hb (220 cm⁻¹ in sperm whale Mb and 216 cm⁻¹ in human Hb), and more similar to those observed in cytochrome *c* peroxidase that contains a triad similar to that of flavoHb.^{42, 43} In cytochrome *c* peroxidase, the extra electron density on the iron weakens the Fe-OO bond and helps in O-O bond activation, and Fe-OO bond weakening is also observed in *G. intestinalis* flavoHb, which has an Fe-OO stretching frequency of 549 cm⁻¹ as compared to sw-Mb's 570 cm⁻¹.

The nature of the ferric species generated by NO dioxygenation (step 1, Scheme 1.1), and the mechanism of its subsequent reduction (step 2, Scheme 1.1), prove to be very important to the overall catalytic cycle. Indeed, Smagghe et al. have noted that, though virtually any oxygenated heme protein is capable of dioxygenating NO, their ability to do so catalytically

is often limited by the efficiency of the re-reduction step.⁴⁵ As will be discussed in more detail in Section 1.4 below and in Chapter 4, loss of water bound to the distal ferric site is often rate-limiting in the re-reduction step, so proteins optimized for dioxygenation are typically designed to lose water efficiently. The contrast between ferric Mbs or Hbs and ferric flavoHbs provides one example of how this can be achieved. Mb and Hb exhibit 6-coordinate ferric species where the 6th ligand is a distal water molecule.⁴⁶ FlavoHbs, on the other hand, exhibit 5-coordinate ferric species where the 6th coordination site is left vacant.⁴⁷ This is thought to be due to the strong proximal Fe-His bond (see above) that prevents the binding of weak ligands like water.

A final key general distinction between globins is how ligands access the distal heme pocket. All globins have pathways by which ligands access the binding site, which is often buried within the protein, but the form of these pathways often varies with the protein's function. Globins such as flavoHbs and trHbN that perform dioxygenation or other catalytic functions often contain well-defined hydrophobic tunnels such as those shown within trHbN in Fig. 1.4 to allow facile ligand passage from solvent to the active site.⁴⁸⁻⁵¹ Mb, on the other hand, relies on hydrophobic pockets connected by pathways that open only transiently via protein dynamics to allow ligand diffusion.⁵² Though not directly related to reactivity, the ease of ligand passage to the active site plays a key role in enabling higher catalytic turnover.

To summarize, the contrast between the structural features of flavoHbs on the one hand and Hbs or Mbs on the other provide a good example of how globins are optimized for specific functions. FlavoHbs appear to be designed with the primary intent of converting NO to NO₃⁻. By contrast, though Mb and Hb are both capable of catalyzing this reaction, they are much less efficient at it due to key differences in their structures, and it is clear that NO

dioxygenation is not their primary function.^{19, 53} As will be shown in the next section, trHbN also appears to be optimized for NO dioxygenation, though it shares only certain features in common with flavoHbs.

1.4. Truncated hemoglobin N

TrHbN belongs to a family of truncated hemoglobins (trHbs) that occur throughout multiple kingdoms of life dating back to an ancient origin. The family is characterized by a tight 2-on-2 α -helical fold around a B-type heme (Fig. 1.4) and is normally broken down into three distinct groups, N-, O-, and P-type trHbs. However, recent topological studies suggest the existence of a smaller, novel fourth group, that encompasses a variety of functionalities such as O₂ storage or detoxification of reactive species that mimic those of other globins.^{4, 54, 55} Interestingly, trHbs are prevalent in many pathological species, and even trHbN itself shares homologues in other infectious mycobacteria.⁵⁶ Research shows that key structural features define a trHb's function, and in the case of trHbN, these features allow the protein to function as an efficient NO dioxygenase. TrHbN shares some of these features with other known NO dioxygenases, such as the flavoHbs discussed in the previous section, but it also lacks some flavoHb features and has others that are unique.

Sequence comparison between trHbN and other globins and trHbs shows a variety of conserved as well as unique residues. Of note is an invariant His at the F8 position that serves as the proximal ligand for the heme cofactor, as well as a Phe at the CD1 position within the distal heme pocket (Fig. 1.3). TrHbN displays a similar distal heme pocket to flavoHbs, with a

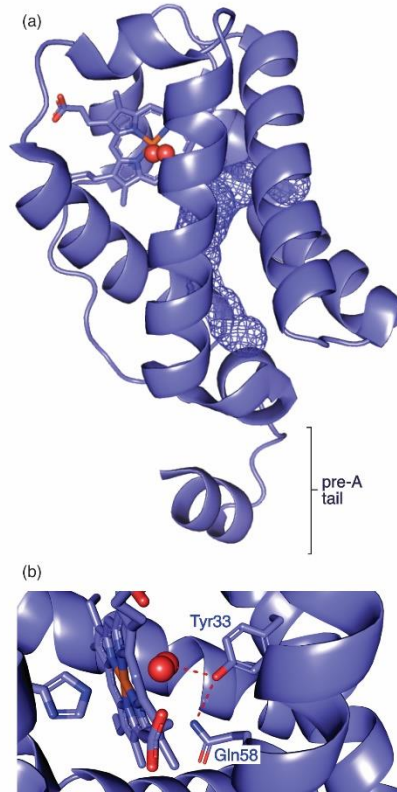


Figure 1.4. (a) Crystal structure of oxy-trHbN_{WT} (PDB entry 1IDR). The heme is shown as sticks, the bound dioxygen as spheres, and the two permanent tunnels as wire mesh. The 12-amino acid N-terminal tail, referred to as the “pre-A tail”, is seen at the bottom. In the crystal structure the pre-A tail appears α -helical; however, an NMR study showed that it is more of a random coil in solution.⁶³ (b) Active site of oxy-trHbN_{WT}, showing the two amino acid residues, Tyr33 and Gln58, that play a crucial role in stabilizing O₂ at the heme center. The structure was illustrated using PyMol.

conserved TyrB10 residue, though the residues at the E7 and E11 positions are reversed, with flavoHb displaying Gln and Leu respectively and trHbN displaying the opposite (Fig. 1.3, and see below).^{2, 19} Within the N-type trHbs, there is good sequence homology; however, an interesting feature appears within the pathogenic variants of mycobacteria at the N-terminus. This motif, which is seen to play a key role in activity, is dubbed the Pre-A region for its appearance before the A-helix, and consists of a 12-amino acid sequence followed by a Pro that separates it from the rest of the protein main body (Fig. 1.4).⁵⁷

TrHbN does not exhibit the proximal triad that is conserved in flavoHbs and gives the proximal histidine in these proteins imidazolate character (see section 1.3). As a result, the Fe-N(His) and Fe-OO stretching frequencies are not as dramatically shifted in trHbNs as they are in flavoHbs. Nevertheless, the trHbN Fe-His stretching frequency is still higher than those of Mb and Hb (226 cm^{-1} in trHbN versus 220 cm^{-1} in sperm whale Mb and 216 cm^{-1} in human Hb). Furthermore, the conserved TyrB10 observed in both trHbN and flavoHbs forms a tight hydrogen-bonding network with distal ligands that leads to lower Fe-OO stretching frequencies (560 cm^{-1} in trHbN versus 570 cm^{-1} in swMb).⁴² FlavoHbs and trHbN share other distal heme pocket architecture similarities that differ greatly from those in Mbs and Hbs. Not only is there good conservation of the key TyrB10 residue, both FlavoHbs and trHbN exhibit a H-bonded Gln residue, though in flavoHb it occurs at the E7 position whereas trHbN displays Gln at the E11 position.^{2, 47, 58} TyrB10 and GlnE7/E11 are proposed to aid in stabilizing highly reactive intermediates during the putative trHbN NO dioxygenation catalytic cycle, as discussed in the next paragraph.^{16, 18}

Figure 1.4b provides a close-up view of trHbN's distal heme pocket and the extensive hydrogen-bonding network between heme-bound ligands and nearby residues. As noted earlier, the Tyr residue at the B10 position plays a key role in ligand stabilization leading to very slow O₂ dissociation rates.^{2, 3, 51, 59} In fact, the inefficiency of O₂-release is a key reason that trHbN and similar globins are not viewed as O₂ transport proteins. The Gln at the E11 position is in close enough proximity to hydrogen-bond to Tyr-B10, and this helps to regulate ligand k_{off} rates, coordination, and orientation of ligands at the active site.^{16, 58} In deoxy-trHbN, the hydrogen-bonding network is seen to extend to a non-coordinated water molecule that has

been proposed to present a kinetic barrier towards ligand binding.⁶⁰ The H-bonding network also facilitates catalysis by directing intermediates and driving product release from the distal heme pocket.^{18, 29}

Though not a part of the distal heme pocket, it should also be noted that the proximal His residue coordinated to the heme Fe occurs with a staggered conformation as opposed to the typical eclipsed conformation found in other globins, and this also contributes towards faster activity at the Fe center.^{3, 49} The Fe within the active site forms a less strained bond with the proximal His, which leads to a geometry in which the Fe is more in plane with the porphyrin ring when compared to other globins.^{2, 3, 49} This leads to faster k_{on} rates and impacts the nature of the Fe-OO bond as described previously, and it may also impact reduction of the ferric trHbN (Step 2, Scheme 1.1), as will be discussed further below.

As briefly mentioned earlier, crystallographic data highlights an extensive tunnel system that connects the distal heme pocket to solvent through two tunnels, one short and one long (Fig. 1.4).⁴⁹ This dual-path tunnel system provides convenient routes for small ligands such as O₂ and NO to enter the active site for catalysis as well as for product release.^{29, 50, 51, 59, 60} Interestingly, the crystallographic data highlights a Phe residue at the E15 position residing at the cross junction between both tunnels and the active site that can be found in two distinct conformations. This finding, with support from MD simulations, has led to the conjecture that PheE15 may act as a gate between tunnels, making sure that each tunnel has access to the active site when necessary.^{17, 61} Xe mapping and MD simulations also highlight key hydrophobic pockets within the tunnel system that could act as binding sites for diatomic ligands, functioning as ligand reservoirs that further facilitate rapid ligand binding.^{51, 62}

As noted earlier, pathogenic forms of trHbs, including trHbN and homologues from *M. avium*, *M. bovis*, *M. microti*, and *M. marinum*, all display a distinct motif at the N-terminus dubbed the Pre-A region (Fig. 1.4). Crystallographic analysis shows the region to form a helix in the solid state, as in Fig. 1.4, but CD and solution NMR evidence suggest that it is a random coil in solution.^{57, 63} Lama et al. demonstrated the importance of the pre-A motif in regulating NO uptake in cells through a series of knockout and reinsertion experiments.⁵⁷ In these experiments they saw a decrease in NO uptake and increase in toxicity in cells lines that featured a variant of the protein with the Pre-A region removed. Even more intriguing, when this motif was inserted onto a homologue of truncated hemoglobin from *M. smegmatis* that normally lacks the motif, NO uptake was increased in cell lines that expressed the variant. The exact role of the pre-A motif in enhancing NO dioxygenase activity has been investigated in several studies. MD simulations revealed significant changes in motions along the protein backbone, primarily along helices B and E, and pointed to possible deregulation of the PheE15 gating residue, when the Pre-A region was deleted.⁵⁷ This explanation was called into question, however, when a solution NMR study by Savard et al. in 2011 found no significant shift in PheE15 after deleting the Pre-A region. The same NMR study supported a random coil conformation of the Pre-A region, which led the authors to warn against fixing the Pre-A region in a helical arrangement in future MD simulations.⁶³ The role of the pre-A region thus remains an open question, and addressing it is a major part of this thesis (see below).

To date, most studies of trHbN have focused on the dioxygenation or re-oxygenation steps (Scheme 1.1, steps 1 and 3, respectively). Markedly less studied is the ferriheme reduction step of the catalytic cycle (Scheme 1.1, step 2). Yet, as noted by Smagghe et al, the

lack of an efficient heme re-reduction system is the factor that eliminates most globins from contention as NO dioxygenases.⁴⁵ Unlike flavoHbs, trHbN lacks a dedicated reductase domain and must depend on an external electron source. Though the innate reductase system utilized by *M. tuberculosis* trHbN has yet to be determined, a 2014 paper by Singh et al. explored the reduction step by using various reductase systems found within the bacteria and the more commonly studied NADH-ferredoxin/flavodoxin (FdR) system from *E. coli*.⁶⁴ Kinetic studies were conducted in which a solution of met-trHbN and NADH in CO-saturated buffer were mixed with FdR to initiate the reaction. The resulting absorbance change in the Soret band was monitored, and a significant decrease in activity was observed in the Pre-A deletion mutant. To probe this result, MD simulations were again employed, and these highlighted a potential disturbance along the simulated protein-protein interface which could hinder electron transfer (ET) from reductase to heme center.

The study by Singh et al. focused on the pre-A tail's possible effect on electron transfer from FdR to trHbN. However, it is also possible that the pre-A tail accelerates ferriheme re-reduction by directly influencing motions in the distal heme pocket. The ferric trHbN's distal heme pocket differs from those of both the oxygen transport/storage proteins (Hb and Mb) and the flavoHb NO dioxygenases. Unlike the flavoHbs, ferric trHbN has a water bound at the distal site,³ and water dissociation has been shown to be rate limiting in ferric Mb or Hb re-reduction. In myoglobin, the relaxation of the Fe out of plane facilitates water release during the transition from $\text{Fe}^{3+}(\text{H}_2\text{O})$ to 5-coordinate Fe^{2+} .⁶⁵ However, as mentioned above, the Fe within the trHbN active site forms a less strained bond with the proximal His, which leads to a geometry in which the Fe is more in plane with the porphyrin ring when compared to other globins.^{2, 3, 49} This may

make it more difficult to reduce trHbN when compared to Mb or Hb, but reduction could be facilitated if pre-A tail motions help to mobilize the water bound at the ferriheme distal site. This possibility is explored in Chapter 4 of the thesis.

1.5. Thesis Objectives

As summarized in this chapter, trHbN activity has already been studied using several experimental and computational methods. Crystallography, computational analysis, and stopped-flow studies have highlighted the importance of the tunnel system for ligand passage.^{17, 29, 49-51, 54, 59, 61, 62, 66} Spectroscopy, crystallography, and computational studies have shed some light on the importance of the distal heme pocket hydrogen-bonding network in controlling reactivity at the active site.^{2, 3, 16, 18, 29, 51, 54, 58-60, 67} More recently, the discovery that the pre-A region significantly impacts activity has spurred investigations aimed at explaining this phenomenon.^{55, 57, 63, 64, 67} The major focus of this thesis is on how the pre-A region influences catalytic activity through effects on key residues within the distal heme pocket. To this end, Chapter 3 describes flash photolysis experiments that utilized a photoactive NO donor to study NO dioxygenation as well as nitrosylation of the wild type protein and a series of mutants, while Chapter 2, describes the synthesis of the photoactive NO generator that was used in the Chapter 3 experiments. Chapter 4 presents a stopped-flow study of ferric trHbN reduction with an artificial reducing agent that probes the effect of various mutations on the rate of heme reduction. Finally, Chapter 5 provides preliminary results obtained with some new trHbN variants, discusses how these variants could be used to answer open questions about the protein, and suggests directions for future study, especially regarding the long-term goal of

designing therapeutic agents to interfere with trHbN activity and make *M. tuberculosis* more susceptible to eradication.

1.6. References

- (1) *Global Tuberculosis Report*; World Health Organization, Geneva, 2022.
- (2) Couture, M.; Yeh, S. R.; Wittenberg, B. A.; Wittenberg, J. B.; Ouellet, Y.; Rousseau, D. L.; Guertin, M. A cooperative oxygen-binding hemoglobin from *Mycobacterium tuberculosis*. *Proc. Natl. Acad. Sci. USA* **1999**, *96*, 11223-11228.
- (3) Yeh, S.-R.; Couture, M.; Ouellet, Y.; Guertin, M.; Rousseau, D. L. A cooperative oxygen binding hemoglobin from *Mycobacterium tuberculosis*. *J. Biol. Chem.* **2000**, *275*, 1679-1684.
- (4) Ouellet, H.; Ouellet, Y.; Richard, C.; Labarre, M.; Wittenberg, B.; Wittenberg, J.; Guertin, M. Truncated hemoglobin HbN protects *Mycobacterium bovis* from nitric oxide. *Proc. Natl. Acad. Sci. USA* **2002**, *99*, 5902-5907.
- (5) Jung, J. Y.; Madan-Lala R Fau - Georgieva, M.; Georgieva M Fau - Rengarajan, J.; Rengarajan J Fau - Sohaskey, C. D.; Sohaskey Cd Fau - Bange, F.-C.; Bange Fc Fau - Robinson, C. M.; Robinson, C. M. The intracellular environment of human macrophages that produce nitric oxide promotes growth of mycobacteria. *Infect Immun.* **2013**, 3198-3209. Jamaati, H.; Mortaz, E.; Pajouhi, Z.; Folkerts, G.; Movassaghi, M.; Moloudizargari, M.; Adcock, I. M.; Garssen, J. Nitric Oxide in the Pathogenesis and Treatment of Tuberculosis. *Front Microbiol* **2017**, *8* (1664-302X (Print)), 2008. DOI: 10.3389/fmicb.2017.02008 From 2017.
- (6) Greenbaum R Fau - Bay, J.; Bay J Fau - Hargreaves, M. D.; Hargreaves Md Fau - Kain, M. L.; Kain Ml Fau - Kelman, G. R.; Kelman Gr Fau - Nunn, J. F.; Nunn Jf Fau - Prys-Roberts, C.; Prys-Roberts C Fau - Siebold, K.; Siebold, K. Effects of higher oxides of nitrogen on the anaesthetized dog. *Br. J. Anaesth* **1967**, 393-404.
- (7) Clean Air Act. EPA, Ed.; 1970.
- (8) Ignarro, L. J.; Buga Gm Fau - Wood, K. S.; Wood Ks Fau - Byrns, R. E.; Byrns Re Fau - Chaudhuri, G.; Chaudhuri, G. Endothelium-derived relaxing factor produced and released from artery and vein is nitric oxide. *Proc Natl Acad Sci U S A* **1987**, 9265-9269. Furchgott Rf Fau - Zawadzki, J. V.; Zawadzki, J. V. The obligatory role of endothelial cells in the relaxation of arterial smooth muscle by acetylcholine. *Nature* **1980**, 373-376.
- (9) Hendriks, J.; Oubrie, A.; Castresana, J.; Urbani, A.; Gemeinhardt, S.; Saraste, M. Nitric oxide reductases in bacteria. *Biochim Biophys Acta* **2000**, *1459* (2-3), 266-273. DOI: 10.1016/s0005-2728(00)00161-4 From 2000 Aug 15. Schreiber, F.; Wunderlin, P.; Udert, K.; Wells, G. Nitric oxide and nitrous oxide turnover in natural and engineered microbial communities: biological pathways, chemical reactions, and novel technologies. *Frontiers in Microbiology* **2012**, *3*, Review. DOI: 10.3389/fmicb.2012.00372.
- (10) Averill, B. A. Dissimilatory Nitrite and Nitric Oxide Reductases. *Chemical Reviews* **1996**, *96*, 2951-2964. Takaya, N. Dissimilatory nitrate reduction metabolisms and their control in fungi. *J. Biosci Bioeng* **2002**, 506-510.
- (11) Moncada, S.; Higgs, A. The L-arginine-nitric oxide pathway. *N Engl J Med* **1993**, 2002-2012.
- (12) Lundberg, J. O.; Weitzberg, E.; Gladwin, M. T. The nitrate-nitrite-nitric oxide pathway in physiology and therapeutics. *Nat Rev Drug Discov* **2008**, *7* (2), 156-167. DOI: 10.1038/nrd2466 From 2008 Feb.

- (13) Blough, N. V.; Zafiriou, O. C. Reaction of superoxide with nitric oxide to form peroxonitrite in alkaline aqueous solution. *Inorganic Chemistry* **1985**, *24* (22), 3502-3504. DOI: 10.1021/ic00216a003.
- (14) Bohle*, D. S.; Glassbrenner, P. A.; Hansert, B. O-atom Transfer versus Aromatic Nitration Reactions of Peroxynitrite. *Tetrahedron Letters* **1997**, *38* (14), 2425-2426. DOI: [https://doi.org/10.1016/S0040-4039\(97\)00419-X](https://doi.org/10.1016/S0040-4039(97)00419-X).
- (15) Szabo, C.; Ischiropoulos, H.; Radi, R. Peroxynitrite: biochemistry, pathophysiology and development of therapeutics. *Nat Rev Drug Discov* **2007**, *6* (8), 662-680. DOI: 10.1038/nrd2222 From 2007 Aug.
- (16) Mishra, S.; Meuly, M. Atomistic simulation of NO dioxygenation in group 1 truncated hemoglobin. *J. Am. Chem. Soc.* **2010**, *132*, 2968-2982.
- (17) Crespo, A.; Marti, M. A.; Kalko, S. G.; Morreale, A.; Orozco, M.; Gelpi, J. L.; Luque, F. J.; Estrin, D. A. Theoretical study of the truncated hemoglobin HbN: exploring the molecular basis of the NO detoxification mechanism. *J. Am. Chem. Soc.* **2005**, *127*, 4433-4444.
- (18) Carabet, L. A.; Guertin, M.; Lague, P.; Lamoureux, G. Mechanism of the nitric oxide dioxygenase reaction of *Mycobacterium tuberculosis* hemoglobin N. *J. Phys. Chem. B.* **2017**, *121*, 8706-8718.
- (19) Gardner, P. R. Nitric oxide dioxygenase function and mechanism of flavohemoglobin, hemoglobin, myoglobin and their associated reductases. *J. Inorg. Biochem.* **2005**, *99*, 247-266.
- (20) Hausladen, A.; Gow, A.; Stamler, J. S. Flavohemoglobin denitrosylase catalyzes the reaction of a nitroxyl equivalent with molecular oxygen. *Proc Natl Acad Sci U S A* **2001**, *98* (18), 10108-10112. DOI: 10.1073/pnas.181199698 From 2001 Aug 28. Ford, P. C. Reactions of NO and Nitrite with Heme Models and Proteins. *Inorganic Chemistry* **2010**, *49* (14), 6226-6239. DOI: 10.1021/ic902073z. Gardner, A. M.; Gardner, P. R. Allosteric in the nitric oxide dioxygenase mechanism of flavohemoglobin. *J. Biol Chem* **2021**.
- (21) Koebke, K. J.; Pauly, D. J.; Lerner, L.; Liu, X.; Pacheco, A. A. Does the oxidation of nitric oxide by oxymyoglobin share an intermediate with the metmyoglobin-catalyzed isomerization of peroxynitrite? *Inorg. Chem.* **2013**, *52*, 7623-7632.
- (22) Ford, P. C.; Lorkovic, I. M. Mechanistic aspects of the reactions of nitric oxide with transition-metal complexes. *Chem. Rev.* **2002**, *102* (4), 993-1017. DOI: 10.1021/Cr0000271. Su, J.; Groves, J. T. Mechanisms of peroxynitrite interactions with heme proteins. *Inorg. Chem.* **2010**, *49*, 6317-6329.
- (23) Herold, S.; Exner, M.; Nauser, T. Kinetic and Mechanistic Studies of the NO-Mediated Oxidation of Oxymyoglobin and Oxyhemoglobin. *Biochemistry* **2001**, *40*, 3385-3395. Olson, J. S.; Foley, E. W.; Rogge, C.; Tsai, A. L.; Doyle, M. P.; Lemon, D. D. *Free Radic. Biol. Med.* **2004**, *36*, 685-697. Goldstein, S.; Merenyi, G.; Samuni, A. Kinetics and mechanism of NO₂ reacting with various oxidation states of myoglobin. *J. Am. Chem. Soc.* **2004**, *126*, 15694-15701.
- (24) Yukl, E. T.; de Vries, S.; Moenne-Loccoz, P. The millisecond intermediate in the reaction of nitric oxide with oxymyoglobin is an iron(III)-nitrate complex, not a peroxynitrite. *J. Am. Chem. Soc.* **2009**, *131*, 7234-7235.
- (25) Bourassa, J. L.; Ives, E. P.; Marqueling, A. L.; Shimanovich, R.; Groves, J. T. Myoglobin catalyzes its own nitration. *J. Am. Chem. Soc.* **2001**, *123*, 5142-5143.
- (26) Su, J.; Groves, J. T. Direct detection of the oxygen rebound intermediates, ferrylMb and NO₂, in the reaction of metMyoglobin with peroxynitrite. *J. Am. Chem. Soc.* **2009**, *131*, 12979-12988.
- (27) Herold, S. Kinetic and spectroscopic characterization of an intermediate peroxynitrite complex in the nitrogen monoxide induced oxidation of oxyhemoglobin 1. *FEBS Letters* **1999**, *443* (1), 81-84, [https://doi.org/10.1016/S0014-5793\(98\)81345-8](https://doi.org/10.1016/S0014-5793(98)81345-8). DOI: [https://doi.org/10.1016/S0014-5793\(98\)81345-8](https://doi.org/10.1016/S0014-5793(98)81345-8) (accessed 2023/04/20). Schopfer, M. P.; Mondal, B.; Lee, D.-H.; Sarjeant, A. A. N.; Karlin, K. D. Heme/O₂/NO nitric oxide dioxygenase (NOD) reactivity: phenolic nitration via a putative heme-peroxynitrite intermediate. *J. Am. Chem. Soc.* **2009**, *131*, 11304-11305.
- (28) Anbar, M.; Taube, H. Interaction of Nitrous Acid with Hydrogen Peroxide and with Water. *Journal of the American Chemical Society* **1954**, *76* (24), 6243-6247. DOI: 10.1021/ja01653a007. Tsai, A. L.; Wei, C.

H.; Kulmacz, R. J. Interaction Between Nitric Oxide and Prostaglandin H Synthase. *Archives of Biochemistry and Biophysics* **1994**, *313* (2), 367-372. DOI: <https://doi.org/10.1006/abbi.1994.1400>.

Beckman, J. S.; Koppenol, W. H. Nitric oxide, superoxide, and peroxynitrite: the good, the bad, and ugly. *Am J Physiol* **1996**, *271* (5 Pt 1), C1424-1437. DOI: 10.1152/ajpcell.1996.271.5.C1424 From 1996 Nov.

Koppenol, W. H.; Moreno, J. J.; Pryor, W. A.; Ischiropoulos, H.; Beckman, J. S. Peroxynitrite, a cloaked oxidant formed by nitric oxide and superoxide. *Chem Res Toxicol* **1992**, *5* (6), 834-842. DOI: 10.1021/tx00030a017 From 1992 Nov-Dec.

(29) Marti, M. A.; Bidon-Chanal, A.; Crespo, A.; Yeh, S.-R.; Guallar, V.; Luque, F. J.; Estrin, D. A. Mechanism of product release in NO detoxification from *Mycobacterium tuberculosis* truncated hemoglobin N. *J. Am. Chem. Soc.* **2008**, *130*, 1688-1693.

(30) Hardison, R. C. A brief history of hemoglobins: plant, animal, protist, and bacteria. *Proc Natl Acad Sci U S A* **1996**, *93* (12), 5675-5679. DOI: 10.1073/pnas.93.12.5675 From 1996 Jun 11. Hardison, R. Hemoglobins from bacteria to man: evolution of different patterns of gene expression. *J Exp Biol* **1998**, *201* (Pt 8), 1099-1117. DOI: 10.1242/jeb.201.8.1099 From 1998 Apr. Hardison, R. C. Evolution of hemoglobin and its genes. *Cold Spring Harb Perspect Med* **2012**, *2* (12), a011627. DOI: 10.1101/cshperspect.a011627 From 2012 Dec 1.

(31) Kendrew Jc Fau - Bodo, G.; Bodo G Fau - Dintzis, H. M.; Dintzis Hm Fau - Parrish, R. G.; Parrish Rg Fau - Wyckoff, H.; Wyckoff H Fau - Phillips, D. C.; Phillips, D. C. A three-dimensional model of the myoglobin molecule obtained by x-ray analysis. *Nature* **1958**, 662-666. Kendrew, J. C.; Dickerson, R. E.; Strandberg, B. E.; Hart, R. G.; Davies, D. R.; Phillips, D. C.; Shore, V. C. Structure of Myoglobin: A Three-Dimensional Fourier Synthesis at 2 Å. Resolution. *Nature* **1960**, *185* (4711), 422-427. DOI: 10.1038/185422a0. Perutz, M. F.; Rossmann, M. G.; Cullis, A. F.; Muirhead, H.; Will, G.; North, A. C. T. Structure of Hæmoglobin: A Three-Dimensional Fourier Synthesis at 5.5-Å. Resolution, Obtained by X-Ray Analysis. *Nature* **1960**, *185* (4711), 416-422. DOI: 10.1038/185416a0.

(32) Doyle Mp Fau - Hoekstra, J. W.; Hoekstra, J. W. Oxidation of nitrogen oxides by bound dioxygen in hemoproteins. *J. Inorg Biochem* **1981**, 351-358.

(33) Gardner, P. R.; Gardner, A. M.; Martin, L. A.; Salzman, A. L. Nitric oxide dioxygenase: An enzymatic function for flavomyoglobin. *Proc. Natl. Acad. Sci. USA* **1998**, *95*, 10378-10383.

(34) Oshino, R.; Oshino, N.; Chance, B.; Hagihara, B. Studies on Yeast Hemoglobin. *European Journal of Biochemistry* **1973**, *35* (1), 23-33, <https://doi.org/10.1111/j.1432-1033.1973.tb02805.x>. DOI: <https://doi.org/10.1111/j.1432-1033.1973.tb02805.x> (accessed 2023/04/20). Zhu, H.; Riggs, A. F. Yeast flavohemoglobin is an ancient protein related to globins and a reductase family. *Proc Natl Acad Sci U S A* **1992**, 5015-5019.

(35) Vinogradov, S. N.; Hoogewijs, D.; Bailly, X.; Arredondo-Peter, R.; Gough, J.; Dewilde, S.; Moens, L.; Vanfleteren, J. R. A phylogenomic profile of globins. *BMC Evol Biol* **2006**, *6*, 31. DOI: 10.1186/1471-2148-6-31.

(36) Moens, L.; Vanfleteren, J.; Van de Peer, Y.; Peeters, K.; Kapp, O.; Czeluzniak, J.; Goodman, M.; Blaxter, M.; Vinogradov, S. Globins in nonvertebrate species: dispersal by horizontal gene transfer and evolution of the structure-function relationships. *Mol Biol Evol* **1996**, *13* (2), 324-333. DOI: 10.1093/oxfordjournals.molbev.a025592.

(37) Raymond, J.; Segre, D. The effect of oxygen on biochemical networks and the evolution of complex life. *Science* **2006**, *311* (5768), 1764-1767. DOI: 10.1126/science.1118439. Falkowski, P. G. Evolution. Tracing oxygen's imprint on earth's metabolic evolution. *Science* **2006**, *311* (5768), 1724-1725. DOI: 10.1126/science.1125937.

(38) Burmester, T.; Hankeln, T. Neuroglobin: a respiratory protein of the nervous system. *News Physiol Sci* **2004**, *19* (0886-1714 (Print)), 110-113. DOI: 10.1152/nips.01513.2003 From 2004 Jun. Tiso, M.; Tejero J Fau - Basu, S.; Basu S Fau - Azarov, I.; Azarov I Fau - Wang, X.; Wang X Fau - Simplaceanu, V.; Simplaceanu V Fau - Frizzell, S.; Frizzell S Fau - Jayaraman, T.; Jayaraman T Fau - Geary, L.; Geary L Fau -

- Shapiro, C.; Shapiro C Fau - Ho, C.; et al. Human neuroglobin functions as a redox-regulated nitrite reductase. *J. Biol Chem* **2011**, 18277-18289.
- (39) Dickerson, R. E. G., I. *Hemoglobin: Structure, function, evolution, and pathology*; The Benjamin/Cummings Publishing Company, 1983.
- (40) Terwilliger, N. B. Functional adaptations of oxygen-transport proteins. *J Exp Biol* **1998**, 201 (Pt 8), 1085-1098. DOI: 10.1242/jeb.201.8.1085 From 1998 Apr.
- (41) Suzuki, T.; Imai, K. Evolution of myoglobin. *Cell Mol Life, Sci* **1998**. Hoy, J. A.; Robinson, H.; Trent, J. T.; Kakar, S.; Smagghe, B. J.; Hargrove, M. S. Plant Hemoglobins: A Molecular Fossil Record for the Evolution of Oxygen Transport. *Journal of Molecular Biology* **2007**, 371 (1), 168-179. DOI: <https://doi.org/10.1016/j.jmb.2007.05.029>.
- (42) Mukai, M.; Mills, C. E.; Poole, R. K.; Yeh, S. R. Flavohemoglobin, a globin with a peroxidase-like catalytic site. *J Biol Chem* **2001**, 276 (10), 7272-7277. DOI: 10.1074/jbc.M009280200 From 2001 Mar 9.
- (43) Lukaszewicz, B.; McColl, E.; Yee, J.; Rafferty, S.; Couture, M. Resonance Raman studies on the flavohemoglobin of the protist *Giardia intestinalis*: evidence of a type I/II-peroxidase-like heme environment and roles of the active site distal residues. *J Biol Inorg Chem* **2017**, 22 (7), 1099-1108. DOI: 10.1007/s00775-017-1487-7 From 2017 Oct.
- (44) Ermler, U.; Siddiqui, R. A.; Cramm, R.; Friedrich, B.; Schröder, D. Crystallization and preliminary X-ray diffraction studies of a bacterial flavohemoglobin protein. *Proteins: Structure, Function, and Bioinformatics* **1995**, 21 (4), 351-353, <https://doi.org/10.1002/prot.340210408>. DOI: <https://doi.org/10.1002/prot.340210408> (accessed 2023/04/20).
- (45) Smagghe, B. J.; Trent, J. T.; Hargrove, M. S. NO dioxygenase activity in hemoglobins is ubiquitous in vitro, but limited by reduction in vivo. *PLoS ONE* **2008**, 3, e2039.
- (46) Coryell, C. D.; Stitt, F.; Pauling, L. The Magnetic Properties and Structure of Ferrihemoglobin (Methemoglobin) and Some of its Compounds. *Journal of the American Chemical Society* **1937**, 59 (4), 633-642. DOI: 10.1021/ja01283a012.
- (47) Bonamore, A.; Boffi, A. Flavohemoglobin: Structure and reactivity. *IUBMB Life* **2008**, 60 (1), 19-28, <https://doi.org/10.1002/iub.9>. DOI: <https://doi.org/10.1002/iub.9> (accessed 2023/04/20).
- (48) Ferreiro, D. N.; Boechi, L.; Estrin, D. A.; Marti, M. A. The key role of water in the dioxygenase function of *Escherichia coli* flavohemoglobin. *J Inorg Biochem* **2013**, 119 (1873-3344 (Electronic)), 75-84. DOI: 10.1016/j.jinorgbio.2012.10.015 From 2013 Feb. Forti, F.; Boechi, L.; Estrin, D. A.; Marti, M. A. Comparing and combining implicit ligand sampling with multiple steered molecular dynamics to study ligand migration processes in heme proteins. *Journal of Computational Chemistry* **2011**, 32 (10), 2219-2231, <https://doi.org/10.1002/jcc.21805>. DOI: <https://doi.org/10.1002/jcc.21805> (accessed 2023/04/20).
- (49) Milani, M.; Pesce, A.; Ouellet, Y.; Ascenzi, P.; Guertin, M.; Bolognesi, M. *Mycobacterium tuberculosis* hemoglobin N displays a protein tunnel suited for O₂ diffusion to the heme. *EMBO J.* **2001**, 20, 3902-3909.
- (50) Bidon-Chanal, A.; Marti, M. A.; Crespo, A.; Milani, M.; Orozco, M.; Bolognesi, M.; Luque, F. J.; Estrin, D. A. Ligand-induced dynamical regulation of NO conversion in *Mycobacterium tuberculosis* truncated hemoglobin-N. *PROT. Struct. Func. Bioinf.* **2006**, 64, 457-464.
- (51) Dantsker, D.; Samuni, U.; Ouellet, Y.; Wittenberg, B. A.; Wittenberg, J. B.; Milani, M.; Bolognesi, M.; Guertin, M.; Friedman, J. M. Viscosity-dependent relaxation significantly modulates the kinetics of CO recombination in the truncated hemoglobin trHbN from *Mycobacterium tuberculosis*. *J. Biol. Chem.* **2004**, 279, 38844-38853.
- (52) Schmidt, M.; Nienhaus, K.; Pahl, R.; Krasselt, A.; Anderson, S.; Parak, F.; Nienhaus, G. U.; Srajer, V. Ligand migration pathway and protein dynamics in myoglobin: a time-resolved crystallographic study on L29W MbCO. *Proc Natl Acad Sci U S A* **2005**, 102 (33), 11704-11709. DOI: 10.1073/pnas.0504932102 From 2005 Aug 16. Teeter, M. M. Myoglobin cavities provide interior ligand pathway. *Protein Science*

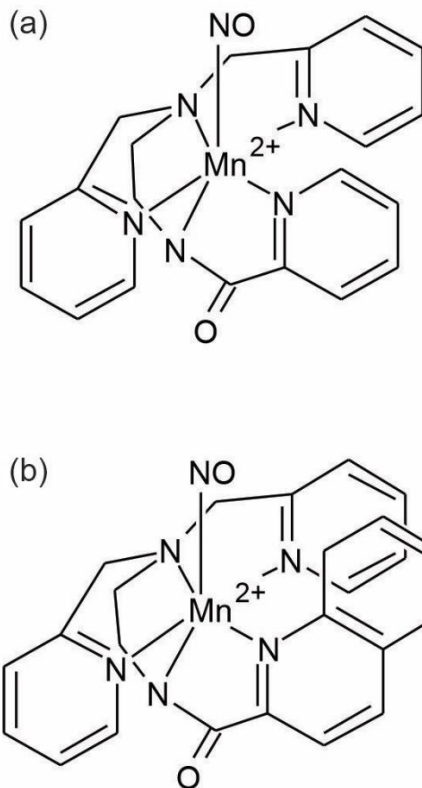
- 2004**, *13* (2), 313-318, <https://doi.org/10.1110/ps.03334304>. DOI: <https://doi.org/10.1110/ps.03334304> (accessed 2023/04/20).
- (53) Gow, A. J.; Luchsinger, B. P.; Pawloski, J. R.; Singel, D. J.; Stamler, J. S. The oxyhemoglobin reaction of nitric oxide. *Proc Natl Acad Sci U S A* **1999**, *96* (16), 9027-9032. DOI: 10.1073/pnas.96.16.9027 From 1999 Aug 3.
- (54) Milani, M.; Pesce, A.; Nardini, M.; Ouellet, H.; Ouellet, Y.; Dewilde, S.; Bocedi, A.; Ascenzi, P.; Guertin, M.; Moens, L.; et al. Structural basis for heme binding and diatomic ligand recognition in truncated hemoglobins. *J. Inorg. Biochem.* **2005**, *99*, 97-109.
- (55) Pesce, A.; Bustamante, J. P.; Bidon-Chanal, A.; Boechi, L.; Estrin, D. A.; Luque, F. J.; Sebiló, A.; Guertin, M.; Bolognesi, M.; Ascenzi, P.; et al. The N-terminal pre-A region of *Mycobacterium tuberculosis* 2/2HbN promotes NO-dioxygenase activity. *FEBS J.* **2016**, *283*, 305-322.
- (56) Nardini, M.; Pesce, A.; Bolognesi, M. Truncated (2/2) hemoglobin: Unconventional structures and functional roles in vivo and in human pathogenesis. *Mol Aspects Med* **2022**, *84* (1872-9452 (Electronic)), 101049. DOI: 10.1016/j.mam.2021.101049.
- (57) Lama, A.; Pawaria, S.; Bidon-Chanal, A.; Anand, A.; Gelpi, J. L.; Swati, A.; Marti, M. A.; Estrin, D. A.; Luque, F. J.; Dikshit, K. L. Role of pre-A motif in nitric oxide scavenging by truncated hemoglobin, HbN of *Mycobacterium tuberculosis*. *J. Biol. Chem.* **2009**, *284*, 14457-14468.
- (58) Ouellet, Y.; Milani, M.; Couture, M.; Bolognesi, M.; Guertin, M. Ligand interactions in the distal heme pocket of *Mycobacterium tuberculosis* truncated hemoglobin N: roles of TyrB10 and GlnE11 residues. *Biochemistry* **2006**, *45*, 8770-8781.
- (59) Samuni, U.; Dantsker, D.; Ray, A.; Wittenberg, J. B.; Wittenberg, B. A.; Dewilde, S.; Moens, L.; Ouellet, Y.; Guertin, M.; Friedman, J. M. Kinetic modulation of carbonmonoxy derivatives of truncated hemoglobins. *J. Biol. Chem.* **2003**, *278*, 27241-27250.
- (60) Ouellet, Y. H.; Daigle, R.; Lague, P.; Dantsker, D.; Milani, M.; Bolognesi, M.; Friedman, J. M.; Guertin, M. Ligand binding to truncated hemoglobin N from *Mycobacterium tuberculosis* is strongly modulated by the interplay between the distal heme pocket residues and internal water. *J. Biol. Chem.* **2008**, *283*, 27270-27278.
- (61) Bidon-Chanal, A.; Marti, M. A.; Estrin, D. A.; Luque, F. J. Dynamical regulation of ligand migration by a gate-opening molecular switch in truncated hemoglobin-N from *Mycobacterium tuberculosis*. *J. Am. Chem. Soc.* **2007**, *129*, 6782-6788. Oliveira, A.; Singh, S.; Bidon-Chanal, A.; Forti, F.; Marti, M. A.; Boechi, L.; Estrin, D. A.; Dikshit, K. L.; Luque, F. J. Role of PheE15 gate in ligand entry and nitric oxide detoxification function of *Mycobacterium tuberculosis* truncated hemoglobin N. *PLoS ONE* **2012**, *7*, e49291.
- (62) Cazade, P.-A.; Meuly, M. Oxygen migration pathways in NO-bound truncated hemoglobin. *ChemPhysChem* **2012**, *13*, 4276-4286.
- (63) Savard, P.-Y.; Daigle, R.; Morin, S.; Sebiló, A.; Meindre, F.; Lague, P.; Guertin, M.; Gagne, S. M. Structure and dynamics of *Mycobacterium tuberculosis* truncated hemoglobin N: insights from NMR spectroscopy and molecular dynamics simulations. *Biochemistry* **2011**, *50*, 11121-11130.
- (64) Singh, S.; Thakur, N.; Oliveira, A.; Petruk, A. A.; Hade, M. D.; Sethi, D.; Bidon-Chanal, A.; Marti, M. A.; Datta, H.; Parkesh, R.; et al. Mechanistic insight into the enzymatic reduction of truncated hemoglobin N of *Mycobacterium tuberculosis*. *J. Biol. Chem.* **2014**, *289*, 21573-21583.
- (65) Della Longa, S.; Arcovito, A.; Congiu-Castellano, A.; Girasole, M.; Hazemann, J. L.; Lo Bosco, A. Redox-induced structural dynamics of Fe-heme ligand in myoglobin by X-ray absorption spectroscopy. *Biophys J.* **2003**, *85*, 549-558.
- (66) Daigle, R.; Guertin, M.; Lague, P. Structural characterization of the tunnels of *Mycobacterium tuberculosis* truncated hemoglobin N from molecular dynamics simulations. *Proteins* **2009**, *75*, 735-747.
- (67) Koebke, K. J.; Waletzko, M. T.; Pacheco, A. A. Direct monitoring of the reaction between photochemically generated nitric oxide and *Mycobacterium tuberculosis* truncated hemoglobin N wild

type and variant forms: an assessment of computational mechanistic predictions. *Biochemistry* **2016**, *55*, 686-696.

Chapter 2 Flash photolysis studies

2.1. Overview

The literature is rich with a variety of NO precursor compounds. A comprehensive review published in 2002 lists 16 distinct classes of NO precursors alone, from organic nitrates and nitrites to hydroxyurea, and with the continued interest in NO chemistry that number has only grown.¹ Compounds in a common class of NO precursor undergo hydrolysis to release NO and are therefore pH sensitive; an example from this class is the organoammonium salt diethylamine NONOate. Compounds in this class though, tend to release NO too slowly for the purposes of the current work because trHbN dioxygenates NO to NO₃⁻ at nearly diffusion-limited rates. Fortunately, many photolytically active compounds can release NO rapidly upon photoexcitation with great control under appropriate experimental conditions. A variety of photolabile metal nitrosyl {M – NO} compounds have been developed by the Mascharak lab, including the diamagnetic ²⁶ complexes [Mn(PaPy₃)(NO)]ClO₄ (**1**), and [Mn(PaPy₂Q)(NO)]ClO₄ (**2**), outlined in Scheme 2.1.^{3, 4} These were utilized for the work described in this thesis, and for work recently published by our group.⁵ The ability of complexes **1** and **2** to be photoactivated, initiating NO release in solution upon irradiation by Visible or Near-IR light, makes them perfect candidates for studying reactions with NO on fast time scales. With the help of a ns pulsed laser, NO can be released from either **1** or **2** in less than 1 ms, after which reactions between trHbN and NO can be monitored on a μs time-scale with a rapidly responding UV/Vis spectrophotometer.



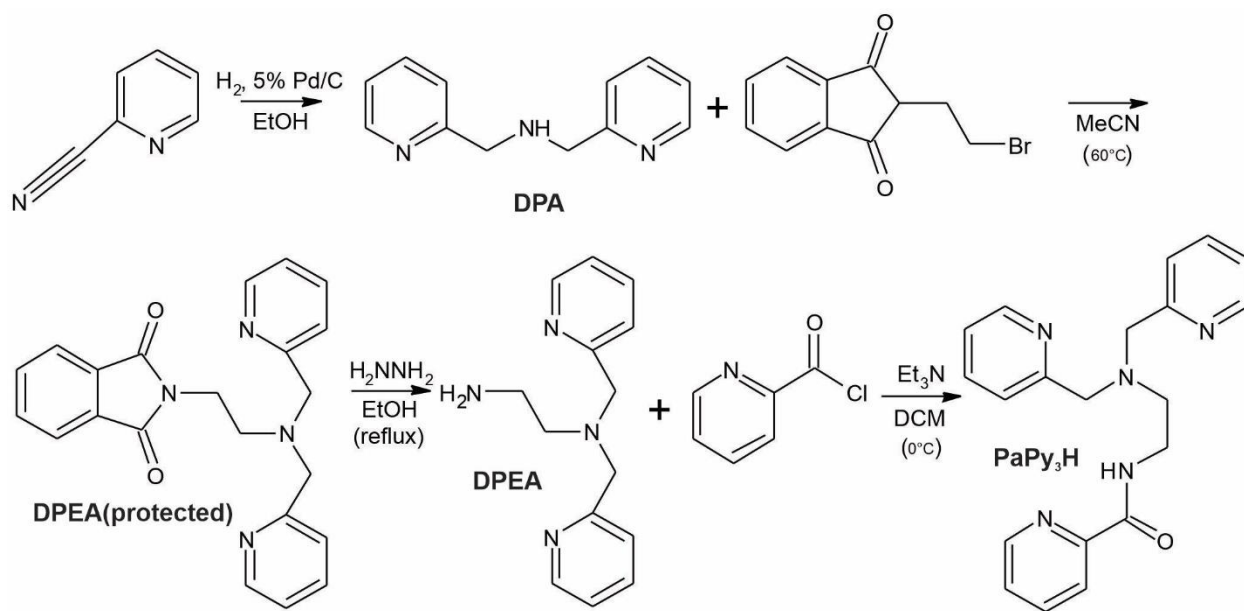
Scheme 2.1. (a) Structure of the $\{\text{Mn} - \text{NO}\}^6$ compound $[\text{Mn}(\text{PaPy}_3)(\text{NO})]^+$ (species **1**). (b) Structure of the $\{\text{Mn} - \text{NO}\}^6$ compound $[\text{Mn}(\text{PaPy}_2\text{Q})(\text{NO})]^+$ (species **2**).

The pentadentate ligand *N,N*-bis(2-pyridylmethyl)amine-*N*-ethyl-2-pyridine-2-carboxamide (PaPy₃H) was first developed by the Mascharak lab to look into mononuclear non-heme iron complexes that could provide insight into the variety of O₂-activating enzymes utilized in nature.⁶ Original interest was in the study of deprotonated carboxamido nitrogen ligation to Fe centers, which was long thought to be improbable due to the fact that iron would most likely precipitate before the pH required for deprotonation. However, the discovery that nature had found ways to circumvent this issue, such as the active site of Fe-dependent nitrile hydratase⁷ and the P-cluster of nitrogenase,⁸ led to an explosion of research on the topic.^{9, 10} Most of these studies focused on ligands featuring multiple carboxamido donors where these anionic ligands are shown to provide much needed stability for maintaining a +3 oxidation

state.¹⁰ However, the development of the low-spin Fe(III) complex $[\text{Fe}(\text{PaPy}_3)(\text{CH}_3\text{CN})]^{2+}$ showed that it was possible to develop ligands that utilize a single carboxamido donor ligand, and interestingly, the acetonitrile group was labile enough to be replaced with a variety of ligands.⁶ This led to the discovery that the acetonitrile ligand could be replaced with a photolabile NO which then led to the development of similar systems utilizing Ru and Mn as the metal centers.^{3, 11, 12} Due to their water solubility and photoactivity in the Visible/IR range, the Mn nitrosyls **1** and **2** mentioned previously have been invaluable studying the reactivity between trHbN and NO.

Complexes **1** and **2** utilize a Mn center chelated by the pentadentate ligands PaPy₃H or PaPy₂QH respectively [PaPy₂QH: *N,N*-bis(2-pyridylmethyl)amine-*N*-ethyl-2-quinoline-2-carboxamide]. The differences in the electronic structure of these ligands tunes their excitation wavelength as well as the quantum yield of NO. While PaPy₃H contains three ligated pyridines along with a bridging amine and carboxamido nitrogen, PaPy₂QH substitutes the pyridyl-carboxamide group for a quinolyl-carboxamide, creating a more conjugated system that red-shifts the absorption spectrum and increases the molar extinction coefficient. The photolability of these complexes has long been believed to arise from excitation of an electron at the metal center to the ligand system, and the stabilization of this $d-\pi^*$ transition due to increased conjugation also leads to an increase in the quantum yield of NO in **2**.^{4, 13} This comes at a cost as the increase in photolability increases premature NO release; nevertheless, species **2** was successfully used by the Pacheco group in an earlier study of trHbN.⁵ Unfortunately, a practical difficulty has arisen since then. The synthesis of **2** employs reductive nitrosylation of Mn(III) complexes under 1 atm of NO, which requires a cylinder of NO gas, the cost of which has

increased ten-fold in a few short years and is now prohibitive. To avoid the need for compressed NO gas, the studies in this thesis were performed using NO precursor **1**, which was synthesized by a new procedure that uses NO generated in situ. As a bonus, species **1** is less photolabile than species **2** and so less prone to premature NO release. This chapter describes the new synthesis of **1**.



Scheme 2.2. Outline for synthesis of the pentadentate ligand PaPy₃H.

2.2. Materials and methods

2.2.1. General methods

All reagents were purchased from Millipore-Sigma, Fisher Scientific, or dot Scientific unless otherwise specified. Routine UV/Vis spectra were obtained using Cary 50 spectrophotometers; where anaerobic conditions were needed, a spectrophotometer installed in a nitrogen-filled glovebox was used. Routine NMR spectra were obtained using a Bruker DPX – 300MHz instrument.

2.2.2. Synthesis of PaPy₃H

2.2.2.1. Bis(2-pyridylmethyl)amine (2,2'-dipicolylamine, DPA).

To a clean and dry round bottom flask equipped with a magnetic stir bar were added 10.1 g of 2-cyanopyridine, 16.5 mL of anhydrous ethanol, and 0.497 g of 5% Palladium on Carbon (Pd/C). The reaction mixture was stirred vigorously while being flushed with hydrogen gas to charge the catalyst and was then left stirring under a continuous flow of hydrogen until the starting material was used up (approximately 72 hr). The extent of reaction was determined by silica TLC monitoring of the reaction mixture using 10% methanol and 90% dichloromethane as an eluent and ninhydrin as an amine stain for developing. The crude product was vacuum filtered through a fritted glass disc covered with a 1 cm layer of celite to remove the Pd/C. After washing the celite cake three times with hot ethanol to maximize recovery of the desired DPA product, the filtrate was transferred to a round bottom flask and concentrated under vacuum, yielding 9.54 g DPA (98.8% yield). ¹H NMR, CDCl₃: δ 8.55-7.16 (m, 8H, aromatic H's), 3.97 (s, 4H, CH₂), 2.63 (s, broad, 1H, NH).

2.2.2.2. *N*-(2-(bis(2-pyridylmethyl)amino)ethyl)-phthalimide.

To a clean and dry round bottom flask, equipped with a magnetic stir bar, were added 8 g of DPA, 10.2 g of *N*-(2-bromoethyl)phthalimide, 6 mL of triethylamine, and 50 mL of anhydrous acetonitrile. The flask was incubated at 60 °C under argon gas until the DPA was consumed (approximately 12 hr). Reaction progress was monitored by TLC using 10% acetonitrile and 90% dichloromethane as an eluent. The mixture was concentrated under vacuum leaving a dark brown paste, which was then vacuum filtered through a fritted glass disk and washed with cold water and diethyl ether (approx. 50mL of each), until only a beige solid remained as the

phthalimide protected intermediate. $^1\text{H NMR}$, (CDCl_3): δ 8.43-7.00 (m, 8H, aromatic H's), 7.83-7.69 (m, 4H, aromatic H's), 3.84 (s, 4H, CH_2), 3.84-3.79 (t, 2H, CH_2), 2.89-2.81 (t, 2H, CH_2).

2.2.2.3. (2-aminoethyl)bis(2-pyridylmethyl)amine (DPEA).

To a clean and dry round bottom flask, equipped with a magnetic stir bar, were added 7.5 g of the phthalimide protected intermediate, 50 mL anhydrous ethanol, and 1 mL hydrazine monohydrate. The solution was refluxed under argon until a gelatinous precipitate formed. After precipitate formation ceased (approx. 2 hr) 10 mL of 12 M HCl were slowly added, and the solution was allowed to reflux to decompose the precipitate-forming phthalyl hydrazide hydrochloride. The solution was cooled, the precipitate filtered off, and the filtrate concentrated under vacuum. The residue was dissolved in RO water and basified with 5 M NaOH to pH 11, and the organic material was extracted in triplicate with 10 mL DCM. The organic layers were then pooled and washed with a salt brine, then dried over Na_2SO_4 . The solid was filtered off and the filtrate concentrated under vacuum, leaving behind *N,N*-Bis(2-pyridylmethyl)ethylenediamine (DPEA) as a yellow oil. $^1\text{H NMR}$, (CDCl_3): δ 8.53-7.13 (m, 8H, aromatic), 3.85 (s, 4H, CH_2), 2.85-2.82 (t, 2H, CH_2), 2.72-2.69 (t, 2H, CH_2).

2.2.2.4. *N,N*-bis(2-pyridylmethyl)amine-*N*-ethyl-2-pyridine-2-carboxamide (PaPy₃H).

2-picolinic acid chloride was first synthesized by adding 0.730 g 2-picolinic acid to a clean and dry three-necked flask that was fitted with a condenser and flushed with argon gas. Excess SOCl_2 (approx. 2 mL) was added to the flask on ice, followed by a drop of catalytic dimethylformamide diluted in dichloromethane. The reaction mixture was then allowed to reflux gently while stirring. The solution starts off as a hunter green color, and as the reaction progresses, turns lavender. After full color change (approx. 2 hr) the SOCl_2 was removed under vacuum. PaPy₃H was synthesized by dissolving 1.44 g of DPEA in dichloromethane cooled in an

ice bath, to which an equivalent of 2-picolinic acid chloride was slowly added. Excess triethylamine was added, and the solution was stirred overnight. The solution was cooled on ice to precipitate the salt byproduct which was then removed by filtration through a fritted glass disk. The solution was basified to pH 11 with 5 M NaOH. The organic product was then extracted three times with 10 mL dichloromethane, and the organic layers were further washed with a salt brine solution, dried over Na₂SO₄, and vacuum filtered. The filtrate was then concentrated under vacuum leaving behind pure PaPy₃H. ¹H NMR (CDCl₃): δ 8.72-7.14 (m, 12H, aromatic), 3.97 (s, 4H), 3.61 (t, 2H), 2.88 (t, 2H).

2.2.3. Synthesis of [Mn(PaPy₃)(NO)]ClO₄ (1)

2.2.3.1. [Mn(PaPy₃)(H₂O)]ClO₄.

CAUTION! Perchlorate salts of metal complexes with organic ligands are potentially explosive.

Only small quantities of these compounds should be prepared and handled with proper protection. 200 mg of PaPy₃H and 60 mg of triethylamine were dissolved in 15 mL of anhydrous methanol. After stirring under argon for 1 hr, 210 mg of Mn(ClO₄)·6H₂O were added and the resulting mixture was stirred vigorously for 15 min, during which time the solution turned a pale yellow color as a beige precipitate formed. The air-sensitive precipitate was collected anaerobically on a fritted glass disk and dried under vacuum, then used in step 2.7 as soon as possible after synthesis.

2.2.3.2. In situ nitric oxide synthesis.

Nitric oxide was prepared in situ by mixing degassed solutions of 1M FeSO₄ in 1M H₂SO₄ with 1M NaNO₂ (5 mL of each) according to the procedure of Blanchard.¹⁴ The evolved gas was manipulated using a specialized gas handling manifold outlined in Figure 2.1 which allowed the NO to be passed through a dry ice/EtOH cold trap and

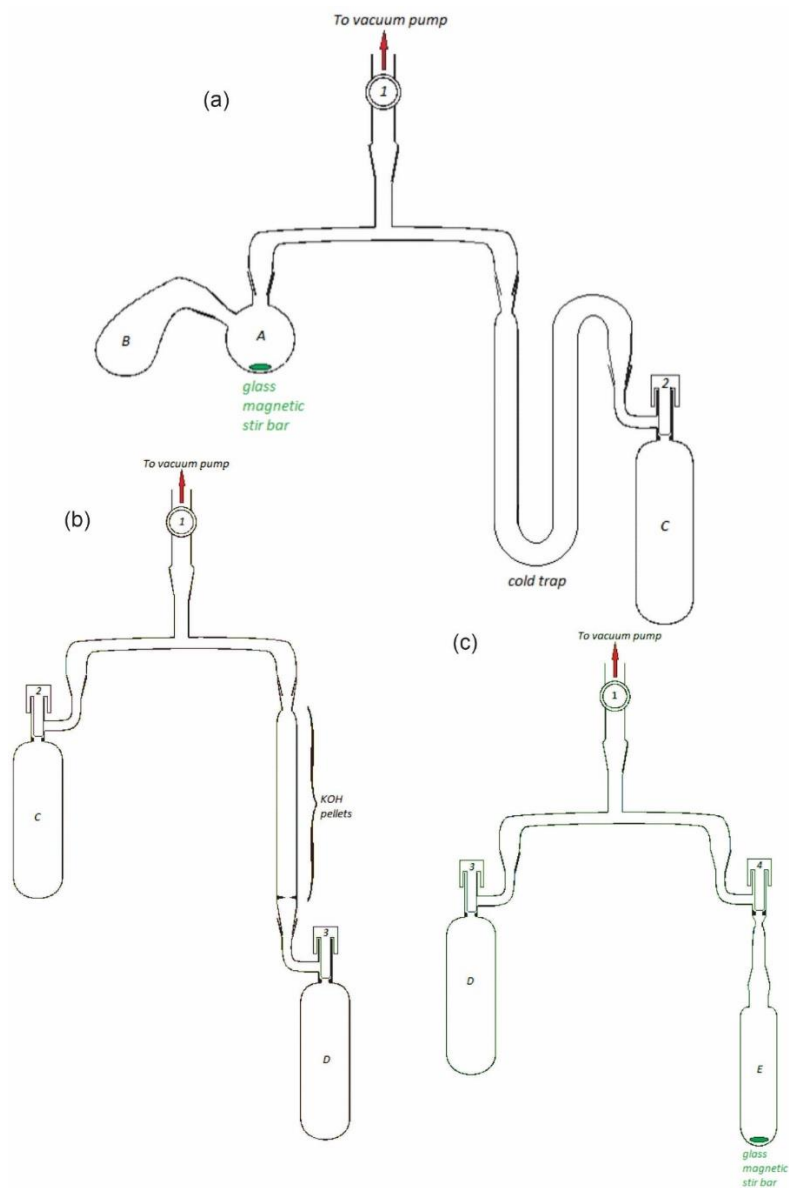


Figure 2.1. Schematic diagram showing the apparatus and procedure used for the synthesis of NO *in situ*. (a) Solutions of 5 mL of 1 M FeSO₄ in 1 M H₂SO₄ and 5 mL of 1 M NaNO₂ in A and B, respectively, are degassed using the freeze-pump-thaw method. The solutions are then mixed *in vacuo* with the system isolated via valve 1, and the resulting gas is transferred to container C, which has been submerged in liquid N₂ with valve 2 open slightly to allow passage, while passing through a dry ice/ethanol cold trap to remove excess water. (b) Valve 2 can be opened slightly to allow NO gas contained in container C to be transferred *in vacuo* to container D, which has been submerged in liquid N₂ with valve 3 open slightly to allow gas passage through a KOH column to remove any acid nitrogen oxides. (c) Valve 3 can be opened slightly to allow NO gas contained in container D to be transferred *in vacuo* to container E, which has been submerged in liquid N₂ with valve 4 open slightly to allow passage and equipped with a magnetic stir bar and a degassed solution of [Mn(PaPy₃)(H₂O)]⁺ in acetonitrile.

a column of potassium hydroxide pellets, which together served to dry the gas and remove NO_x impurities. The pure, dry, NO was stored in a 65 mL Schlenk-type flask sealed with a high vacuum Teflon valve but used within hours of its synthesis.

2.2.3.3. [Mn(PaPy₃)(NO)]ClO₄.

100mg of **3** was suspended in 10mL degassed acetonitrile in a Schlenk-type flask. The flask was connected to the gas handling manifold (Fig. 2.1) and evacuated by freeze-pump-thaw cycles, after which the NO prepared in Step 2.2.3.3 was vacuum transferred in the dark to the evacuated vessel. A solution of **3** was stirred under NO pressure in the dark for 2 hrs. After formation of a green solution, the solvent was removed under vacuum. The resulting solid was recrystallized from MeCN/Et₂O in the dark, which generated dark green crystals of **1** that were collected on a fritted glass disk. An example of the absorbance of a 751 μM solution of **1** in MeCN is shown in Figure 2.2, along with the changes observed upon the irradiation of a 378 μM solution of **1** by white light.

2.3. Results and discussion

2.3.1. PaPy₃H synthesis

Scheme 2.2 provides an outline of the procedure used to synthesize PaPy₃H. For the most part, the synthesis of PaPy₃H followed procedures established earlier.^{3, 6, 15} However, the procedure for synthesizing the tridentate ligand DPA, developed by Trevor Hageman and Alan Schwabacher of the UWM Chemistry department, (Hageman, unpublished) is new and more efficient than established procedures. It provides near stoichiometric yield of product, (98.8%) as compared to the 40% yield obtained following the method that was used earlier to prepare

PaPy₃H.¹⁵ Furthermore, the new method uses much milder conditions than those outlined in the original literature.¹⁵

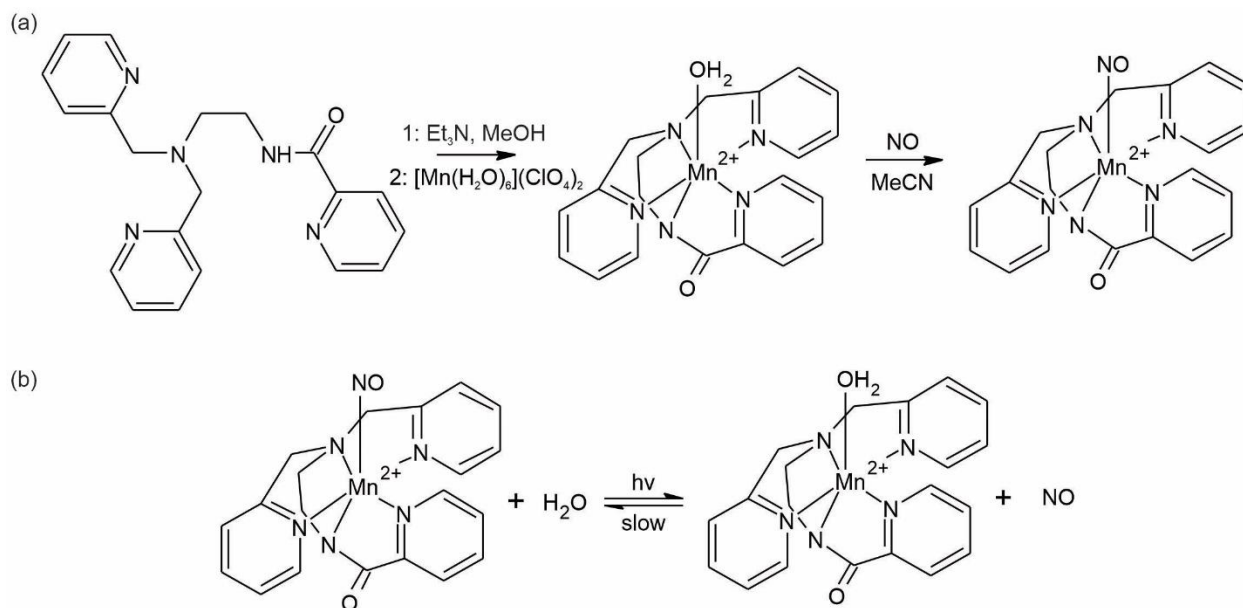
The selective hydrogenation of nitriles to form amines using precious metal catalysts is not a new concept, with a 1991 paper in *Journal of Organic Chemistry* highlighting the synthesis of secondary amines using a Rhodium catalyst.¹⁶ A more in depth analysis showed the versatility of using Rh and Pd catalysts on alkyl and aryl nitriles in different solvents and the subsequent formation of different substituted amines.¹⁷ In the DPA synthesis reported herein, the use of a Pd/C catalyst and presence of the aromatic pyridine bound nitrile group follows a path similar to that outlined in Monguchi et al., though with much higher yield.¹⁷ Contrary to what was observed in the study of Monguchi et al., the use of Pd as opposed to Rh yielded negligible, if any, of the tertiary amine. This is most likely due to steric constraints created by the bulky pyridine group, as the imine intermediate is most likely stabilized due to the presence of the pyridine nitrogen interaction with Pd.¹⁸ The ammonia side product can easily be neutralized, and is actually beneficial when monitoring the reaction as the basicity of the fumes can be monitored with pH paper, alongside monitoring for amine formation via ninhydrin-stained TLC. The one drawback to the hydrogenation methods just discussed is that they typically require long reaction times, and in this, the DPA synthesis was no exception. However, the reaction mixture required minimal monitoring during the synthesis, which made the long reaction time less onerous. According to a recent report, attempts to cut down on reaction time are underway using Pd and Pt catalysts on nanoparticles.¹⁹

Apart from the novel DPA synthesis, the only other minor change made to the original PaPy₃H synthesis^{3, 6, 15} was to use acetonitrile as a solvent and lower temperature for refluxing

during the synthesis of the phthalimide-protected DPEA intermediate. This change seemed to prevent the formation of undesirable side products.

2.3.2. Synthesis of complex 1

With the rising costs for transporting hazardous materials such as NO, plus the waste generated when solutions are bubbled constantly with the gas, the procedure outlined in Fig. 2.1a and 2.1b for generating NO in situ allows the synthesis of controlled amounts of NO at a much cheaper cost. Any acidic nitrogen oxides can be neutralized via the use of KOH columns (Fig. 2.1b), and careful manipulation of the gas through cold traps as described in Fig. 2.1a results in the removal of any excess water as well. The system must be kept anaerobic so as to prevent the formation of NO₂.



Scheme 2.3. (a) Synthesis of $[\text{Mn}(\text{PaPy}_3)(\text{NO})]^+$ from PaPy_3H and $[\text{Mn}(\text{H}_2\text{O})_6]^{2+}$. (b) Photolysis of $[\text{Mn}(\text{PaPy}_3)(\text{NO})]^+$ to yield one equivalent of NO in solution.

Scheme 2.3a summarizes the 2-step procedure used to prepare complex **1**. In the first step, $\text{Mn}(\text{H}_2\text{O})_6^{2+}$ reacts with PaPy_3H in basic methanol to generate the air-sensitive

$[\text{Mn}(\text{PaPy}_3)(\text{H}_2\text{O})]^+$ complex. A solution of $[\text{Mn}(\text{PaPy}_3)(\text{H}_2\text{O})]^+$ in degassed, anhydrous acetonitrile is put under NO pressure using the vacuum line setup shown in Fig. 2.1c and stirred vigorously in the dark to yield a green solution of complex **1**. Recrystallization by MeCN/Et₂O proved tricky; however, removal of the solvent in vacuo in the dark yielded green crystals that could be stored for future use.

A UV/Vis spectrum of the green crystals (Fig. 2.2) matches well with that of **1** reported earlier in the literature,³ and equally importantly, the spectrum shifts in the predicted way when the sample is exposed to white light, due to the loss of NO and generation of the aquo complex (Scheme 2.3b). Complex **1** is strongly coupled in a {low-spin Mn (II) – NO}¹¹ electron configuration, leaving a diamagnetic $S = 0$ state that in principle allows for analysis by NMR. However, any paramagnetic Mn(III) impurities in solution can strongly affect the resulting NMR spectra, and in practice, no clean spectra were obtained. Mn(III) is a strong oxidizer, and Mn(III) impurities in some preparations of **1** also caused complications in the experiments with trHbN, as will be discussed in the following chapter.

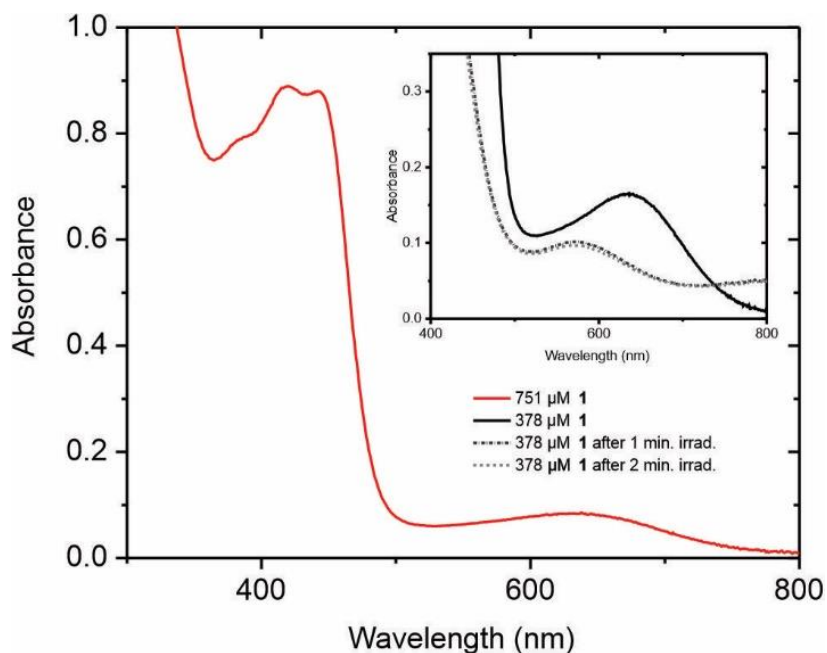


Figure 2.2. Absorption spectrum of $[\text{Mn}(\text{PaPy}_3)(\text{NO})]^+$ in acetonitrile and upon irradiation with white light.

2.4. Summary

In conclusion, the synthesis route for $[\text{Mn}(\text{PaPy}_3)(\text{NO})]\text{ClO}_4$ presented in the current work shows increased yield and lowered cost when compared to the method reported earlier,^{3, 6, 15} though one piece of business left unfinished in the project is to optimize the protocol for recrystallizing **1** and getting more consistent purity. The improved synthesis of the chelating ligand DPA shows promise for the synthesis of transition metal catalysts that selectively hydrogenate nitriles under ambient conditions. Similarly, the ability to generate and manipulate NO in situ may prove useful not only for the synthesis of **1** but also in other applications that require controlled amounts of NO.

2.5. References

- (1) Wang, P. G.; Xian, M.; Tang, X.; Wu, X.; Wen, Z.; Cai, T.; Janczuk, A. J. Nitric oxide donors: chemical activities and biological applications. *Chem Rev* **2002**, *102* (4), 1091-1134. DOI: 10.1021/cr000040l.
- (2) Ghosh, K.; Eroy-Reveles, A. A.; Avila, B.; Holman, T. R.; Olmstead, M. M.; Mascharak, P. K. Reactions of NO with Mn(II) and Mn(III) centers coordinated to carboxamido nitrogen: synthesis of a manganese nitrosyl with photolabile NO. *Inorg Chem* **2004**, *43* (9), 2988-2997. DOI: 10.1021/ic030331n.
- (3) Ghosh, K.; Eroy-Reveles, A. A.; Avila, B.; Holman, T. R.; Olmstead, M. M.; Mascharak, P. K. Reactions of NO with Mn(II) and Mn(III) centers coordinated to carboxamido nitrogen: synthesis of a manganese nitrosyl with a photolabile NO. *Inorg. Chem.* **2004**, *43*, 2988-2997.
- (4) Eroy-Reveles, A. A.; Leung, Y.; Beavers, C. M.; Olmstead, M. M.; Mascharak, P. K. Near-infrared light activated release of nitric oxide from designed photoactive manganese nitrosyls: strategy, design, and potential as NO donors. *J Am Chem Soc* **2008**, *130* (13), 4447-4458. DOI: 10.1021/ja710265j.
- (5) Koebke, K. J.; Waletzko, M. T.; Pacheco, A. A. Direct monitoring of the reaction between photochemically generated nitric oxide and *Mycobacterium tuberculosis* truncated hemoglobin N wild type and variant forms: an assessment of computational mechanistic predictions. *Biochemistry* **2016**, *55*, 686-696.
- (6) Rowland, J. M.; Olmstead, M. M.; Mascharak, P. K. Syntheses, structures, and reactivity of low spin iron(III) complexes containing a single carboxamido nitrogen in a [FeN₅L] chromophore. *Inorg. Chem.* **2001**, *40*, 2810-2817.
- (7) Nagashima, S.; Nakasako, M.; Dohmae, N.; Tsujimura, M.; Takio, K.; Odaka, M.; Yohda, M.; Kamiya, N.; Endo, I. Novel non-heme iron center of nitrile hydratase with a claw setting of oxygen atoms. *Nat Struct Biol* **1998**, *5* (5), 347-351. DOI: 10.1038/nsb0598-347. Huang, W.; Jia, J.; Cummings, J.; Nelson, M.; Schneider, G.; Lindqvist, Y. Crystal structure of nitrile hydratase reveals a novel iron centre in a novel fold. *Structure* **1997**, *5* (5), 691-699. DOI: 10.1016/s0969-2126(97)00223-2.
- (8) Peters, J. W.; Stowell, M. H.; Soltis, S. M.; Finnegan, M. G.; Johnson, M. K.; Rees, D. C. Redox-dependent structural changes in the nitrogenase P-cluster. *Biochemistry* **1997**, *36* (6), 1181-1187. DOI: 10.1021/bi9626665.
- (9) Tao, X.; Stephan, D. W.; Mascharak, P. K. Synthetic analog approach to metallobleomycins. 2. Synthesis, structure, and properties of the low-spin iron(III) complex of N-(2-(4-imidazolyl)ethyl)pyridine-2-carboxamide. *Inorganic Chemistry* **1987**, *26* (5), 754-759. DOI: 10.1021/ic00252a022. Noveron, J. C.; Olmstead, M. M.; Mascharak, P. K. Effect of Carboxamido N Coordination to Iron on the Redox Potential of Low-Spin Non-Heme Iron Centers with N,S Coordination: Relevance to the Iron Site of Nitrile Hydratase. *Inorg Chem* **1998**, *37* (6), 1138-1139. DOI: 10.1021/ic971388a. Bartos, M. J.; Kidwell, C.; Kauffmann, K. E.; Gordon-Wylie, S. W.; Collins, T. J.; Clark, G. C.; Münck, E.; Weintraub, S. T. A Stable Aquairon(III) Complex with S = 1: Structure and Spectroscopic Properties. *Angewandte Chemie International Edition in English* **1995**, *34* (11), 1216-1219, <https://doi.org/10.1002/anie.199512161>. DOI: <https://doi.org/10.1002/anie.199512161> (accessed 2023/04/10).
- (10) Marlin, D. S.; Olmstead, M. M.; Mascharak, P. K. Carboxamido Nitrogens Are Good Donors for Fe(III): Syntheses, Structures, and Properties of Two Low-Spin Nonmacrocyclic Iron(III) Complexes with Tetracarboxamido-N Coordination. *Inorganic Chemistry* **1999**, *38* (13), 3258-3260. DOI: 10.1021/ic981461c.
- (11) Patra, A. K.; Afshar, R.; Olmstead, M. M.; Mascharak, P. K. The first non-heme iron(III) complex with a ligated carboxamido group that exhibits photolability of a bound NO ligand. *Angew Chem Int Ed Engl* **2002**, *41* (14), 2512-2515. DOI: 10.1002/1521-3773(20020715)41:14<2512::AID-ANIE2512>3.0.CO;2-7.

- (12) Patra, A. K.; Mascharak, P. K. A ruthenium nitrosyl that rapidly delivers NO to proteins in aqueous solution upon short exposure to UV light. *Inorg Chem* **2003**, *42* (23), 7363-7365. DOI: 10.1021/ic030110h.
- (13) Greene, S. N.; Richards, N. G. J. Theoretical Investigations of the Electronic Structure and Spectroscopy of Mononuclear, Non-Heme {Fe-NO}₆ Complexes. *Inorganic Chemistry* **2004**, *43* (22), 7030-7041. DOI: 10.1021/ic0499695.
- (14) Blanchard, A. A. Nitric oxide. In *Inorganic Syntheses*, Fernelius, W. C. Ed.; Vol. II; McGraw-Hill, 1946; pp 126-128.
- (15) Matouzenko, G. S.; Bousseksou, A.; Lecocq, S.; van Koningsbruggen, P. J.; Perrin, M.; Kahn, O.; Collet, A. Spin transition in [Fe(DPEA)(NCS)₂], a compound with the new tetradentate ligand (2-Aminoethyl)bis(2-pyridylmethyl)amine (DPEA): crystal structure, magnetic properties, and Mossbauer spectroscopy. *Inorg. Chem.* **1997**, *36*, 2975-2981.
- (16) Galan, A.; De Mendoza, J.; Prados, P.; Rojo, J.; Echavarren, A. M. Synthesis of secondary amines by rhodium catalyzed hydrogenation of nitriles. *The Journal of Organic Chemistry* **1991**, *56* (1), 452-454. DOI: 10.1021/jo00001a088.
- (17) Monguchi, Y.; Mizuno, M.; Ichikawa, T.; Fujita, Y.; Murakami, E.; Hattori, T.; Maegawa, T.; Sawama, Y.; Sajiki, H. Catalyst-Dependent Selective Hydrogenation of Nitriles: Selective Synthesis of Tertiary and Secondary Amines. *J Org Chem* **2017**, *82* (20), 10939-10944. DOI: 10.1021/acs.joc.7b01823.
- (18) Ahmad, G.; Rasool, N.; Rizwan, K.; Altaf, A. A.; Rashid, U.; Hussein, M. Z.; Mahmood, T.; Ayub, K. Role of Pyridine Nitrogen in Palladium-Catalyzed Imine Hydrolysis: A Case Study of (E)-1-(3-bromothiophen-2-yl)-N-(4-methylpyridin-2-yl)methanimine. In *Molecules*, 2019; Vol. 24.
- (19) Nishida, Y. S., K.; Chaudhari, C.; Yamada, H.; Toriyama, T.; Yamamoto, T.; Matsumura, S.; Menez Aspera, S.; Nakanishi, H.; Haneda, M.; Nagaoka, K. Nitrile hydrogenation to secondary amines under ambient conditions over palladium-platinum random alloy nanoparticles. *Catalysis Science & Technology* **2022**, (13), 4128-4137.

Chapter 3 Reaction of oxy-trHbN and red-trHbN variants with photogenerated NO

3.1. Overview

As outlined in Chapter 1, many structural features have been shown to play an integral role in trHbN activity by crystallographic, computational, and other experimental techniques. This chapter focuses on the effect that the pre-A tail (Fig. 1.4) has on the rates of NO dioxygenation by the oxygenated form of trHbN (oxy-trHbNO) and NO nitrosylation by the reduced form of trHbN (red-trHbN). Scheme 1.1 shows where these steps fit within the putative NO dioxygenation catalytic cycle. Step 1 of Scheme 1.1 is the dioxygenation step, which generates the aquomet ferric form of trHbN (met-trHbN). This is reduced to red-trHbN in Scheme 1.1 step 2, and then re-oxygenated to the oxy-trHbN form in Scheme 1.1 step 3. In this chapter, nitrosylation of red-trHbN is used as a surrogate for oxygenation.

Koebke et al. showed that by utilizing the photolabile NO precursor **2** (Scheme 2.1) and a flash photolysis system, both dioxygenation of NO and nitrosylation of red-trHbN could be monitored on the μs time scale.¹ The photolysis method was used to study the wild type (trHbN_{wt}) and a series of variants, and it yielded several interesting observations. Of special importance to the present study, Koebke et al. reported that mutations produced changes to NO dioxygenation rates that were modest when compared to the changes they produced in red-trHbN nitrosylation rates.¹ Notably, mutations of active site residues Tyr33 and Gln58 (Fig. 1.4) led to increases in nitrosylation rates, while deletion of the Pre-A tail led to a dramatic decrease in nitrosylation rate.

Based on their results, and on an earlier study by Ouellet et al., Koebeke et al. proposed that motions of the pre-A tail play a crucial role in displacing a non-coordinated water molecule that blocks access to the distal heme site in red-trHbN_{wt} and provides the main kinetic barrier for ligand binding to red-trHbN_{wt}.^{1, 2} Thus, when the pre-A sequence is deleted (trHbN_{delN} variant), conversion of red-trHbN_{delN} to the oxygenated form (oxy-trHbN_{delN}) slows down greatly, as does the reaction of red-trHbN_{delN} with other diatomic gases such as NO, and presumably, CO.

The water molecule that blocks access to the distal heme site is held in place by a tight interaction with Tyr33, which is aided by hydrogen bonding interactions between Tyr33 and Gln58.² Therefore, to test the hypothesis that deletion of the pre-A sequence slows displacement of the obstructive water molecule, in this chapter the nitrosylation rates of the red-trHbN_{delN} variant are compared with those of a variant that lacks the pre-A tail and also has the point mutations Tyr33Phe and Gln58Val. The triple variant will be referred to as trHbN_{TM}. Koebeke et al showed that the ferrous form of a double variant with Tyr33 and Gln58 mutations (red-trHbN_{DM}) is nitrosylated about 4× faster than red-trHbN_{WT}, presumably because access to the distal heme site is no longer blocked by water once Tyr33 and Gln58 are removed.¹ If the pre-A tail plays a role in facilitating water displacement, then removing Tyr33 and Gln58 should counteract the loss of pre-A in the triple variant red-trHbN_{TM}. The study presented in this chapter used the NO photoprecursor **1** rather than species **2** (Scheme 2.1), but otherwise, the photolysis protocol was comparable.

3.2. Materials and methods

3.2.1. General methods

All reagents were purchased from Millipore-Sigma, Fisher Scientific, or dot Scientific unless otherwise specified. Routine UV/Vis spectra were obtained using Cary 50 spectrophotometers; where anaerobic conditions were needed, a spectrophotometer installed in a nitrogen-filled glovebox was used. Wild type and variant trHbN were expressed and purified using the method previously described, summarized below with slight alterations.¹ Unless otherwise specified, all experiments with trHbN were carried out in 50 mM tris(hydroxymethyl)aminomethane (tris), 0.5 mM ethylenediaminetetraacetic acid disodium salt (EDTA), pH 8.1 (hereafter referred to as “tris buffer”).

3.2.2. trHbN expression and purification

The gene for trHbN from *M. tuberculosis* was synthesized for optimal codon usage by Genscript before cloning into a pUC19 vector and transforming into BL21(DE3) *Escherichia coli* for expression. Mutants were either produced in the lab by phusion site-directed mutagenesis PCR (Thermo Scientific Phusion Site-Directed Mutagenesis Kit) or purchased from Integrated DNA technologies as a gBlock gene fragment before ligation into pUC19. Bacterial cultures were grown overnight at 37 °C in LB media, after which the cells were concentrated and lysed using a sonic dismembrator (model CL334) to release the cell contents, and the resulting suspension clarified by addition of streptomycin sulfate to a final concentration of 1% and centrifugation. Protein was purified using a two-step purification procedure. In the first step the clarified cell lysate was loaded onto a 50 mL anion exchange Q-Sepharose column (GE Healthcare) using standard tris buffer. The protein mixture was then eluted using 500 mL of a linear gradient

starting with tris buffer and ending with the elution buffer, which contained 0.2 M NaCl in tris buffer. In the second purification step the trHbN-containing fraction from step 1 was concentrated to ~1-2 mL and passed through a 300 mL Sephacryl S-100 Size Exclusion Column (GE Healthcare) using a buffer consisting of tris buffer with 0.15 M NaCl. At each stage of the purification protein purity was assessed by monitoring the ratio of A_{416}/A_{280} in the UV/Vis spectrum, the goal being to get ratios of 3 or higher. The final purity of the trHbN was assessed by SDS-PAGE gel electrophoresis. The concentration of each purified protein stock solution was determined by quantifying its heme content with the pyridine hemochrome assay,³ after which molar extinction coefficient spectra of each variant in the oxy-trHbN, red-trHbN, met-trHbN, and nitroso-trHbN forms were obtained as well. Examples are shown in Fig. 3.1 for trHbN_{TM}.

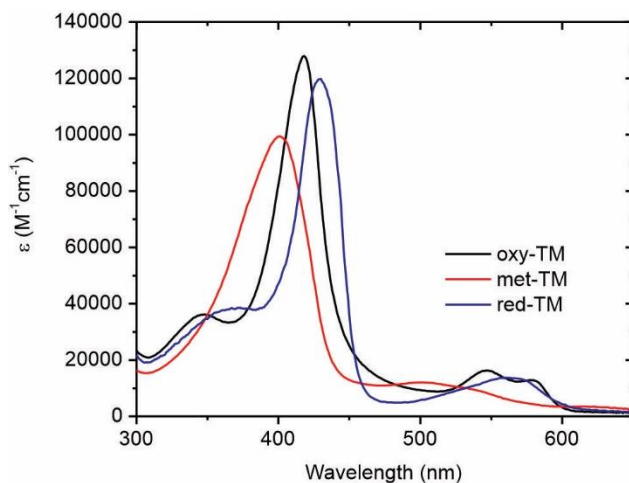


Figure 3.1. Molar extinction coefficient spectra for oxy-trHbN_{TM} (black), met-trHbN_{TM} (red), and red-trHbN_{TM} (blue).

Variants containing double mutations to the active site required additional steps before they could be used in further experiments. Samples of purified trHbN_{DM} and trHbN_{TM} were first oxidized with excess potassium ferricyanide trihydrate to generate the ferric forms. The potassium ferricyanide trihydrate was removed by exchanging with tris buffer, using 10 kDa

molecular weight cutoff centrifugal filters (Amicon Ultra). The protein was then reduced to the 5-coordinate ferrous form in an anaerobic glovebox using an equivalent of electrolytically produced methyl viologen monocation radical, after which the reduced solutions were either brought out of the glovebox to bind oxygen or used directly in the glovebox for experiments requiring ferrous trHbN.

3.2.3. Time-resolved flash photolysis

The apparatus used for these experiments, outlined in Fig. 3.2, was as described by Koebe et al.¹ Briefly, an OPO tunable laser (Opotec Rainbow Vis) was used to irradiate with 10

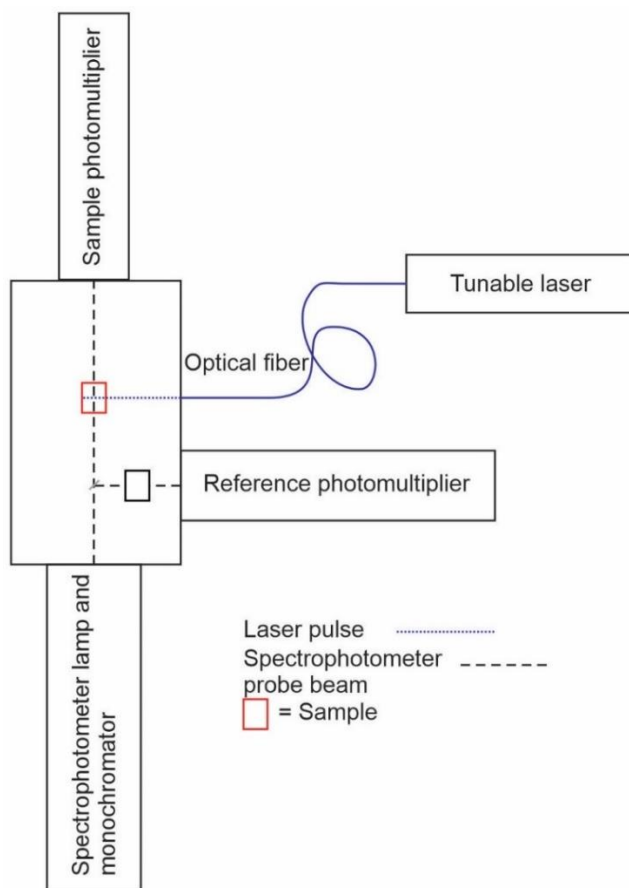


Figure 3.2. Schematic of the apparatus used for the flash photolysis experiments outlined in this chapter. Laser pulses generated by the tunable laser are transmitted via the fiber optic cable shown in blue to irradiate a sample cuvette shown as a red box. A spectrophotometer beam shown as the black dashed line is transmitted perpendicular to the laser pulse.

ns, 455 nm laser pulses, solutions held in 1.5mm×1.5mm fluorometer submicro cuvettes (Starna), after which spectral changes at selected wavelengths were monitored on the microsecond timescale with an Olis RSM-1000 spectrophotometer in fixed wavelength mode. Solutions for the experiments were made up in tris buffer. Each solution contained 30 μM of the NO photoprecursor **1** (Scheme 2.1) and either red-trHbN or oxy-trHbN of the appropriate variant, in concentrations varying from 10-100 μM . Under these conditions, each laser pulse generated about 3 μM NO. Thus, protein was in at least 10 \times excess of NO in all experiments, which maintained pseudo first-order conditions. All solutions for these experiments were prepared fresh daily and kept in the dark to prevent premature release of NO from **1**. Data were plotted and analyzed using the software program Origin 8.0.

3.3. Results

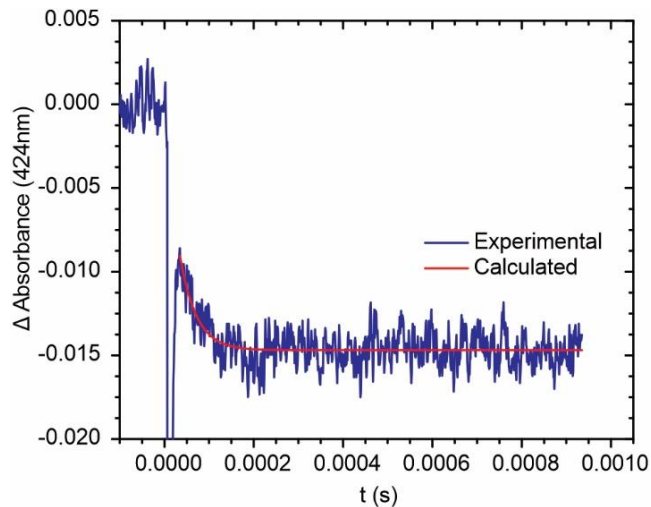


Figure 3.3. Blue trace: spectral changes at 424 nm that follow irradiation by a 455 nm, 10 ns laser pulse of a solution initially containing 24.5 μM oxy-trHbN_{TM}, 30 μM of photoactive species **1**, and 0.5 mM EDTA, in a 50 mM Tris buffer, pH 8.1. Red trace: least-squares fit to a single exponential decay (see main text for details).

The blue trace in Fig. 3.3 shows the spectral changes observed at 424nm after exposing to a 10 ns, 455 nm laser pulse a solution initially containing 24.5 μM oxy-trHbN_{TM}, 30 μM of **1**, and 0.5 mM EDTA in a 50 mM Tris buffer, pH 8.1. After an initial sharp negative deflection in A_{424} due to oversaturation of the photomultiplier tubes' voltage output by the laser pulse, a decrease in absorbance due to the reaction of oxy-trHbN_{TM} with NO to yield the aquo-met adduct (met-trHbN_{TM} Scheme 1.1) is clearly visible. Under these conditions, the amount of NO generated by the laser pulse is roughly 3 μM ,¹ so the reaction between NO and protein is expected to be pseudo-first-order. The experimental trace was fit with the exponential decay equation $A_{424} = A_0 + \text{Amp} \cdot [1 - \exp(-k_{\text{obs}} \cdot t)]$ (red trace, Fig. 3.3), where A_{424} is the absorbance at 424 nm and time t , A_0 is the absorbance at 424 nm and time zero, and k_{obs} is the apparent rate constant. In the fit, A_0 was fixed at zero, while the least-squares best values of the parameters Amp and k_{obs} were determined by the nonlinear least-squares fitting routine. The experiment of Fig. 3.3 was repeated using concentrations of oxy-trHbN_{TM} varying from 10-35 μM , and k_{obs} values were obtained at each individual concentration. A replot of k_{obs} as a function of oxy-trHbN_{TM} concentration (Fig. 3.4a) afforded a linear fit (red trace, Fig. 3.4a) from which a second-order rate constant of $(1.15 \pm 0.05) \times 10^9 \text{ M}^{-1}\text{s}^{-1}$ was obtained for the reaction of oxy-trHbN_{TM} with NO.

The second-order rate constant for nitrosylation of deoxy reduced trHbN_{TM} (red-trHbN_{TM}) was obtained in experiments analogous to those just described. This time, red-trHbN_{TM} was varied from 12-40 μM while keeping the concentration of photoactive species **1** constant at 30 μM as before. In any given experiment, absorbance changes with time were monitored at 439 nm, where absorbance decreases as red-trHbN_{TM} is nitrosylated. Once more,

A_{439} vs t plots could be fit with exponential decay functions, and a plot of k_{obs} vs $[\text{red-trHbN}_{TM}]$ (blue circles, Fig. 3.4b) afforded a linear fit (red trace, Fig. 3.4b); from this, a second-order rate constant of $(2.4 \pm 0.1) \times 10^8 \text{ M}^{-1}\text{s}^{-1}$ was calculated for the reaction of red-trHbN_{TM} with NO.

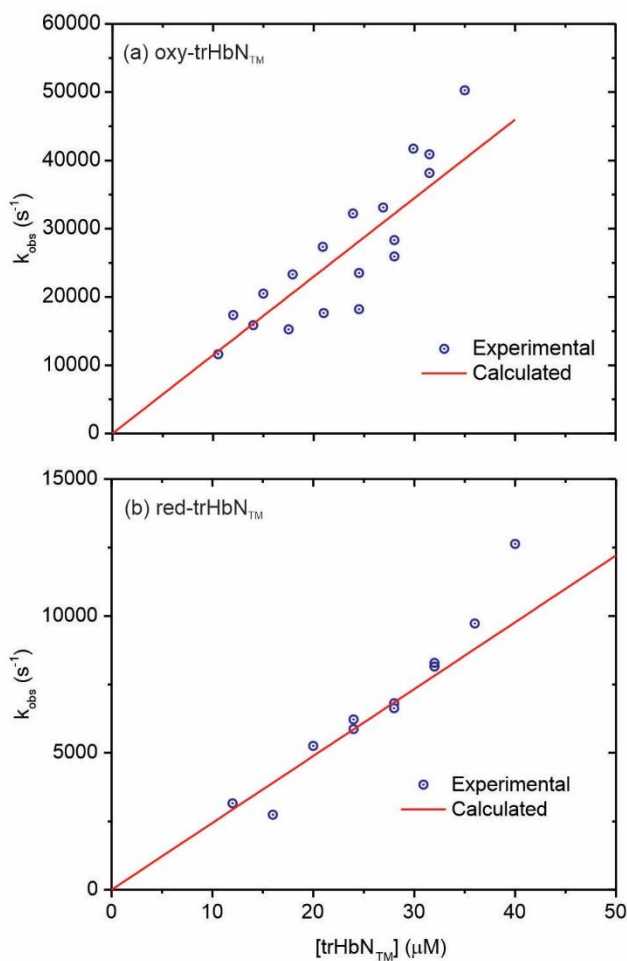


Figure 3.4. Blue circles: dependence of the apparent rate constants on trHbN_{TM} concentrations for (a) reaction of oxy-trHbN_{TM} with NO, and (b) nitrosylation of red-trHbN_{TM}. Red lines: linear least-squares fits of the data (y-intercepts fixed at zero).

Table 3.1 compares the second-order rate constants obtained for the reactions of NO with the WT, DM, TM and delN variants of oxy-trHbN and red-trHbN. Koebeke et al had previously reported values for trHbN_{WT} and the trHbN_{DM} and trHbN_{DeIN} variants,¹ but the

experiments were repeated in this study to check for reproducibility. Table 3.1 shows that the rate constants obtained in our recent experiments match those obtained earlier, with the notable exception of the one obtained for nitrosylation of red-trHbN_{deIN}. Koebke et al reported

	NO Dioxygenation (k_{diox} , $\mu\text{M}^{-1}\text{s}^{-1}$)			Nitrosylation (k_{NO} $\mu\text{M}^{-1}\text{s}^{-1}$)		
		(<i>Lit. value</i>)	% of WT		(<i>Lit. value</i>)	% of WT
trHbN _{WT}	1000 ± 30	(1370 ¹ , 745 ⁷)	-	250 ± 10	(220 ¹)	-
trHbN _{DeIN}	610 ± 10	(1030 ¹)	61	110 ± 20	(N/A ¹)	50
trHbN _{DM}	1820 ± 50	(750 ¹)	182	710 ± 50	(900 ¹)	284
trHbN _{TM}	1150 ± 50	-	115	240 ± 10	-	96

Table 3.1. Second-order rate constants obtained for the reactions of NO with WT, DeIN, DM, and TM variants of oxy-trHbN and red-trHbN. Values in parentheses are for comparison to earlier literature values.

that red-trHbN_{deIN} nitrosylation was first-order overall with a rate constant k of $3300 \pm 1200 \text{ s}^{-1}$, unlike all the other reactions, which are second-order overall.¹ However, the current study shows that a clear linear dependence on protein concentration can be resolved (blue circles and red line, Fig. 3.5), from which a second-order rate constant of $(1.1 \pm 0.2) \times 10^8 \text{ M}^{-1}\text{s}^{-1}$ was obtained. This value is half that obtained for red-trHbN_{WT} nitrosylation (Table 3.1); thus, the slope of the k_{obs} vs [red-trHbN_{DeIN}] is shallow and was obscured by scatter in the earlier study. Nevertheless, when the results from the previous study are overlaid on those of the current one (green squares, Fig. 3.5),¹ a positive slope is discernible in the earlier data if one knows a priori that it is there.

Note that the data points obtained at the two highest red-trHbN_{deIN} concentrations were not included in the least-squares fit shown in Fig. 3.5. The rationale for this is that the k_{obs} values for these points fall well below the linear trend exhibited by the other data points, and it is possible that at these high protein concentrations, absorbance of some 450 nm laser pulse

the triple variant that also lacks Tyr33 and Gln 58 (Table 3.1). Ouellet et al. first reported that binding of O₂ and CO to red-trHbN_{DM} is faster than in the wild type, and based on a computational analysis, proposed that this is because in the wild type a non-coordinated water that blocks access to the distal heme site is held tightly in place by Tyr33 and Gln 58.² When these residues are mutated, water no longer blocks the active site and gas binding accelerates. Koebke et al. later showed that NO binding to the distal heme is faster in red-trHbN_{DM} but slower in red-trHbN_{delIN} when compared to red-trHbN_{WT}, and proposed that the pre-A tail promotes motions of Tyr33 and Gln 58 which help release the non-coordinated water molecule that otherwise blocks access to the distal site.¹ The results reported herein with red-trHbN_{TM} are consistent with this hypothesis, since making the mutations Tyr33Phe and Gln58Val counteracts the effect of deleting the pre-A tail, restoring nitrosylation rates in the triple variant to those observed in the wild type (Table 3.1). On the other hand, the new study of red-trHbN_{delIN} nitrosylation summarized in Fig. 3.5 (blue circles and red linear fit) weakens the hypothesis relative to the earlier corresponding study by Koebke et al.¹ In the earlier study, the first-order dependence of k_{obs} on [red-trHbN_{delIN}] was obscured by scatter in the data (green squares, Fig. 3.5), making it appear as if red-trHbN_{delIN} nitrosylation was much more dramatically affected than NO dioxygenation by oxy-trHbN_{delIN}. This is what one would expect if the pre-A tail's primary role was to mobilize the non-coordinated water that blocks access to the active site in red-trHbN. According to the new results, though, the effect of pre-A tail loss on red-trHbN nitrosylation is comparable to its effect on NO dioxygenation by oxy-trHbN; that is, both processes are diminished by a modest 50% (Table 3.1). Thus, though it is still clear that the role of the pre-A tail deletion is tied to the roles of Tyr33 and Gln 58, a direct connection to these

amino acids' roles in anchoring the non-coordinating water molecule in the red-trHbN active site is less clear.

The linear least-squares fit to a subset of the red-trHbN_{delIN} nitrosylation data (Fig 3.5) suggests a non-zero y-intercept, and this is still unique when compared to nitrosylation of other red-trHbN variants or NO dioxygenation by oxy-trHbN variants. The Fig. 3.5 non-zero intercept value is small enough that it may be due to experimental error ($700 \pm 400 \text{ s}^{-1}$). However, if one were to include in the least-squares fit all the data points in Fig. 3.5, not just the selected subset, then the y-intercept would be much more substantial, thus setting the nitrosylation behavior of red-trHbN_{delIN} further apart from other trHbN variant reactions with NO.

Establishing whether the non-zero intercept in red-trHbN_{delIN} is real, and if so, how big it is, should be a top priority in future studies of trHbN. If the non-zero intercept is real and large, then the effect of pre-A tail deletion on red-trHbN nitrosylation is unique, as proposed by Koebke et al.¹ On the other hand, if the apparent intercept is due to data scatter only, pre-A tail deletion will be seen to affect red-trHbN nitrosylation and NO dioxygenation by oxy-trHbN more uniformly, as suggested by the Table 3.1 data collected for this thesis. Clearly, distinguishing between these possibilities will be critical to understanding the effects of the pre-A tail on microsecond timescale dynamics within the trHbN active site. In support of this goal, the Pacheco group recently acquired a flash photolysis apparatus that should generate data with less scatter than the current system can provide.

Two technical points will be of importance to researchers that continue with the current research. First, they should be aware that, when the DM and TM variants of oxy-trHbN are irradiated with a laser pulse, some of the bound O₂ is photolyzed by the pulse. This

phenomenon is most likely due to the decreased O₂ affinity observed upon mutation of active site residues Tyr33 and Gln58 as it was not observed in the WT. Fortunately, the rapid rate of NO dioxygenation as compared to O₂ re-binding (or red-trHbN nitrosylation) makes it easy to distinguish the processes kinetically. The photolysis process itself occurred during the deadtime of the current instrumentation but may be detectable with the new flash photolysis apparatus, which will be capable of monitoring processes occurring on the ns timescale. TrHbN ligand photolysis is a non-issue while observing nitrosylation of red-trHbN variants as there is then no bound ligand susceptible to photolysis.

The second technical point that should be considered when conducting laser flash photolysis experiments is that some preparations of species **1** were found to contain Mn(III) impurities capable of oxidizing red-trHbN variants (though these impurities had no effect on oxy-trHbN variants). Such reactivity has precedent; previous studies showed that myoglobin could be reduced by certain metal complexes, and that the reaction rate depends heavily on ligand dissociation, which implicates deoxymyoglobin as the reactive species.⁴ The reorganizational energy at the active site also plays a role, as the formation of the aquomet-species is heavily influenced by the nature of the distal pocket.⁵ This would explain the differences in susceptibility for different trHbN variants towards oxidation compared to the WT. To eliminate the Mn(III) impurities, solutions of **1** were titrated with reduced methyl viologen until the sharp MV_{red} signal at 395 nm was just detectable. Further reduction of the Mn (II) in **1** is of no concern due to the properties of the carboxamido-Mn bond as discussed in Ghosh et al.⁶

3.5. Summary

The results of the current study provide a useful follow-up to the work reported by Koebke et al.¹ At a practical level, they show that the NO precursor [Mn(PaPy₃)(NO)]ClO₄ (**1**) can be used as a reliable NO donor in the study of NO dioxygenation of oxy-trHbN variants and nitrosylation of red-trHbN variants. The generally good agreement between the rate constants derived in the current work and those previously obtained further solidifies the validity of the flash photolysis methodology.^{1, 7} Nevertheless, the data scatter generated by the instrumentation available to date leaves important mechanistic questions open for future study with better instrumentation.

The top question to be addressed in future studies is whether the kinetic behavior of red-trHbN_{delIN} nitrosylation is unique in having a k_{obs} vs [red-trHbN] dependence with non-zero y-intercept. If it does, then follow-up experiments and computational studies can focus on finding an explanation for this behavior. If, on the other hand, the non-zero intercept vanishes upon making more precise measurements, then follow-up studies should instead focus on explaining the modest effects of pre-A tail deletion on both red-trHbN nitrosylation and NO dioxygenation by oxy-trHbN.

3.6. References

- (1) Koebke, K. J.; Waletzko, M. T.; Pacheco, A. A. Direct monitoring of the reaction between photochemically generated nitric oxide and *Mycobacterium tuberculosis* truncated hemoglobin N wild type and variant forms: an assessment of computational mechanistic predictions. *Biochemistry* **2016**, *55*, 686-696.
- (2) Ouellet, Y. H.; Daigle, R.; Lague, P.; Dantsker, D.; Milani, M.; Bolognesi, M.; Friedman, J. M.; Guertin, M. Ligand binding to truncated hemoglobin N from *Mycobacterium tuberculosis* is strongly modulated by the interplay between the distal heme pocket residues and internal water. *J. Biol. Chem.* **2008**, *283*, 27270-27278.

- (3) Berry, E. A.; Trumpower, B. L. Simultaneous determination of hemes a, b, and c from pyridine hemochrome spectra. *Anal. Biochem.* **1987**, *161*, 1-15.
- (4) Hegetschweiler K Fau - Saltman, P.; Saltman P Fau - Dalvit, C.; Dalvit C Fau - Wright, P. E.; Wright, P. E. Kinetics and mechanisms of the oxidation of myoglobin by Fe(III) and Cu(II) complexes. (0006-3002 (Print)). From 1987 Apr 30.
- (5) Dunn, C. J.; Rohlf's Rj Fau - Fee, J. A.; Fee Ja Fau - Saltman, P.; Saltman, P. Oxidation of deoxy myoglobin by [Fe(CN)₆]³⁻. (0162-0134 (Print)). From 1999 Jul 15.
- (6) Ghosh, K.; Eroy-Reveles, A. A.; Avila, B.; Holman, T. R.; Olmstead, M. M.; Mascharak, P. K. Reactions of NO with Mn(II) and Mn(III) centers coordinated to carboxamido nitrogen: synthesis of a manganese nitrosyl with a photolabile NO. *Inorg. Chem.* **2004**, *43*, 2988-2997.
- (7) Ouellet, H.; Ouellet, Y.; Richard, C.; Labarre, M.; Wittenberg, B.; Wittenberg, J.; Guertin, M. Truncated hemoglobin HbN protects *Mycobacterium bovis* from nitric oxide. *Proc. Natl. Acad. Sci. USA* **2002**, *99*, 5902-5907.

Chapter 4 Stopped-Flow analysis of met-trHbN reduction

4.1. Overview of ferriglobin reduction chemistry

A critical step in the proposed NO dioxygenation catalytic cycle is reduction of the met-trHbN after the dioxygenation step (step 2, Scheme 1.1). Indeed, it has been noted that though the ability of oxy-hemoglobins and oxy-myoglobins to dioxygenate NO in vitro is virtually universal, their ability to do so in vivo is often curtailed by rate-limiting re-reduction of the oxidized heme so generated.¹ Unlike flavoHb, which incorporates a distinct reductase domain, trHbN has no such domain and the physiological electron donor is to date unknown, though NADH-flavodoxin reductase from *E. coli* has been shown to be competent in this role.² Most likely due to the lack of knowledge about the physiological electron source, the process of trHbN reduction has not been well studied to date. Thankfully, there are much more well studied systems, myoglobin in particular, that share enough similarity as to provide a reference point when looking at trHbN. As touched on in Chapter 1, the literature is saturated with studies of myoglobin, perhaps to a fault. In fact, at the time of writing this thesis, a quick search of “myoglobin” using Dimensions yields 254,057 published results, with 97,202 results listed under the categories “Biological Sciences”, “Chemical Sciences”, or “Biochemistry and Cell Biology”. By comparison, the words “truncated hemoglobin” yield only 19,748 results in the same categories, with quite a bit of overlap referencing a truncated form of the more well-studied tetrameric hemoglobin. With that in mind, this chapter begins with a detailed review of previous myoglobin reduction studies.

4.1.1. Myoglobin oxidation

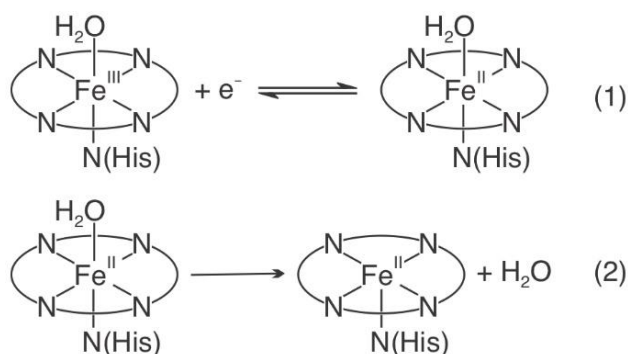
The oxidation of myoglobin, and hemoglobin for that matter, has been a topic of great interest from a physiological standpoint. Just as with NO dioxygenases, the oxygen storage and transport proteins Mb and Hb must be in the ferrous state to bind oxygen.

Methemoglobinemia, a condition in which some of the hemoglobin in the bloodstream has been converted to methemoglobin (with the iron in a ferric Fe^{3+} state), hampers oxygen transport throughout the body. This can be genetic, via disruption of physiological systems that regulate hemoglobin reduction, or acquired, for example by inadvertently ingesting certain oxidizing agents.³ Even under normal physiological conditions though, some ferrous Mb and Hb is continuously oxidized, so organisms that use these proteins have systems in place to re-reduce them.

Given the importance of heme oxidation state regulation, studies of the ferric state date back nearly a century. A seminal paper published by Linus Pauling and Charles Coryell described the magnetic properties of hemoglobin, oxyhemoglobin, and carbonmonoxyhemoglobin in 1936.⁴ Of note was the drastic change in magnetic susceptibility upon binding of O_2 , from the paramagnetic state observed in hemoglobin, to the diamagnetic state observed in oxyhemoglobin. The following year, a follow up paper was published by the two researchers, along with Fred Stitt, covering the nature of methemoglobin in a variety of ligand-bound states.⁵ It was in this paper that the authors suggested the occupancy of the sixth coordination site by a water molecule in methemoglobin (thus referred to as aquomethemoglobin), as opposed to the five coordinate state previously hypothesized. Together, these two papers could be considered the catalyst which opened the door for the field of bioinorganic chemistry.

4.1.2. Reduction of metmyoglobin

The field of bioinorganic chemistry has evolved greatly since 1936; as instrumentation and theory have advanced, so have the understandings of complex biological systems. The advent of techniques such as rapid-mixing stopped-flow and faster spectrometers have allowed researchers to look at kinetics on increasingly smaller time scales, and during the 1970s, researchers started to investigate the mechanism by which aquometmyoglobin undergoes reduction.⁶⁻⁸ Wilting and co-workers looked into the reduction of aquomethemoglobin and aquometmyoglobin by hydrated electrons, noticing distinct kinetic phases that differed between the two species, owing to the occurrence of quaternary structure in hemoglobin but not myoglobin.⁶ They also observed kinetic phases shared by the two proteins, and attributed these to distinct processes of heme reduction and ligand dissociation. The question then became, which came first: reduction or ligand dissociation? Scheme 4.1 shows the case where heme reduction precedes ligand dissociation (“liganded intermediate” pathway), but initially, the so-called “ligand off” pathway, in which ligand dissociation precedes reduction, seemed equally plausible. This question was further investigated by Raymond Cox and Michael Holloway, who studied via stopped-flow the reduction by dithionite of metmyoglobin with several different ligands bound at the distal position. Among the metmyoglobin derivatives studied were ones with cyanide and azide axial ligands whose $k_{\text{off}(\text{ox})}$ rates for ligand substitution were independently known. Cox and coworkers observed reduction rates that exceeded those predicted by $k_{\text{off}(\text{ox})}$, which supported the liganded-intermediate pathway of Scheme 4.1, in which the $k_{\text{off}(\text{red})}$ governing ligand dissociation from the ferrous heme was presumably greater than $k_{\text{off}(\text{ox})}$.⁸ This conclusion was supported by Olivas et al. in a similar study published around



Scheme 4.1. The two mechanistic steps typically involved in ferric heme reduction, as ascertained from studies with myoglobin and other model proteins.^{10, 16-19} Both the 6-coordinate Fe(III) and 5-coordinate Fe(II) states are high-spin, whereas the 6-coordinate Fe(II) intermediate is low-spin.¹⁶

the same time when looking at the CN^- , NO_2^- , and imidazole adducts; however, these authors suggested a ligand off pathway for other variants.⁷ It should be noted that neither study found evidence for an intermediate formed during the reduction of aquometmyoglobin.^{7, 8}

Research over the next few decades provided further evidence supporting the liganded-intermediate pathway (Scheme 4.1) proposed by Cox and Holloway. A paper by Gasyna et al. reported on changes in absorption spectra at low-temperature during reduction via g-irradiated electrons.⁹ They observed that intermediates could be trapped at 77 K, which they attributed to liganded Fe(II) species, that only formed the 5-coordinate Fe(II) species upon warming to temperatures above 100K. Intermediates were observed for most of the metmyoglobin derivatives studied including aquometmyoglobin. A possible exception was the fluoride bound species which exhibited characteristics of both a liganded-intermediate and ligand-off pathway.⁹

A decade after the paper of Gasyna et al, Keiichi Tsukahara published a rather interesting paper comparing metmyoglobin with a version in which the distal His residue had been cyanated.¹⁰ The distal His hydrogen bonds to the distal water ligand in metMb and helps

to stabilize its binding to the heme. Cyanated histidine can no longer hydrogen bond with the distal water ligand, and as a result, the cyanated metMb heme is 5-coordinate instead of 6-coordinate.¹¹ Tsukahara showed that cyanated metMb was consistently reduced more rapidly than native metMb by a variety of electron donors (over 700× faster in the case of $\text{Ru}(\text{NH}_3)_6^{2+}$).¹⁰ Furthermore, temperature-dependent stopped-flow studies showed that the faster reduction in the cyanated metMb was attributable to a large decrease in the enthalpic activation energy when compared to the native metMb.¹⁰ In turn, the difference in enthalpic activation energy is readily attributable to the much greater change in geometry associated with reduction of native metMb, where water must leave the heme binding pocket upon reduction.

In a result similar to that of Tsukahara, reduction of cyanide-bound native metmyoglobin was found to be substantially slower when compared to cyanide-bound variants in which the distal His residue had been mutated to either Gly or Val.^{12, 13} Once again, this could be attributed to the disruption in the variants of the hydrogen-bonding network that helps stabilize the distal ligand on the heme. It is important to also keep in mind, though, that cyanide release is accompanied by protonation, which is also heavily influenced by protein environment.^{12, 13}

In 1992, a paper published by Fred Hawkrige and Brian Hoffmann with the help of Bertha King studied the reduction of metmyoglobin and the cyano- and fluoride- derivatives by cyclic voltammetry (CV), expanding on previous work done by the same groups when monitoring electron transfer between mixed metal hemoglobin hybrids.^{14, 15} What they found was that changes in scan rate gave rise to changes in anodic character, and fitting of the

voltammograms required fitting to a sequential mechanism in which reduction of the iron was followed by ligand dissociation, as opposed to a concerted mechanism.¹⁵ At the turn of the century, a number of papers by Fritz Parak and Valeri Prusakov looked into low-temperature reduction of metmyoglobin by different spectroscopic methods.¹⁶⁻¹⁸ Their work provided further evidence that electron transfer initially results in reduction of Fe(III)(H₂O) to Fe(II)(H₂O), after which thermal relaxation is required to yield the 5-coordinate Fe(II) product (as shown in Scheme 4.1). During this process the protein can adopt a number of conformational substates, and these low-frequency dynamics drive the reaction as the temperature is increased.¹⁸ Parak's 1994 publication also solved a rather interesting open question by showing that, during the process of aquometmyoglobin reduction, there is indeed a change in spin state.¹⁶ This was proved by the detection of a low-spin Fe(II) intermediate by Mössbauer spectroscopy.¹⁶ Previously, reduction had been assumed to proceed without a change in spin-state.

Numerous additional studies of metMb reduction over the past 20 years have provided further mechanistic details about the process,¹⁹ so that at present a fairly complete picture is available. The key conclusions are still those of Scheme 4.1: reduction of metmyoglobin is not a concerted process and instead goes by a) reduction of the iron center followed by b) dissociation of the distal ligand, which is the rate limiting step during the process and heavily influenced by the environment within the distal heme pocket.^{6, 12, 20} Myoglobin starts in a high-spin Fe(III)(H₂O) state and ends in a high-spin Fe(II) 5-coordinate state, but in between, a low-spin Fe(II)(H₂O) is detectable (Scheme 4.1).¹⁶ The driving force for this reaction appears to be geometric relaxation to the 5-coordinate Fe(II) product where the iron relaxes out of the heme plane, as well as dissociation of the water molecule.

The extensive knowledge available for myoglobin provides very helpful guidance for trying to understand the less studied trHbN. In some ways, the two proteins are similar. They are both monomeric heme proteins whose ferric state is high-spin aquomet, and both reduce to high-spin 5-coordinate deoxy- states in which O₂ can readily bind.²¹ Beyond that, though, the proteins are also rather different structurally. For example, as related in Chapter 1, in trHbN, the bond between the iron and proximal His exhibits very low strain, meaning that the iron sits closer to the heme plane compared to many other globins, myoglobin included.²¹ This means the geometric change between ligand-bound ferric and ligand-free ferrous states is much smaller, which could be advantageous from a reorganizational energy perspective, but could also hamper the ability to drive ligand release. Another key difference is the extensive hydrogen-bonding network within the distal heme pocket of trHbN.^{21, 22} This is already known to lead to low k_{off} rates for O₂, and could extend to other ligands, such as water. In general, many of the features that help to optimize oxy-trHbN for NO dioxygenation could very well hamper the met-trHbN heme reduction step, which would limit efficiency in terms of overall turnover (Scheme 1.1).

As mentioned earlier, the met-trHbN reduction step of Scheme 1.1 remains understudied, primarily because the native reductase system utilized by *M. tuberculosis* is to date unknown. In a study of cyanide binding to truncated hemoglobins, reduction using dithionite as a reducing agent produced a transient Fe(II)-CN⁻ species in agreement with the results of a similar experiment done with myoglobin.^{20, 23} Interestingly, the authors note that reduction rates were highly variable between systems, though this result should be interpreted with caution because, as mentioned earlier, cyanide release from metal binding is accompanied

by protonation, which is heavily influenced by protein environment. Thus, when contrasting reduction of two ferriheme proteins with cyanide distal ligands, it isn't clear which differences are unique to the cyanide system and which are more generally attributable to differences in the ferrihemes themselves.

As briefly mentioned in section 1.4, Singh et al investigated met-trHbN reduction by using NADH-ferredoxin/flavodoxin (FdR) system from *E. coli* as the electron donor.² This group reported a drastic decrease in met-trHbN reduction rate upon deletion of the N-terminal tail, which they attributed to decreased ability of met-trHbN_{delN} to properly interface with a reductase.² However, as shown in Chapter 3, the N-terminal tail appears to influence NO dioxygenation by oxy-trHbN and red-trHbN nitrosylation via induced conformational changes directly at the active site, and we conjectured that the tail might similarly affect water release from aquomet-trHbN. In support of this conjecture, it has been shown that active site residue TyrB10, with support from GlnE11, is responsible for maintaining proper coordination of the water molecule in the aquomet-state, as evidenced by the appearance of 5-coordinate character in UV/Vis absorption and resonance Raman spectra of TyrB10Phe variants.²¹ This means that, upon mutation of this residue, water is no longer tightly bound to the iron at the active site, and theoretically should behave similarly during reduction to myoglobin mutants that have penta-coordinate ferrihemes. This chapter presents kinetics experiments in which met-trHbN_{wt}, met-trHbN_{delN}, met-trHbN_{DM}, and met-trHbN_{TM}, were reduced with the non-biological electron donor hexaamineruthenium(II). It seems unlikely that deletion of the pre-A tail would affect the ability of met-trHbN_{delN} to properly interface with a small molecule donor

such as hexaammineruthenium(II), so the goal of the experiments was to assess the pre-A tail deletion's effect directly on the active site of met-trHbN.

4.2. Materials and methods

Stock solutions of 10 mM hexaammineruthenium(III) chloride (Ru^{III}) and 0.2 M NaCl in tris buffer were fully reduced in a glovebox to hexaammineruthenium(II) (Ru^{II}) using controlled potential electrolysis with a BASi Epsilon EC potentiostat before each experiment. An Ag/AgCl electrode (BASi model RE-5B) was used as the reference and was routinely calibrated against the methyl viologen midpoint potential.²⁴ Kinetic measurements for the reaction between Ru^{II} and met-trHbN_{WT}, met-trHbN_{DeIN}, met-trHbN_{DM}, or met-trHbN_{TM} were measured using an Applied Photophysics SX20 stopped-flow apparatus. UV/Vis detection was with a photodiode array to collect the whole spectrum from 200-800 nm with the system scanning in logarithmic mode, and a temperature of 25 °C, unless otherwise specified. Total data acquisition time varied from 20 s to upwards of 500 s, depending on the variant being studied. The final concentrations for each sample were 1 mM Ru^{II} , and approximately 5 μM met-trHbN. Experiments were completed in triplicate and the data averaged before further analyses, which were completed using custom-built programs in Mathcad 15 (PTC Software) previously outlined by Shahid et al. with slight modifications outlined below.²⁵

4.3. Results

The blue, green, light blue, and yellow traces in Figure 4.1a show the averaged UV/Vis spectral changes observed at selected times after a solution containing approximately 9 μM trHbN_{wt} was mixed in a 1:1 ratio with one containing 2 mM hexaammineruthenium(II) (Ru^{II}). Figure 4.1b shows absorbance vs time slices taken at 407 nm and 426 nm from the spectra

depicted in Fig. 4.1a. Singular value decomposition (SVD) analysis^{26, 27} of the Fig. 4.1a spectra showed that four components were needed to faithfully reconstruct a noise-reduced absorbance matrix. The SVD-treated data were then fit empirically to the model shown in Scheme 4.2 (dashed red traces, Fig. 4.1). In the scheme, $S_0(\lambda) - S_3(\lambda)$ are the spectral components that are generated sequentially as shown in Eq. 1. At any given time t , the absorbance at a given wavelength λ ($A_{\lambda,t}$) is obtained by taking the product of $S_n(\lambda)$ and a time-dependent variable $y_n(t)$, then summing the products from $n = 0$ to $n = 3$ (Scheme 4.2, Eq. 2). The values of $y_n(t)$, in turn, are obtained by numerical integration of the differential Eqs. (3) – (6) in Scheme 4.2, with the initial conditions $y_{0(0)} = 1$ and $y_{1(0)} = y_{2(0)} = y_{3(0)} = 0$. In Eqs. (1) – (6), $k_1 - k_3$ and $S_0(\lambda) - S_3(\lambda)$ are adjustable parameters obtained by a combination of linear and nonlinear least-squares fitting of the data set shown in Fig. 4.1a.²⁶

Figure 4.2 shows the spectral components $S_0 - S_3$ obtained from the Fig. 4.1 fitting process. For each component, the dashed red traces are least-squares Beer's law fits of the components with the independently obtained extinction coefficient spectra of wild type met-trHbN, red-trHbN, and oxy-trHbN. The components were fit only in the range from 395 nm to 456 nm, which is where the biggest spectral changes took place. The excellent fits in each case provide good evidence that met-trHbN_{wt}, red-trHbN_{wt}, and oxy-trHbN_{wt} are the only species contributing to the components. Table 4.1 summarizes the concentrations of met-trHbN_{wt}, red-trHbN_{wt}, and oxy-trHbN_{wt} that contribute to each spectral component, as determined by the Beer's law fits. These concentrations, together with the $y_{0(t)} - y_{3(t)}$ values generated in the

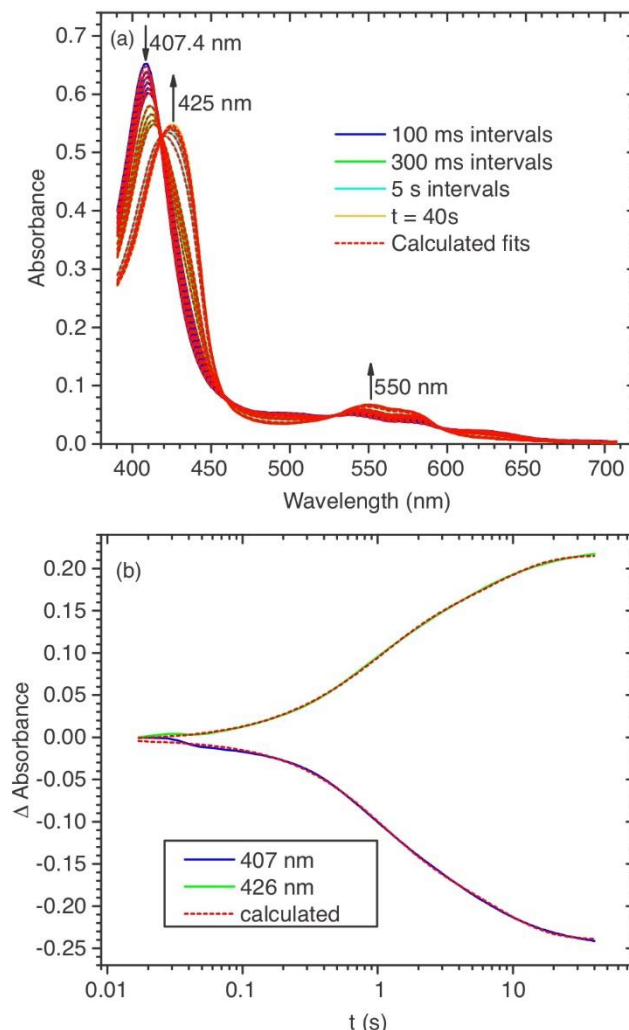


Figure 4.1. (a) blue, green, light blue, and yellow traces: UV/Vis spectral changes observed at selected times after a solution containing approximately $9 \mu\text{M}$ trHbN_{wt} was mixed in a 1:1 ratio with one containing 2 mM hexaammineruthenium(II) (Ru^{II}); 50 mM tris buffer, pH 8.1. (b) absorbance vs time slices taken at 407 nm and 426 nm from the spectra depicted in (a). Dashed red traces: least-squares best fits to the model of Scheme 4.1.

empirical Scheme 4.2 fit described above, were then used to calculate how the met-trHbN, red-trHbN, and oxy-trHbN concentrations evolved with time (Fig. 4.3). Scheme 4.3 shows how this was done. In Scheme 4.3, $[\text{met-trHbN}]_t$, $[\text{red-trHbN}]_t$, and $[\text{oxy-trHbN}]_t$ are the concentrations of each species at time t , while $[\text{met-trHbN}]_n$, $[\text{red-trHbN}]_n$, and $[\text{oxy-trHbN}]_n$ ($n = 0 - 3$) are the concentrations of each species that contribute to $S_0 - S_3$, respectively, as listed in Table 4.1.



$$A_{\lambda,t} = S_{0(\lambda)} \cdot y_{0(t)} + S_{1(\lambda)} \cdot y_{1(t)} + S_{2(\lambda)} \cdot y_{2(t)} + S_{3(\lambda)} \cdot y_{3(t)} \quad (2)$$

$$\frac{dy_0}{dt} = -k_1 y_0 \quad (3)$$

$$\frac{dy_1}{dt} = k_1 y_0 - k_2 y_1 \quad (4)$$

$$\frac{dy_2}{dt} = k_2 y_1 - k_3 y_2 \quad (5)$$

$$\frac{dy_3}{dt} = k_3 y_2 \quad (6)$$

Scheme 4.2. Equations 3 – 6 were integrated numerically with initial conditions: $y_{0(0)} = 1$; $y_{1(0)} = y_{2(0)} = y_{3(0)} = 0$.

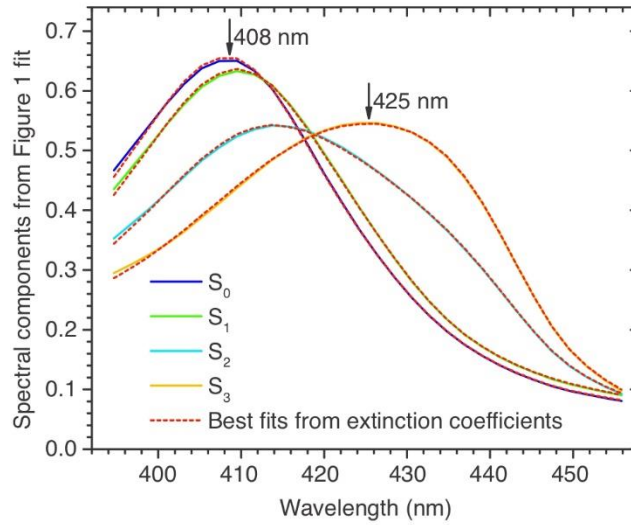


Figure 4.2. Blue, green, aqua, and yellow traces: spectral components $S_0 - S_3$ obtained by fitting the Fig. 4.1a spectra to the Scheme 4.2 model. Dashed red traces: least-squares Beer's law fits of the spectral components with the independently obtained extinction coefficient spectra of met-trHbN_{WT}, red-trHbN_{WT}, and oxy-trHbN_{WT}.

$$[\text{met-trHbN}]_t = [\text{met-trHbN}]_0 \cdot y_{0(t)} + [\text{met-trHbN}]_1 \cdot y_{1(t)} + [\text{met-trHbN}]_2 \cdot y_{2(t)} + [\text{met-trHbN}]_3 \cdot y_{3(t)} \quad (7)$$

$$[\text{red-trHbN}]_t = [\text{red-trHbN}]_0 \cdot y_{0(t)} + [\text{red-trHbN}]_1 \cdot y_{1(t)} + [\text{red-trHbN}]_2 \cdot y_{2(t)} + [\text{red-trHbN}]_3 \cdot y_{3(t)} \quad (8)$$

$$[\text{oxy-trHbN}]_t = [\text{oxy-trHbN}]_0 \cdot y_{0(t)} + [\text{oxy-trHbN}]_1 \cdot y_{1(t)} + [\text{oxy-trHbN}]_2 \cdot y_{2(t)} + [\text{oxy-trHbN}]_3 \cdot y_{3(t)} \quad (9)$$

Scheme 4.3. Equations used to obtain the Fig. 4.3 plots of met-trHbN_{WT}, red-trHbN_{WT}, and oxy-trHbN_{WT} concentrations as a function of time. $[\text{met-trHbN}]_n$, $[\text{red-trHbN}]_n$, and $[\text{oxy-trHbN}]_n$ ($n = 0 - 3$) are the concentrations of each species that contribute to $S_0 - S_3$, respectively, as listed in Table 4.1, while $y_{0(t)} - y_{3(t)}$ are the values generated in the empirical Scheme 4.2 fit (see main text for details).

	S_0	S_1	S_2	S_3
[met-trHbN _{WT}] (μM)	3.42	2.35	1.07	0.27
[red-trHbN _{WT}] (μM)	0.05	-0.14	1.89	3.64
[oxy-trHbN _{WT}] (μM)	0.97	2.21	1.48	0.51

Table 4.1. Concentrations of met-trHbN_{WT}, red-trHbN_{WT}, and oxy-trHbN_{WT} that contribute to the $S_0 - S_3$, components obtained in the Fig. 4.1 fits, as calculated from the $S_0 - S_3$ Beer's law fits (Fig. 4.2).

The Fig. 4.3 fits show that about 1 μM of oxy-trHbN and 3.4 μM met-trHbN are present at $t = 0$, before any reaction between the protein and Ru^{II} has taken place; the concentration of red-trHbN at $t = 0$ is negligible. Over the first 500 ms, the major event taking place is conversion of met-trHbN to oxy-trHbN. Oxy-trHbN concentration peaks at around 500 ms and then decreases, while production of red-trHbN, which initially lags the appearance of oxy-trHbN, increases steadily after 100 ms. It appears that red-trHbN is being generated both from met-trHbN and from oxy-trHbN, with the latter taking place either through dissociation of the oxygen ligand, or through reduction of the oxy-trHbN moiety by Ru^{II}.

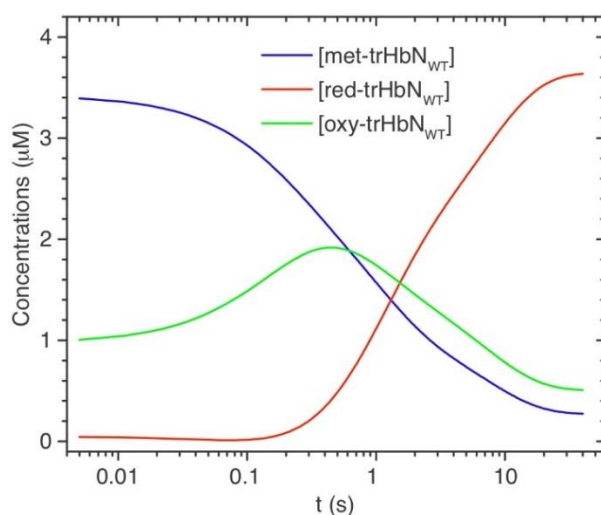


Figure 4.3. Concentrations of met-trHbN_{WT}, red-trHbN_{WT}, and oxy-trHbN_{WT} as a function of time, calculated from the Fig. 4.1 and 4.2 fits using the Scheme 4.3 equations.

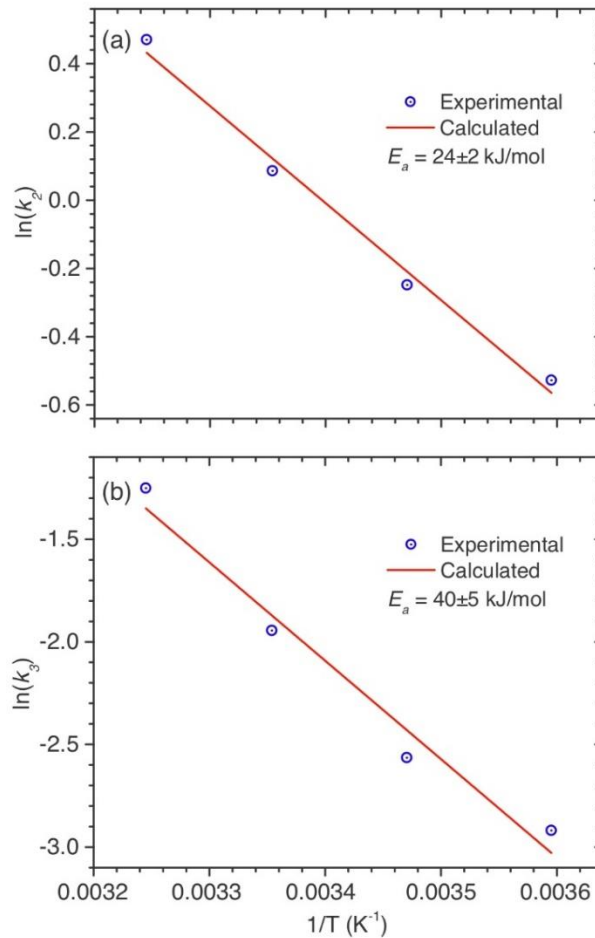


Figure 4.4. Arrhenius plots showing how the rate constants k_2 (a) and k_3 (b) obtained from the Fig. 4.1 fits vary with temperature.

Repeating the experiment of Figs. 4.1 – 4.3 at temperatures varying from 5 °C to 30 °C showed that the values of k_2 and k_3 varied with temperature as predicted by the Arrhenius equation (Fig. 4.4), whereas that of k_1 , which primarily governed appearance of oxy-trHbN, was essentially independent of temperature. Fitting of the Fig. 4.4 data with the Arrhenius equation yielded activation energies $E_{a2} = 24 \pm 2$ kJ/mol and $E_{a3} = 40 \pm 5$ kJ/mol for the second and third kinetic phases, respectively.

When the experiment of Figs. 4.1 – 4.3 was repeated with the variants trHbN_{deIN}, trHbN_{DM}, and trHbN_{TM}, SVD analysis^{26, 27} once again showed that four components were needed

to faithfully reconstruct a noise-reduced absorbance matrix, and once again the experimental data could be well fit using the Scheme 4.2 model. However, the kinetic behavior of the variants differed substantially from that of the wild type, as is evident from Fig. 4.5, which compares the rates of red-trHbN appearance of the four variants. It is clear from Fig. 4.5 that

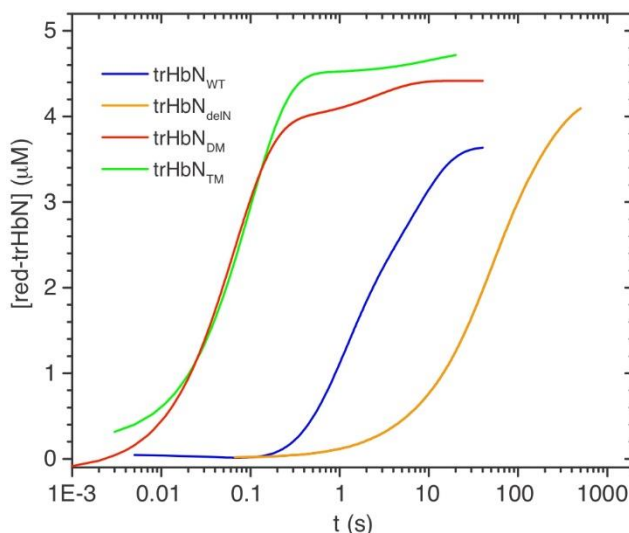


Figure 4.5. Concentrations of red-trHbN_{WT}, red-trHbN_{deIN}, red-trHbN_{DM}, and red-trHbN_{TM} as a function of time after mixing 8 - 10 μM of the corresponding met-trHbN variant in a 1:1 ratio with one containing 2 mM Ru^{II} ; 50 mM tris buffer, pH 8.1, temperature fixed at 25.0 $^{\circ}\text{C}$.

heme reduction by Ru^{II} is much slower for the trHbN_{deIN} variant than for the wild type, but faster for both the trHbN_{DM} and trHbN_{TM} variants. Table 4.2 summarizes the values of the individual rate constants obtained by fitting each data set with the Scheme 4.2 model.

Comparing trHbN_{wt} and trHbN_{deIN} shows that the $k_1 - k_3$ values for trHbN_{deIN} are all 2% - 5% of the wild type values. Notably, experiments with trHbN_{deIN} carried out at temperatures varying from 5 $^{\circ}\text{C}$ to 30 $^{\circ}\text{C}$ showed that none of the rate constants vary significantly with temperature (data not shown); this is in contrast to the wild type case, where k_2 and k_3 were found to vary with temperature (Fig. 4.4). For trHbN_{DM} and trHbN_{TM}, the effects on each rate constant are more varied than they are for trHbN_{deIN}; k_1 and k_2 are about 5 \times and 10 \times higher, respectively, for

trHbN_{DM} and trHbN_{TM} than for trHbN_{wt}, but k_3 for trHbN_{DM} is higher than for the wild type whereas for trHbN_{TM} it's lower (Table 4.2). Note though, that the spectral changes associated with k_3 are minor for trHbN_{DM} and trHbN_{TM} when compared with trHbN_{WT}.

	k_1 (s ⁻¹)	(% of wt)	k_2 (s ⁻¹)	(% of wt)	k_3 (s ⁻¹)	(% of wt)
trHbN _{wt}	5.7	(-)	1.1	(-)	0.14	(-)
trHbN _{delN}	0.31	(5.4)	0.026	(2.4)	0.0058	(4.1)
trHbN _{DM}	20.1	(350)	12	(1090)	0.41	(300)
trHbN _{TM}	27.4	(480)	10.1	(920)	0.09	(64)

Table 4.2. Comparison of the $k_1 - k_3$ rate constant values for trHbN_{wt}, trHbN_{delN}, trHbN_{DM}, and trHbN_{TM}, obtained by fitting experimental data with the Scheme 4.2 model. In each case, the temperature was fixed at 25 °C, and hexaammineruthenium(II) concentrations were 1 mM after stopped-flow dilution.

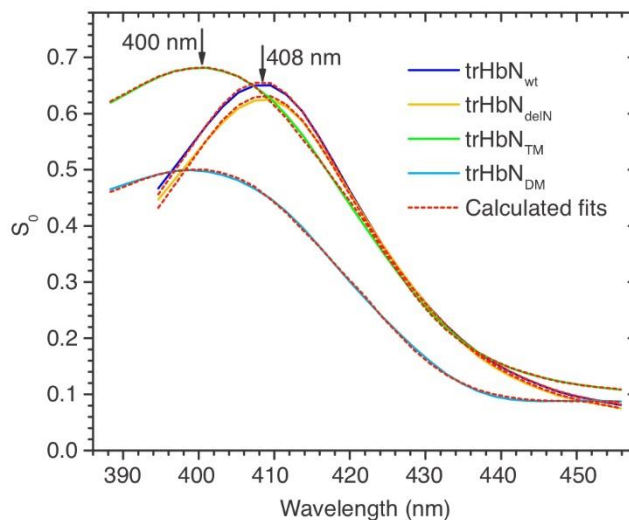


Figure 4.6. S_0 components obtained for each variant in the Fig. 4.5 experiments. The dashed red traces are the least-squares Beer's law fits of the spectral components with the independently obtained extinction coefficient spectra of met-trHbN, red-trHbN, and oxy-trHbN for each variant.

Figure 4.6 compares the S_0 spectral components of trHbN_{TM}, trHbN_{DM}, trHbN_{wt}, and trHbN_{delN}, which primarily reflect the shapes of the met-trHbN Soret bands, as met-trHbN is the dominant protein species at $t = 0$. From Fig. 4.6, one can see that the S_0 spectral component shapes fall into two groups: trHbN_{wt} and trHbN_{delN} have absorbance maxima centered around

408 nm, whereas the trHbN_{DM} and trHbN_{TM} bands are blue-shifted by 8 nm and are significantly broader. This broadening and blue-shift of the Soret band is diagnostic of a 5-coordinate high-spin met-trHbN heme and was expected because a previous study had shown that the heme in met-trHbN double mutants where Y33 and Q58 had been replaced by nonpolar residues is 5-coordinate. By contrast, the wild type met-trHbN heme is 6-coordinate high-spin, with a water occupying the distal site; the narrower Soret band centered around 408 nm is diagnostic of this.²⁸ The comparable shape of the met-trHbN_{delN} Soret band shows that heme coordination in this ferric variant is 6-coordinate as well.

4.4. Discussion

This work provides strong evidence that the met-trHbN reduction rate is highly regulated by the nature of the coordination sphere surrounding the active site, which in turn is influenced by pre-A tail-induced motions. The drastic increase in the appearance of deoxy-character upon mutation of active site residues Tyr33 and Gln58 shows that reduction rate is limited by release of the ligated water molecule. When no water is bound, an electron can rapidly transfer without the need to change coordination number. This mimics results observed by Tsukahara after cyanating a distal His residue in Mb, where a vacant active site in the oxidized state led to increased reduction rates (Section 4.1.2).¹⁰ The decrease in reduction rate after deletion of the N-terminal tail was more surprising, but not wholly unexpected given the earlier results of Singh et al.² The fact that reduction was slowed using Ru^{II} as an electron donor as opposed to the ferredoxin reductase utilized in the Singh paper² supports the conjecture that N-tail deletion affects the trHbN active site directly rather than altering the protein-protein interface between trHbN and its physiological donor.

Given the high positive charge on Ru^{II}, we examined the possibility that the coulombic attraction between Ru^{II} and met-trHbN_{wt} was different than between Ru^{II} and met-trHbN_{delN}. However, using the Adaptive Poisson-Boltzmann Solver electrostatics calculation program in PyMol shows similar electrostatics mapping in both variants, and the overall isoelectric point of the protein is lowered due to the basicity of the N-terminal tail.

Crucially, the reduction kinetics of met-trHbN_{TM}, in which Y33 and Q58 were mutated simultaneously with pre-A tail deletion, were virtually identical to those of met-trHbN_{DM}, which had the same Y33 and Q58 mutations but not the pre-A tail deletion. We conclude that, when the hydrogen-bonding network created between Y33, Q58, and the distal water molecule, are intact and water is coordinated in the oxidized state, deletion of the Pre-A tail lowers the rate of reduction due to slowed ligand release. When the hydrogen-bonding network is broken and the distal site is left vacant, as in the case of the Y33F/Q58V variants, deletion of the Pre-A tail has no effect on reduction rate, as is expected if the pre-A tail plays a key role in facilitating water release during reduction.

For all the variants studied, after SVD analysis of the spectra that tracked met-trHbN reduction, four spectral components were needed to reconstruct the noise-reduced spectra. These spectral components could be fit with reasonable certainty using the individually derived extinction coefficients for the variants in the met-, oxy-, and red- states, leading us to believe that these are the only species contributing to the overall spectra. Note that in all experiments some oxy-trHbN was present at $t = 0$. Met-trHbN was prepared from oxy-trHbN by reacting it with $[\text{Fe}(\text{CN})_6]^{3-}$, and it appears that this reaction was incomplete to varying degrees in the various experiments. In future experiments, the oxy-trHbN oxidation reaction should be

monitored by UV/Vis to ensure that it goes to completion before carrying out buffer-exchange to remove $[\text{Fe}(\text{CN})_6]^{3-}$.

Figure 4.3 shows that after trHbN_{WT} is mixed with Ru^{II} , the concentration of oxy-trHbN initially increases, reaches a maximum concentration after about 500 ms, then decreases to about half of the initial concentration over the next 20 s as it is converted to red-trHbN. A similar result was seen with $\text{trHbN}_{\text{deIN}}$; however, interestingly, the transient oxy formation was not observed for either trHbN_{DM} or trHbN_{TM} (not shown). The results shown in Figs. 4.3 and A1.1 for trHbN_{WT} and $\text{trHbN}_{\text{deIN}}$ could be explained if red-trHbN formed in step 2 of Scheme 4.1 then reacted rapidly with residual O_2 to form oxy-trHbN, which was in turn reduced to red-trHbN on a longer timescale. However, two factors call this hypothesis into question. First, if red-trHbN is reacting with residual oxygen, why do red-trHbN_{DM} or red-trHbN_{TM} appear to be immune? If anything, based on the Chapter 3 results, they should react more rapidly with oxygen. Second, when oxy-trHbN_{WT} was allowed to react with Ru^{II} in the glovebox, UV/Vis analysis showed that, while oxy-trHbN_{WT} was indeed reduced to red-trHbN_{WT}, (not shown) the reaction proceeded far more slowly than the rate shown in Fig. 4.3 ($k_{\text{obs}} = 0.0014 \text{ s}^{-1}$, $t_{0.5} \sim 8.3 \text{ min}$).

An alternative explanation of the Fig. 4.3 and other results is that, despite appearances, the species that grows in over 500 ms and then decreases over the next 20 s is not oxy-trHbN, but rather some other species with a very similar UV/Vis spectrum. A plausible alternative candidate for the species growing in would be the reduced trHbN with water still bound that is predicted to form in step 1 of Scheme 4.1. Parak et al showed that such a species would be low-spin like oxy-trHbN, but unlike met-trHbN and red-trHbN.¹⁶ Thus, it could well have a UV/vis

spectrum similar to that of oxy-trHbN. Furthermore, a 6-coordinate intermediate wouldn't form upon reduction of met-trHbN_{DM} or met-trHbN_{TM} because these species are largely 5-coordinate (Fig. 4.6). As mentioned in section 4.1, 6-coordinate aquoferrous intermediates have never been detected for Mb at room temperature, but perhaps they are longer lived in trHbN because of the decreased strain in the trHbN Fe-N(His) bond that allows the iron to sit closer to the heme plane compared to Mb.²¹

Further experiments will be needed to clarify the true nature of the transient species observed in Fig. 4.3. The obvious first experiment that should be done is to repeat the experiment under more rigorously anaerobic conditions. If the intermediate appears under such conditions, it will be shown to be something other than oxy-trHbN. If it does not appear, then the intermediate is due to residual oxygen as initially postulated. In that case, a new question arises: why does the transient oxy-trHbN disappear within 20s whereas bulk oxy-trHbN has a much longer half-life in the presence of Ru^{II}? A possible answer to that question is that oxy-trHbN can exist in several conformations, some of which are more rapidly reduced than others. This too would be an interesting result worthy of further analysis.

The exact physical mechanism by which the pre-A tail affects the processes taking place at the distal heme pocket is still not understood and will require further experimental and computational studies to clarify. One plausible hypothesis is that the tail applies an entropic pressure on the main body of the protein, which shifts the conformational landscape to favor conformations which facilitate fast reduction. This hypothesis is in line with studies done by the group of Zachary Wood that will be further discussed in Chapter 6,²⁹ and would explain why similar kinetic phases ($k_1 - k_3$) are identified for all variants that nevertheless vary greatly in

both their amplitudes and rate constants. For example, k_3 is 300× greater for trHbN_{DM} than it is for trHbN_{WT}, while it is smaller for trHbN_{TM}. This could mean that the conformational substate governing k_3 could heavily depend on the N-terminal tail, while the other constants are solely reliant on the composition of the active site.

The dependence of rate constants k_1 , k_2 , and k_3 on temperature in both trHbN_{WT} and trHbN_{DeIN} provides further interesting insight. In the wild type, both k_2 and k_3 display linear Arrhenius behavior, while k_1 shows concave behavior (Fig. 4.4). By contrast, in trHbN_{DeIN}, all three constants vary wildly with temperature, showing at times concave, convex, or no dependence on temperature (not shown). A paper by Truhlar and Kohen provides great insight into how and why reactions, especially ones involving enzyme kinetics, can deviate from expected Arrhenius behavior.³⁰ Based on previous work outlined much earlier (in the 1920s) by Tolman,³¹ complex chemical systems such as enzymes can exist in a large variety of conformations, some of which are catalytically active while others are inactive. As the temperature increases, the phase space of available conformations increases, and this typically increases the fraction of nonreactive conformers. This phenomenon counters typical Arrhenius behavior, whereby rate constants are expected to increase with temperature. Instead, with enzymes, one may see so-called “convex” Arrhenius plots, in which k_{obs} initially increases with temperature but later decreases. In terms of trHbN, the fact that k_2 and k_3 deviate from Arrhenius behavior upon deletion of the N-terminal tail could mean that the N-terminal tail provides stability to conformational substates governing these processes. Since these later rate constants relate closely to the appearance of final red-trHbN, this could mean that the pre-A

region plays a critical role in facilitating vacancy of the active site and formation of the final reduced species.

4.6. Summary

In conclusion, the stopped-flow studies presented in this chapter show that the pre-A tail's primary influence on the rate of met-trHbN reduction arises from its ability to affect active site residues Tyr33 and Gln 58 in ways that accelerate the rate-limiting release of water from the heme distal site during reduction (Scheme 4.1, step 2). The importance of Tyr33 and Gln58 in maintaining water coordination and regulating the rate of reduction is highlighted by the significant rate increase seen in both the DM and TM variants (Fig. 4.5). Subsequently, the link between the pre-A tail and the roles of Tyr33 and Gln58 in maintaining water coordination is established by the observation that deletion of the tail profoundly affects reduction rate only when Tyr33 and Gln58 are still present in the active site. Pre-A tail deletion has no significant effect on the reduction rate of met-trHbN_{TM} (Fig. 4.5). The pre-A tail's main mode of action is not in promoting proper protein-protein interaction with its physiological electron donor as previously hypothesized.² Instead, its role seems to be to shift the conformational landscape of trHbN in favor of species in which water is more easily released in the rate limiting step (step 2, Scheme 4.1).

Comparing the results from Chapters 3 and 4 it is clear that, though the pre-A tail deletion's effects on Tyr33 and Gln58 influence all three steps in the NO dioxygenation catalytic cycle (Scheme 1.1), its effect on the reductive step (step 2, Scheme 1.1) is by far the greatest and most likely to be physiologically relevant. This agrees with earlier studies published by Lama et al and Singh et al.^{2, 32} Future studies on met-trHbN reduction should first establish

whether the transient species seen in Fig. 4.3 is due to oxy-trHbN generated from residual oxygen, as modeled in the figures, or to a ferrous aquo intermediate that has very similar spectral properties. With this question clarified, the role of the pre-A tail could be further investigated with molecular dynamics simulations, stopped-flow studies under the more rigorously anaerobic conditions, and studies of new variants, as described in Chapter 5.

4.7. References

- (1) Smagghe, B. J.; Trent, J. T.; Hargrove, M. S. NO dioxygenase activity in hemoglobins is ubiquitous in vitro, but limited by reduction in vivo. *PLoS ONE* **2008**, *3*, e2039.
- (2) Singh, S.; Thakur, N.; Oliveira, A.; Petruk, A. A.; Hade, M. D.; Sethi, D.; Bidon-Chanal, A.; Marti, M. A.; Datta, H.; Parkesh, R.; et al. Mechanistic insight into the enzymatic reduction of truncated hemoglobin N of *Mycobacterium tuberculosis*. *J. Biol. Chem.* **2014**, *289*, 21573-21583.
- (3) Ludlow, J. T.; Wilkerson, R. G.; Nappe, T. M. Methemoglobinemia. BTI - StatPearls. **2021**. From 2023 Jan.
- (4) Pauling, L.; Coryell, C. D. The Magnetic Properties and Structure of Hemoglobin, Oxyhemoglobin and Carbonmonoxyhemoglobin. *Proc Natl Acad Sci U S A* **1936**, *22* (4), 210-216. DOI: 10.1073/pnas.22.4.210 From 1936 Apr.
- (5) Coryell, C. D.; Stitt, F.; Pauling, L. The Magnetic Properties and Structure of Ferrihemoglobin (Methemoglobin) and Some of its Compounds. *Journal of the American Chemical Society* **1937**, *59* (4), 633-642. DOI: 10.1021/ja01283a012.
- (6) Wilting, J.; Raap, A.; Braams, R.; De Bruin, S. H.; Rollema, H. S.; Janssen, L. H. M. Conformational Changes and Ligand Dissociation Kinetics following Rapid Reduction of Human Aquomethemoglobin and Horse Aquometmyoglobin by Hydrated Electrons. *Journal of Biological Chemistry* **1974**, *249* (19), 6325-6330. DOI: [https://doi.org/10.1016/S0021-9258\(19\)42256-4](https://doi.org/10.1016/S0021-9258(19)42256-4).
- (7) Olivas E Fau - De Waal, D. J.; De Waal Dj Fau - Wilkins, R. G.; Wilkins, R. G. Reduction of metmyoglobin derivatives by dithionite ion. *J. Biol Chem* **1977**, (0021-9258 (Print)), 4038-4042.
- (8) Cox, R. P.; Hollaway, M. R. The Reduction by Dithionite of Fe(III) Myoglobin Derivatives with Different Ligands Attached to the Iron Atom. *European Journal of Biochemistry* **1977**, *74* (3), 575-587, <https://doi.org/10.1111/j.1432-1033.1977.tb11427.x>. DOI: <https://doi.org/10.1111/j.1432-1033.1977.tb11427.x> (accessed 2023/04/25).
- (9) Gasyňa, Z. Transient intermediates in the reduction of Fe(III) myoglobin-ligand complexes by electrons at low temperature. *Biochim Biophys Acta* **1979**, 90022-90029.
- (10) Tsukahara, K. Kinetics and mechanisms of reduction of metmyoglobins. Importance of the geometry change at the heme iron site upon reduction. *J. Am. Chem. Soc.* **1989**, *111*, 2040-2044.
- (11) Shiro Y Fau - Morishima, I.; Morishima, I. Modification of the heme distal side in myoglobin by cyanogen bromide. Heme environmental structures and ligand binding properties of the modified myoglobin. *Biochemistry* **1984**, 4879-4884. Morishima, I.; Shiro, Y.; Wakino, T. Meso deuterium NMR hyperfine shift as a probe for determining five- or six-coordination at heme iron binding site in ferric

- high-spin hemoproteins. *Journal of the American Chemical Society* **1985**, *107* (4), 1063-1065. DOI: 10.1021/ja00290a055.
- (12) Bellelli, A.; Antonini, G.; Brunori, M.; Springer, B. A.; Sligar, S. G. Transient spectroscopy of the reaction of cyanide with ferrous myoglobin. Effect of distal side residues. *Journal of Biological Chemistry* **1990**, *265* (31), 18898-18901. DOI: [https://doi.org/10.1016/S0021-9258\(17\)30600-2](https://doi.org/10.1016/S0021-9258(17)30600-2).
- (13) Brunori, M.; Antonini, G.; Castagnola, M.; Bellelli, A. Cooperative cyanide dissociation from ferrous hemoglobin. *Journal of Biological Chemistry* **1992**, *267* (4), 2258-2263. DOI: [https://doi.org/10.1016/S0021-9258\(18\)45871-1](https://doi.org/10.1016/S0021-9258(18)45871-1). Antonini, G.; Bellelli, A.; Concetti, A.; Falcioni, G.; Brunori, M. Cyanide dissociation from the hemoglobin of *Parascaris equorum*. *Biochimica et biophysica acta* **1994**, *1205* 2, 252-257.
- (14) Natan, M. J.; Kuila, D.; Baxter, W. W.; King, B. C.; Hawkridge, F. M.; Hoffman, B. M. Modulation of interprotein electron transfer energetics by heme-ligand variation. *Journal of the American Chemical Society* **1990**, *112* (10), 4081-4082. DOI: 10.1021/ja00166a079.
- (15) King, B. C.; Hawkridge, F. M.; Hoffman, B. M. Electrochemical studies of cyanometmyoglobin and metmyoglobin: implications for long-range electron transfer in proteins. *Journal of the American Chemical Society* **1992**, *114* (26), 10603-10608. DOI: 10.1021/ja00052a066.
- (16) Parak, F. G.; Prusakov, V. E. Relaxation of non-equilibrium states of myoglobin studied by Mossbauer spectroscopy. *Hyperfine Interactions* **1994**, *91*, 885-890.
- (17) Prusakov, V. E.; Steyer, J.; Parak, F. G. Mossbauer spectroscopy on nonequilibrium states of myoglobin: a study of r-t relaxation. *Biophys J* **1995**, *68* (6), 2524-2530. DOI: 10.1016/S0006-3495(95)80435-2. Lamb, D. C.; Ostermann, A.; Prusakov, V. E.; Parak, F. G. From metmyoglobin to deoxy myoglobin: relaxations of an intermediate state. *Eur. Biophys. J.* **1998**, *27*, 113-125.
- (18) Engler, N.; Ostermann, A.; Gassmann, A.; Lamb, D. C.; Prusakov, V. E.; Schott, J.; Schweitzer-Stenner, R.; Parak, F. G. Protein dynamics in an intermediate state of myoglobin: optical absorption, resonance Raman spectroscopy, and X-ray structure analysis. *Biophys J.* **2000**, *78*, 2081-2092.
- (19) Della Longa, S.; Arcovito, A.; Congiu-Castellano, A.; Girasole, M.; Hazemann, J. L.; Lo Bosco, A. Redox-induced structural dynamics of Fe-heme ligand in myoglobin by X-ray absorption spectroscopy. *Biophys J.* **2003**, *85*, 549-558. Oang, K. Y.; Kim, K. H.; Jo, J.; Kim, Y.; Kim, J. G.; Kim, T. W.; Jun, S.; Kim, J.; Ihee, H. Sub-100-ps structural dynamics of horse heart myoglobin probed by time-resolved X-ray solution scattering. *Chem Phys* **2014**, *422* (0301-0104 (Print)), 137-142. DOI: 10.1016/j.chemphys.2014.03.004.
- (20) Dantsker, D.; Samuni, U.; Ouellet, Y.; Wittenberg, B. A.; Wittenberg, J. B.; Milani, M.; Bolognesi, M.; Guertin, M.; Friedman, J. M. Viscosity-dependent relaxation significantly modulates the kinetics of CO recombination in the truncated hemoglobin trHbN from *Mycobacterium tuberculosis*. *J. Biol. Chem.* **2004**, *279*, 38844-38853.
- (21) Yeh, S.-R.; Couture, M.; Ouellet, Y.; Guertin, M.; Rousseau, D. L. A cooperative oxygen binding hemoglobin from *Mycobacterium tuberculosis*. *J. Biol. Chem.* **2000**, *275*, 1679-1684.
- (22) Ouellet, Y. H.; Daigle, R.; Lague, P.; Dantsker, D.; Milani, M.; Bolognesi, M.; Friedman, J. M.; Guertin, M. Ligand binding to truncated hemoglobin N from *Mycobacterium tuberculosis* is strongly modulated by the interplay between the distal heme pocket residues and internal water. *J. Biol. Chem.* **2008**, *283*, 27270-27278.
- (23) Lambeth Do Fau - Palmer, G.; Palmer, G. The kinetics and mechanism of reduction of electron transfer proteins and other compounds of biological interest by dithionite. *J. Biol Chem* **1973**, 6095-6103.
- (24) Watanabe, T.; Honda, K. Measurement of the extinction coefficient of the methyl viologen cation radical and the efficiency of its formation by semiconductor photocatalysis. *J. Phys. Chem.* **1982**, *86*, 2617-2619.

- (25) Shahid, S.; Ali, M.; Legaspi-Humiston, D.; Wilcoxon, J.; Pacheco, A. A. A kinetic investigation of the early steps in cytochrome *c* nitrite reductase (ccNiR)-catalyzed reduction of nitrite. *Biochemistry* **2021**, *60*, 2098-2115.
- (26) Press, W. H.; Teukolsky, S. A.; Vetterling, W. T.; Flannery, B. P. Numerical Recipes the art of scientific computing. 3rd ed.; Cambridge University Press, 2007; pp 773-839.
- (27) Henry, E. R.; Hofrichter, J. Singular Value Decomposition: Application to Analysis of Experimental Data. In *Meth. Enzymol.*, Brand, L., Johnson, M. L. Eds.; Vol. 210; Academic Press, 1992; pp 129-192.
- (28) Ouellet, Y.; Milani, M.; Couture, M.; Bolognesi, M.; Guertin, M. Ligand interactions in the distal heme pocket of Mycobacterium tuberculosis truncated hemoglobin N: roles of TyrB10 and GlnE11 residues. *Biochemistry* **2006**, *45*, 8770-8781.
- (29) Keul, N. D.; Oruganty, K.; Schaper Bergman, E. T.; Beattie, N. R.; McDonald, W. E.; Kadirvelraj, R.; Gross, M. L.; Phillips, R. S.; Harvey, S. C.; Wood, Z. A. The entropic force generated by intrinsically disordered segments tunes protein function. *Nature* **2018**, *563* (7732), 584-588. DOI: 10.1038/s41586-018-0699-5.
- (30) Truhlar, D.; Kohen, A. Convex Arrhenius plots and their interpretation. *Proc Natl Acad Sci U S A* **2001**, 848-851.
- (31) Tolman, R. C. STATISTICAL MECHANICS APPLIED TO CHEMICAL KINETICS. *Journal of the American Chemical Society* **1920**, *42* (12), 2506-2528. DOI: 10.1021/ja01457a008. Thomas, J. S. G. Statistical mechanics with applications to physics and chemistry. By R. C. Tolman, Ph.D. American Chemical Society Monograph Series. Pp. 334. New York: The Chemical Catalog Company, Inc., 1927. Price \$7.00. *Journal of the Society of Chemical Industry* **1927**, *46* (43), 985-985. DOI: <https://doi.org/10.1002/jctb.5000464313>.
- (32) Lama, A.; Pawaria, S.; Bidon-Chanal, A.; Anand, A.; Gelpi, J. L.; Swati, A.; Marti, M. A.; Estrin, D. A.; Luque, F. J.; Dikshit, K. L. Role of pre-A motif in nitric oxide scavenging by truncated hemoglobin, HbN of *Mycobacterium tuberculosis*. *J. Biol. Chem.* **2009**, *284*, 14457-14468.

Chapter 5 Preparation of pre-A tail variants of trHbN

5.1. Overview

The experiments described in chapters 3 and 4 provide further evidence that the pre-A tail plays essential roles in the proper functioning of trHbN. This is evidenced by the decrease in nitrosylation rates (chapter 3) and more drastic decrease in reduction rates (chapter 4) observed upon deletion of the tail. The importance of the tail is also highlighted by its conserved nature amongst the trHbNs of pathogenic slow-growing mycobacteria, which suggests that it gives a potential evolutionary advantage against nitrosative stress to these bacteria.¹ Furthermore, as will be discussed in more detail in Chapter 6, studies published in the last five years have begun to show that other proteins, not just trHbNs, also exhibit elongated N- or C-terminal disordered regions that greatly affect activity. Given the emerging understanding of how important disordered regions such as trHbN's pre-A tail may be to the proper functioning of some proteins, this chapter describes the preparation of a series of trHbN pre-A tail variants designed to probe whether or to what extent the composition and length of the tail are of importance to its proper functioning.

5.2. Materials and methods

5.2.1. General methods

All chemical reagents were purchased from Millipore-Sigma, Fisher Scientific, or dot Scientific unless otherwise specified. Codons for each variant were designed and codon optimized using the Benchling R&D Cloud software platform(Benchling), then purchased as gBlock fragments from Twist Bioscience. Enzymes and chemically competent cells were

purchased from New England Biolabs and used according to the manufacturer's protocol.

QIAGEN kits were utilized according to manufacturer's protocols. Routine UV/Vis spectra were obtained using Cary 50 spectrophotometers; where anaerobic conditions were needed, a spectrophotometer installed in a nitrogen-filled glovebox was used. Unless otherwise specified, all experiments with trHbN were carried out in tris buffer as described in Chapter 3.

5.2.2. Expression and purification of trHbN variants

Figure 5.1 outlines the key features of the DNA fragments that were used to express each trHbN variant. Each gene fragment contained a forward and reverse primer sequence containing BamHI and HindIII restriction sites, a ribosome binding site, and the stop codon TAA. Purchased fragments were amplified by PCR with complementary forward and reverse primer sequences using an annealing temperature of 46 °C, after which the PCR product was cleaned using a QIAGEN PCR cleanup kit. DNA fragments and pUC19 plasmid were then digested individually using BamHI and HindIII. Digest products were isolated using gel electrophoresis in a 2% agarose gel at 60 V for 60 min (Figure 5.2), and the appropriate bands extracted using a QIAGEN gel extraction kit. Digested fragments were ligated into a digested pUC19 plasmid using Instant Sticky-Ends Ligase, and the ligated DNA was then transformed into chemically competent NEB 5- α strain *Escherichia coli*. Cells were then screened for efficiency using a blue/white screening method by growing overnight at 37 °C on LB agar plates supplemented with 150 μ L of 1000 X concentrated (1 g/10 mL) Ampicillin, 40 μ L of 100 mM IPTG, and 120 μ L X-GAL (200 mg X-GAL in 10 mL DMF). White colonies were selected and grown overnight in 5 mL of LB supplemented with 5 mL of 1000 X concentrated Ampicillin in a 37 °C shaker, after which the DNA was extracted using a QIAGEN Mini-Prep kit. DNA was then transformed into

BL21(DE3) chemically competent cells, after which 100 mL of cells were plated onto LB agar plates

```

AAAATTTTAAGCTTATAACTAACTAAAAGGAGGACAGCTATGCGCAAGCGCGAGCCGATCAGCATCTATGATAAAATTGGGGGCCATGAAGCGATTGAAGTGGTTGT
GGAAGATTTCTATGTTTCGTGTACTCGCAGACGACCCAGTTGAGTGCGTTCTTTTCTGGCACCAACATGAGCCGGCTTAAAGGGAAACAGGTGGAATTTTTTCGCGGCGG
CGCTGGGTGGTCTGAACCCCTACACCGGAGCCCCGATGAAACAAGTTCATCAGGGTCGTGGTATTACCATGCATCACTTTAGTCTGGTGGCTGGACACCTGGCCGAT
GCTTTAACAGCAGCCGGCGTCCCCTGGGAGACGATCACCGAAATTCTGGGCGTGATAGCTCCACTGGCAGTCGATGTCACGTCCGGCGAGTCAACTACTGCCCGGT
ATAACGCCGGGTGTAAGGATCCATATATAT

```

Figure 5.1. Full DNA fragment for the expression of trHbN_{HALF}. Shown in blue are the complimentary segments for the forward and reverse primer sequences, with restriction sites for HindIII and BamHI restriction endonucleases shown in bold. Shown in red is the ribosomal binding site and shown in black is the codon optimized sequence for trHbN_{HALF}.

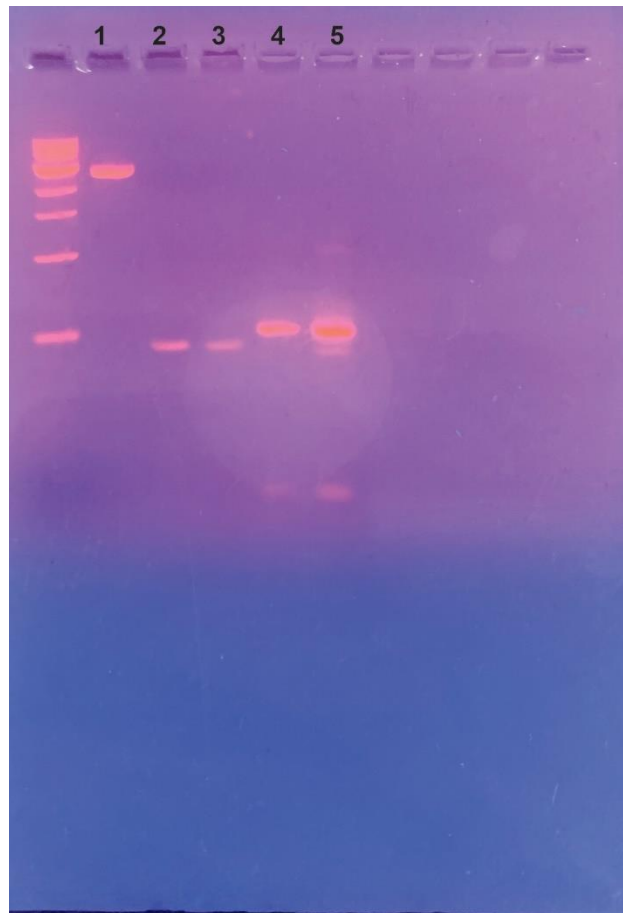


Figure 5.2. Agarose gel (2% w/v) of pUC19 and gene fragments for trHbN_{BTA} and trHbN_{DC} variants with a 1 kb DNA ladder on the left. The numbered lanes contain the following: (1) pUC19 fragment after restriction digest, (2) and (3) gene fragments for trHbN_{BTA} and trHbN_{DC} respectively after restriction digest, (4) and (5) PCR products after ligation of digested pUC19 and trHbN_{BTA} and trHbN_{DC} fragments respectively using M13 primers.

supplemented with 100 mL of 1000 X concentrated Ampicillin and grown overnight at 37 °C. Colonies were selected from the plate and grown in 5 mL of LB supplemented with 5 mL of 1000 X concentrated Ampicillin overnight in a 37 °C shaker. To ensure that the cells now expressed the desired gene, DNA was extracted using a QIAGEN Mini-prep kit, after which PCR was performed using M13 primers with an annealing temperature of 55 °C. DNA fragments were then isolated using the previously described gel electrophoresis method (Figure 5.2), and the extracted fragments were shipped to the University of Chicago Comprehensive Cancer Center for sequencing.

Each variant was purified using the method outlined in Section 3.2 with two major exceptions for the double Cys (DC) and hexa-his tagged (HT) variants. For the DC variant, 4 L cultures were inoculated with 5-aminolevulinic acid (5ALA) to a final concentration of 150 μ M while grown at 37 °C for 16 hr, after which the cells were collected, and the protein purified as previously described. Given the availability of a hexa-His tail in the His-tag variant, the protein was purified using Immobilized Metal Affinity Chromatography instead of the usual method. After centrifugation to collect the cell pellet, the cells were resuspended in 20 mM HEPES, 30 mM Imidazole, 500 mM NaCl, pH = 7.0 resuspension buffer. Cells were then sonicated and centrifuged to clarify the lysate as usual; however, no Streptomycin sulfate was added, and the lysate was loaded onto a 25mL Ni-Sepharose 6 Fast Flow column charged with 0.1 M NiSO₄ and equilibrated with resuspension buffer. After non-specific proteins were washed off the column using resuspension buffer, trHbN_{HT} was eluted using 20 mM HEPES, 500 mM Imidazole, 500 mM NaCl, pH = 7.0 elution buffer. Protein containing samples were then immediately concentrated and buffer exchanged into 50mM Tris, 0.5mM EDTA, pH = 8.1 buffer A.

The purity of each trHbN variant was verified by SDS-PAGE gel electrophoresis using NuPAGE 10 %, Bis-Tris gels and MES running buffer at 200 V for 35 min (Figure 5.3). The concentration of trHbN in a given solution could be ascertained from the heme concentration in the solution, which in turn was obtained from the pyridine hemochrome assay.² Once a given solution's concentration was known the individual extinction coefficient spectra were then obtained for each variant in the oxy-, red-, and met- states.

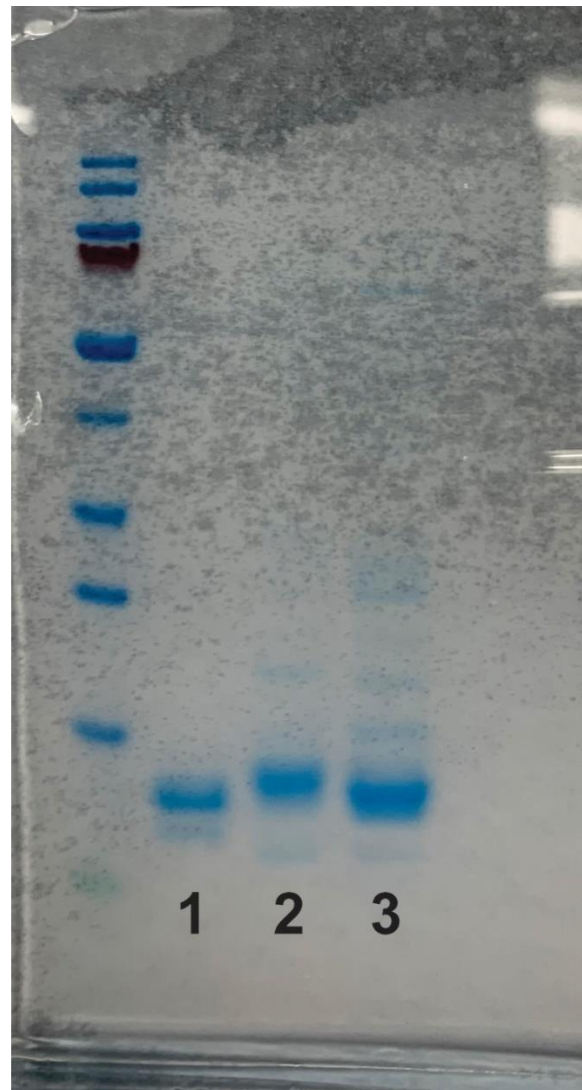


Figure 5.3. SDS-PAGE gel of trHbN_{WT} (1), trHbN_{SC} (2), and trHbN_{DC} (3) with a prestained protein ladder on the left.

5.3. Results and Discussion

Figure 5.4 lists the pre-A tail variants whose preparation is outlined in Section 5.2.2 and the acronyms used to refer to them. The design and expression of the variants follows the method previously outlined in Koebke et al.³ The high-copy number pUC19 plasmid does not use the T7 polymerase system often used in recombinant protein expression systems, and relies on leaky expression of the target proteins. However, the need to induce with IPTG is avoided, and expression levels are still adequate.

The level of expression of most variants was found to be comparable to that of trHbN_{WT} with the one exception being the trHbN_{DC} variant. Two common reasons for low recombinant protein expression are toxicity to the cell of the protein product and formation of undesirable disulfide bonds. However, cellular replication rates were uninhibited by cells containing plasmid encoding for trHbN_{DC}, which ruled out the first possible problem, and the use of reducing agents such as dithiothreitol in buffer after collection of cells and during purification did not lead to any increase in the amount of protein purified, which ruled out problems due to disulfide bond formation. 5ALA is a small, delta-amino acid and a known precursor in the biological synthesis of heme.^{4, 5} In fact, the biosynthesis of 5ALA has been shown to be rate-limiting during heme formation,⁶ and earlier researchers found that in some cases supplementing cells with 5ALA would stimulate the expression of hemeproteins.^{5, 7} With these earlier successes in mind, cells carrying the trHbN_{DC} gene were grown in medium supplemented with 5ALA. This approach increased the yield of trHbN_{DC} to levels comparable to those of trHbN_{WT} and other variants.

(a) -----MGLLSRLRKREPISIIYDKIGGHEAIEVVVEDFYVRVLADDQLSAFFSGTNMSRLKKGKQVEFFAAAL
 (b) -----MGLLCRLRKREPISIIYDKIGGHEAIEVVVEDFYVRVLADDQLSAFFSGTNMSRLKKGKQVEFFAAAL
 (c) MHHHHHHHGLLSRLRKREPISIIYDKIGGHEAIEVVVEDFYVRVLADDQLSAFFSGTNMSRLKKGKQVEFFAAAL
 (d) -----MRKREPISIIYDKIGGHEAIEVVVEDFYVRVLADDQLSAFFSGTNMSRLKKGKQVEFFAAAL
 (e) -----MGLLSELEEEEPISIIYDKIGGHEAIEVVVEDFYVRVLADDQLSAFFSGTNMSRLKKGKQVEFFAAAL
 (f) -----MGLLSCLRKREPISIIYCKIGGHEAIEVVVEDFYVRVLADDQLSAFFSGTNMSRLKKGKQVEFFAAAL

Figure 5.4. Truncated sequence comparison between trHbN (a) wild type (WT), and the variants (b) single Cys (SC), (c) hexa-His tag (HT), (d) half tail (HALF), (e) base to acid (BTA), (f) double Cys (DC).

Each new variant was chosen to test how the mutation would affect the pre-A tail's ability to modulate reactivity at the trHbN distal heme site, though the actual reactivity experiments have not yet been performed. For the benefit of future researchers, the questions that can be addressed with each variant are as follows.

Early studies have hinted towards potential interactions between the tail and main body via salt bridges, those these have somewhat been debated over the years.⁸ In the variant trHbN_{BTA}, the pre-A tail's basic amino acids have all been replaced by acidic ones, to test whether this has any effect. If it does, this could mean that a negatively charged tail is less mobile than a positively charged one, perhaps because it interacts with the globular part of the protein. It could also be due to maintaining proper charge distribution along the protein surface to facilitate proper function. If the switch has no effect, it will likely mean that any charged amino acids could mobilize the tail equally by making the tail soluble in aqueous solution.

Two variants were designed to test how the length of the Pre-A tail could alter enzyme activity. In the variant trHbN_{HT}, a hexa-His segment was added to the N-terminus. This was chosen because polyhistidine tags have been shown to have negligible effect on the overall

structure of the protein,⁹ but in some cases have caused differences in protein dynamics.^{10, 11}

The work of Thielges et al is particularly relevant as it reports on changes in myoglobin dynamics at short time scales.¹¹ As an added bonus with trHbN_{HT}, the ability to purify polyhistidine tagged proteins by IMAC simplifies the purification process, although care needs to be taken to promptly remove the imidazole as it is a known ligand of heme. The “half-tail” variant, trHbN_{HALF}, was designed to be one of a series of variants with progressively shorter tails that will ultimately test the relationship between tail length and the effect on the distal heme site’s reactivity. Such a study may not provide direct insights for designing anti-TB therapeutics, but it would be very helpful for answering fundamental questions about the allosteric effects of intrinsically disordered domains on enzymatic functions.

The last two variants could provide further insight on not only the importance of the Pre-A tail in maintaining proper protein function, but also whether or not the Pre-A tail could be a potential target towards inhibition. The trHbN_{DC} variant was designed to see if disulfide bond formation will inhibit the pre-A tail’s motions sufficiently to inhibit its effect on the heme distal site. If it does, perhaps a therapeutic agent could be henceforth designed to similarly inhibit the pre-A tail’s motions in trHbN_{WT}. The last variant developed, trHbN_{SC}, could provide multiple avenues of study. Originally, the variant with a single Cys within the Pre-A tail was developed to attach a spin label and study protein dynamics via EPR. Though these experiments have yet to prove fruitful, trHbN_{SC} could be used to nucleophilically add any number of bulky molecules, or even to other proteins. These could provide further insight on whether targeting the Pre-A tail is a viable option towards inhibition.

5.4. References

- (1) Lama, A.; Pawaria, S.; Bidon-Chanal, A.; Anand, A.; Gelpi, J. L.; Swati, A.; Marti, M. A.; Estrin, D. A.; Luque, F. J.; Dikshit, K. L. Role of pre-A motif in nitric oxide scavenging by truncated hemoglobin, HbN of *Mycobacterium tuberculosis*. *J. Biol. Chem.* **2009**, *284*, 14457-14468.
- (2) Berry, E. A.; Trumpower, B. L. Simultaneous determination of hemes a, b, and c from pyridine hemochrome spectra. *Anal. Biochem.* **1987**, *161*, 1-15.
- (3) Koebke, K. J.; Waletzko, M. T.; Pacheco, A. A. Direct monitoring of the reaction between photochemically generated nitric oxide and *Mycobacterium tuberculosis* truncated hemoglobin N wild type and variant forms: an assessment of computational mechanistic predictions. *Biochemistry* **2016**, *55*, 686-696.
- (4) Hendry Ga Fau - Jones, O. T.; Jones, O. T. Haems and chlorophylls: comparison of function and formation. *J. Med Genet* **1980**, (0022-2593 (Print)), 1-14. DOI: D - NASA: 80162745 EDAT- 1980/02/01 00:00 MHDA- 1980/02/01 00:01 CRDT- 1980/02/01 00:00 PHST- 1980/02/01 00:00 [pubmed] PHST- 1980/02/01 00:01 [medline] PHST- 1980/02/01 00:00 [entrez] AID - 10.1136/jmg.17.1.1 [doi] PST - ppublsh.
- (5) Ishizuka, M.; Abe, F.; Sano, Y.; Takahashi, K.; Inoue, K.; Nakajima, M.; Kohda, T.; Komatsu, N.; Ogura, S.; Tanaka, T. Novel development of 5-aminolevulinic acid (ALA) in cancer diagnoses and therapy. *Int Immunopharmacol* **2011**, *11* (3), 358-365. DOI: 10.1016/j.intimp.2010.11.029 From 2011 Mar.
- (6) Sassa, S. Heme stimulation of cellular growth and differentiation. *Semin Hematol* **1988**, *25* (4), 312-320. From 1988 Oct.
- (7) Sugiyama, Y.; Hagiya, Y.; Nakajima, M.; Ishizuka, M.; Tanaka, T.; Ogura, S. The heme precursor 5-aminolevulinic acid disrupts the Warburg effect in tumor cells and induces caspase-dependent apoptosis. *Oncol Rep* **2014**, *31* (3), 1282-1286. DOI: 10.3892/or.2013.2945 From 2014 Mar. Nishio, Y.; Fujino, M.; Zhao, M.; Ishii, T.; Ishizuka, M.; Ito, H.; Takahashi, K.; Abe, F.; Nakajima, M.; Tanaka, T.; et al. 5-Aminolevulinic acid combined with ferrous iron enhances the expression of heme oxygenase-1. *Int Immunopharmacol* **2014**, *19* (2), 300-307. DOI: 10.1016/j.intimp.2014.02.003 From 2014 Apr.
- (8) Milani, M.; Pesce, A.; Ouellet, Y.; Ascenzi, P.; Guertin, M.; Bolognesi, M. Mycobacterium tuberculosis hemoglobin N displays a protein tunnel suited for O₂ diffusion to the heme. *EMBO J.* **2001**, *20*, 3902-3909. Savard, P.-Y.; Daigle, R.; Morin, S.; Sebilio, A.; Meindre, F.; Lague, P.; Guertin, M.; Gagne, S. M. Structure and dynamics of *Mycobacterium tuberculosis* truncated hemoglobin N: insights from NMR spectroscopy and molecular dynamics simulations. *Biochemistry* **2011**, *50*, 11121-11130.
- (9) Carson, M.; Johnson, D. H.; McDonald, H.; Brouillette, C.; Delucas, L. J. His-tag impact on structure. *Acta Crystallogr D Biol Crystallogr* **2007**, *63* (Pt 3), 295-301. DOI: 10.1107/S0907444906052024 From 2007 Mar.
- (10) Booth, W. T.; Schlachter, C. R.; Pote, S.; Ussin, N.; Mank, N. J.; Klapper, V.; Offermann, L. R.; Tang, C.; Hurlburt, B. K.; Chruszcz, M. Impact of an N-terminal Polyhistidine Tag on Protein Thermal Stability. *ACS Omega* **2018**, *3* (1), 760-768. DOI: 10.1021/acsomega.7b01598 From 2018 Jan 31.
- (11) Thielges, M. C.; Chung, J. K.; Axup, J. Y.; Fayer, M. D. Influence of Histidine Tag Attachment on Picosecond Protein Dynamics. *Biochemistry* **2011**, *50* (25), 5799-5805. DOI: 10.1021/bi2003923.

Chapter 6 Possible strategies for designing trHbN-based anti-mycobacterial therapeutics

6.1. Overview

As was briefly mentioned in Chapter 5, studies published in the last five years have begun to show that other proteins, not just trHbNs, also exhibit elongated N- or C-terminal disordered regions that greatly affect activity. This chapter begins with a brief review of how the effects of disordered regions on protein function are currently understood. Based on this understanding, the chapter then suggests possible strategies by which the trHbN pre-A tail's function could be hindered by anti-mycobacterial therapeutics.

6.2. N- and C- terminal modulation of conformational dynamics in proteins

A paper published in 2011 looked into the effect of a hexahistidine tail on pico-second myoglobin dynamics, concluding that the addition of the His-tag had a definite effect on the dynamics at the heme site.¹ More recently, an article by Keul et al. reported that human UDP- α -D-glucose-6-dehydrogenase (UGDH) contains an intrinsically disordered C-terminal tail which greatly enhances affinity for an allosteric inhibitor through modification of the protein energy landscape.² UGDH catalyzes the oxidation of UDP-glucose by NAD^+ and is allosterically inhibited by UDP-xylose. Interestingly, Keul et al found that when the UGDH C-terminal tail was deleted, UDP-xylose no longer inhibited the enzyme, even though the enzyme's kinetic parameters, k_{cat} and K_m , were otherwise normal. By varying the length of the tail, the authors showed that the affinity enhancement for UDP-xylose increased with length to a maximum value, in behavior that could be modeled with an increasing exponential decay function. On the other hand,

various changes to tail composition or amino acid sequence had minimal effect. From this, the authors concluded that UGDH exists as an ensemble of substates with low- and high-affinity for UDP-xylose, and that the C-terminal tail provides an entropic force that shifts the distribution of substates to favor the high-affinity forms.²

Since the Keul paper, several more studies have looked into the effect of disordered tails on protein function.³⁻⁹ The studies provide examples of systems that require disordered tails for proper function, such as ligand binding to glutaredoxin I,⁷ others in which the tail is required for proper protein interfacing, as in the nucleoprotein of measles virus,⁸ and still others where the tail is essential for allosteric regulation, as in the Gag capsid linker in HIV.⁶ Bioinformatics are allowing identification of whole families of proteins that include intrinsically disordered domains, such as the lytic polysaccharide monooxygenase family.³

In parallel with experimental identification of proteins with disordered tails, other investigators are taking more theoretical and computational approaches to study such systems, though challenges remain when attempting to calculate absolute entropy using traditional atomistic simulations.¹⁰ Victor de Souza and Bronowska have shown that quasiharmonic methods are more successful when studying such flexible systems, applying their method coined SQuE to the UGDH studied in the Keul paper.⁹ Another aspect that is challenging for computational studies is determining the effect of charged surfaces on intrinsic disorder, a question looked into by Taneja and Holehouse.⁵ A review published in 2021 summarized many of the points made in the aforementioned studies, though the underlying tone was that more information is necessary in order to fully understand the extent to which these disordered tails affect protein function.⁴

Though the importance of disordered tails on protein dynamics is only recently being recognized, similar effects in other systems have been known for longer, and provide useful insights. A brief dive into the dynamics of fluid membranes, in particular the effect of surface polymers, will serve as an example. Two papers published by Bickel et al. at the turn of the century took a statistical mechanics approach towards explaining the effect that a tethered polymer has on a membrane surface. Essentially, a tethered polymer pinches a membrane at its contact point, causing a cone-like distortion to the surface. This effect is explained as an entropic pressure applied by the polymer on the surface in eq. 1:

$$p(r) = \frac{1}{2\pi} \frac{K_B T}{(r^2 + a^2)^{\frac{3}{2}}} \left(1 + \frac{(r^2 + a^2)}{2R_g^2} \right) \exp\left(-\frac{(r^2 + a^2)}{4R_g^2}\right) \quad (1)$$

where the pressure (p) at some distance (r) from the point of contact is related to the size of the polymer (R_g), absolute temperature (T), and Boltzmann constant (K_b).¹¹ A globular protein with a disordered tail could be visualized with a similar model if we substitute the tail for the tethered polymer and the globular part of the protein for the fluid membrane surface, though the model is complicated by changes to the electronic surface that can be induced by either addition of charged polymers or general changes to the curvature of the surface itself.¹²

6.3. Towards treating trHbN as a therapeutic target

A key long-term goal underlying the current research is to find ways of inhibiting trHbN activity and thus hopefully disrupting one of the defensive mechanisms used by *M. tuberculosis* against the immune system during infection. This is not a new notion with regards to trHbN, as the possibility was previously probed in a study by Ascenzi et al. who looked into isoniazid binding to the heme active site.¹³ Isoniazid, a hydrazide derivative of isonicotinic acid, is a first-

line drug that has been used in combatting tuberculosis since the 1950s.¹⁴ Early studies showed that isoniazid's primary effect is to disrupt the mycobacterial cell wall, though its exact mechanism eluded scientists for many years.¹⁵ It wasn't until the mid-90's that scientists began to unfurl isoniazid's precise mode of action. In 1995, Johnsson et al. published a report showing that InhA, an enoyl-reductase critical for fatty acid synthesis in mycobacterial cell wall production, was inhibited by the oxidation of isoniazid by KatG, the physiological catalase system found in *M. tuberculosis*, in the presence of NADH.¹⁶ Further studies by Sacchetti and Blanchard that included X-ray crystallographic characterization showed that isoniazid itself acted as a pro-drug in InhA inhibition, and that isonicotinic-acyl NADH was the active drug compound.¹⁷ This mechanism is proposed to proceed via a radical intermediate.

Though isoniazid has been a front line anti-mycobacterial drug for decades, it has several drawbacks. For one, mutations to the KatG gene have led to increasing cases of multi-drug resistant TB.¹⁸ Furthermore, the reactive nature of isoniazid and its radical product lead to increased disruption of essential cellular processes in infected individuals. Liver toxicity was long known to be associated with isoniazid consumption, especially when administered concomitantly with other drugs, and the drug was later found to be a reversible inhibitor of varying isoforms of cytochrome P450 in the liver.¹⁹ Pyridine and pyridine derivatives have long been known to bind to cytochrome P450, due to the high affinity of the iron in hemes for pyridine.²⁰ As such, it comes as no surprise that isoniazid could act as an inhibitor for trHbN activity, which has a very expansive tunnel system and heme pocket capable of allowing access to molecules such as isoniazid. Since isoniazid is already in use as an anti-tubercular drug acting on a target other than trHbN, its ability to bind trHbN doesn't really add to the anti-tubercular

arsenal. However, it does point towards the possibility of producing similar derivatives designed to selectively block the trHbN tunnel system through specific interactions with both the heme distal site and the tunnel residues.

Given the increasing evidence that the Pre-A tail facilitates protection against reactive nitrogen species,²¹ the alternative of most interest to our group is the possibility of therapeutically targeting the trHbN pre-A tail. If motion of the pre-A tail shifts the conformational landscape of trHbN to facilitate met-trHbN reduction (Chapter 4), then in theory, limiting its movement should also limit enzymatic activity. Furthermore, considering the reports summarized in Section 6.2 above regarding other proteins in which disordered tails play important functional roles, studies aimed at targeting the trHbN pre-A tail could not only yield therapeutics for the fight against TB, but they could also reveal new avenues for targeting C- and N-terminal domains in other proteins.

Future studies aimed at targeting the pre-A tail therapeutically should first focus on establishing exactly how tail motions are coupled to motions in the distal heme pocket. HDX experiments that show where the largest changes in side-chain mobility occur upon deletion of the Pre-A tail could be especially useful here. The recently prepared variants described in Chapter 5 may also provide valuable information about coupling between pre-A tail and distal heme pocket motions. For example, the wild type crystal structure showed salt bridge formation between Arg6 within the Pre-A tail and Asp17 on the A-helix.²² This inspired the design of the double-Cys variant described in Chapter 5. Though an NMR study showed that trHbN's solution structure is considerably more disordered than its solid state structure,²³ it is possible that even in solution residues 6 and 17 spend enough time in close proximity to allow

disulfide bond formation. If a disulfide bond does form in trHbN_{DC}, and if such bond formation proves to inhibit met-trHbN_{DC} reduction, then perhaps a small molecule that enhances interaction between the tail and the globular body of trHbN would make a promising therapeutic.

There are many possible strategies for designing molecules that can interact with proteins, but due to the intrinsic disorder that the pre-A tail seems to exhibit, many traditional methods may prove difficult to implement. Two methods that may prove fruitful are sequence-based protein-peptide interaction and lysine modification. Protein-protein interactions are very common in nature and have been studied in great detail. These interactions are often due to non-covalent binding between amino acid residues in the form of salt-bridges and van der Waals forces, though disulfide bond formation also plays important roles in some cases. With the wealth of structural data now available and major advances in *in silico* methods such as machine-learning, it is becoming easier to design small peptides capable of interacting with protein targets.²⁴ Two primary routes exist for predicting protein-protein interactions: similarity-based techniques such as SPRINT²⁵ and PIPE4²⁶, and deep-learning methods that rely on applying patterns from real systems to query proteins.²⁷ One limitation is the fact that most FDA-approved peptides bind to surface proteins, most likely due to the highly polar nature of peptide fragments. However, this may not be a limitation in the case of *M. tuberculosis*-expressed trHbN because a recent study showed that the protein is largely localized at the cell membrane, and actually exposed at the cell surface, thanks to post-translational glycosylation of the C-terminus (this likely provides a convenient location for rapid conversion of NO as it enters the cell).²⁸

It is still true that intrinsic disorder is hard to characterize structurally, limiting the opportunity for rational design. However, this does not mean that intrinsically disordered proteins are untargettable, and in fact, the targeting of intrinsically disordered peptides has been a key area of research due to the prevalence of disordered proteins in disease.^{29, 30} The inherent nature of disordered peptides means they exist in a highly dynamic state which, though a hurdle for characterizing and modeling, can allow protein to exhibit what some call “multiconformational affinity”.³¹ The first and most well studied intrinsically disordered system is the heterodimeric interaction between c-Myc, an oncogenic transcription factor, and the protein Max.³² High-throughput screening of potential inhibitors of this protein-protein interface has been a successful target of study since the turn of the century.³³ Many other inhibitors of intrinsically disordered proteins have been characterized since, though most have relied on targeting protein-protein interactions or hydrophobic pockets.^{30, 31} This could be challenging with trHbN, as there are no known protein-protein interactions with the N-terminal domain and the composition of the tail is largely polar.

Other than developing peptides for sequence-based protein-peptide interaction with trHbN, a second possible source of therapeutics would be covalent lysine inhibitors. The basicity of the amine side chain in Lys residues allows for the use of electrophiles for covalent inhibition, and many types of inhibitors exist.³⁴ Backbone amines, though much less basic, are still a target for bioconjugation.³⁵ Thankfully, the Pre-A tail has both. Once again, the possibility for rational design of covalent inhibitors could prove difficult, but the targets are there, and with the recent advances in homology modeling, a specific inhibitor for the Pre-A tail of trHbN could be found.³⁶ The variants described in Chapter 5 will hopefully help in the search.

6.4 References

- (1) Thielges, M. C.; Chung, J. K.; Axup, J. Y.; Fayer, M. D. Influence of Histidine Tag Attachment on Picosecond Protein Dynamics. *Biochemistry* **2011**, *50* (25), 5799-5805. DOI: 10.1021/bi2003923.
- (2) Keul, N. D.; Oruganty, K.; Schaper Bergman, E. T.; Beattie, N. R.; McDonald, W. E.; Kadirvelraj, R.; Gross, M. L.; Phillips, R. S.; Harvey, S. C.; Wood, Z. A. The entropic force generated by intrinsically disordered segments tunes protein function. *Nature* **2018**, *563* (7732), 584-588. DOI: 10.1038/s41586-018-0699-5.
- (3) Tamburrini, K. C.; Terrapon, N.; Lombard, V.; Bissaro, B.; Longhi, S.; Berrin, J.-G. Bioinformatic Analysis of Lytic Polysaccharide Monooxygenases Reveals the Pan-Families Occurrence of Intrinsically Disordered C-Terminal Extensions. In *Biomolecules*, 2021; Vol. 11.
- (4) Malagrino, F.; Diop, A.; Pagano, L.; Nardella, C.; Toto, A.; Gianni, S. Unveiling induced folding of intrinsically disordered proteins - Protein engineering, frustration and emerging themes. *Curr Opin Struct Biol* **2022**, *72* (1879-033X (Electronic)), 153-160. DOI: 10.1016/j.sbi.2021.11.004 From 2022 Feb.
- (5) Taneja, I.; Holehouse, A. S. Folded domain charge properties influence the conformational behavior of disordered tails. *Curr Res Struct Biol* **2021**, *3* (2665-928X (Electronic)), 216-228. DOI: 10.1016/j.crstbi.2021.08.002 From 2021.
- (6) Koma, T.; Kotani, O.; Miyakawa, K.; Ryo, A.; Yokoyama, M.; Doi, N.; Adachi, A.; Sato, H.; Nomaguchi, M. Allosteric Regulation of HIV-1 Capsid Structure for Gag Assembly, Virion Production, and Viral Infectivity by a Disordered Interdomain Linker. LID - 10.1128/JVI.00381-19 [doi] LID - e00381-19. *J Virol* **2019**, *93* (1098-5514 (Electronic)).
- (7) Balatti, G. E.; Barletta, G. P.; Parisi, G.; Tosatto, S. C. E.; Bellanda, M.; Fernandez-Alberti, S. Intrinsically Disordered Region Modulates Ligand Binding in Glutaredoxin 1 from *Trypanosoma Brucei*. *J Phys Chem B* **2021**, *125* (49), 13366-13375. DOI: 10.1021/acs.jpcc.1c07035 From 2021 Dec 16.
- (8) Bignon, E. A.-O.; Albornoz, A. A.-O.; Guardado-Calvo, P. A.-O.; Rey, F. A.-O.; Tischler, N. A.-O. Molecular organization and dynamics of the fusion protein Gc at the hantavirus surface. LID - 10.7554/eLife.46028 [doi] LID - e46028. *eLife* **2019**, *8* (2050-084X (Electronic)).
- (9) Victor de Souza, J. B., A. Long-Range Entropic Effects on Protein Intrinsically Disordered Regions. *ChemRxiv* **2019**.
- (10) Gilson, M. K.; Given, J. A.; Bush, B. L.; McCammon, J. A. The statistical-thermodynamic basis for computation of binding affinities: a critical review. *Biophys J* **1997**, *72* (3), 1047-1069. DOI: 10.1016/S0006-3495(97)78756-3.
- (11) Bickel, T.; Marques, C.; Jeppesen, C. Pressure patches for membranes: The induced pinch of a grafted polymer. *Physical Review E* **2000**, *62* (1), 1124-1127. DOI: 10.1103/PhysRevE.62.1124. Bickel, T.; Jeppesen, C.; Marques, C. M. Local entropic effects of polymers grafted to soft interfaces. *The European Physical Journal E* **2001**, *4* (1), 33-43. DOI: 10.1007/s101890170140.
- (12) Landau, L. D. L., E. M. *The Classical Theory of Fields*; Pergamon Press, 1995.
- (13) Ascenzi, P.; Coletta, A.; Cao, Y.; Trezza, V.; Leboffe, L.; Fanali, G.; Fasano, M.; Pesce, A.; Ciaccio, C.; Marini, S.; et al. Isoniazid inhibits the heme-based reactivity of *Mycobacterium tuberculosis* truncated hemoglobin N. *PLoS ONE* **2013**, *8*, e69762.
- (14) Bernstein J Fau - Lott, W. A.; Lott Wa Fau - Steinberg, B. A.; Steinberg Ba Fau - Yale, H. L.; Yale, H. L. Chemotherapy of experimental tuberculosis. V. Isonicotinic acid hydrazide (nydrazid) and related compounds. *Am Rev, Tuberc* **1952**, (0096-0381 (Print)), 357-364. DOI: D - CLML: 5221:34073:259:385 OTO - NLM.
- (15) Albert, A. Mode of Action of Isoniazid. *Nature* **1956**, *177* (4507), 525-526. DOI: 10.1038/177525a0. Cohn MI Fau - Kovitz, C.; Kovitz C Fau - Oda, U.; Oda U Fau - Middlebrook, G.; Middlebrook, G. Studies on isoniazid and tubercle bacilli. II. The growth requirements, catalase activities, and pathogenic properties

of isoniazid-resistant mutants. *Am Rev, Tuberc* **1954**, (0096-0381 (Print)). DOI: D - CLML: 5527:9375:98:303:320 OTO - NLM. Takayama K Fau - Schnoes, H. K.; Schnoes Hk Fau - Armstrong, E. L.; Armstrong El Fau - Boyle, R. W.; Boyle, R. W. Site of inhibitory action of isoniazid in the synthesis of mycolic acids in Mycobacterium tuberculosis. *J. Lipid Res* **1975**, (0022-2275 (Print)), 308-317.

(16) Johnsson, K.; King, D. S.; Schultz, P. G. Studies on the Mechanism of Action of Isoniazid and Ethionamide in the Chemotherapy of Tuberculosis. *Journal of the American Chemical Society* **1995**, *117* (17), 5009-5010. DOI: 10.1021/ja00122a038.

(17) Rozwarski, D. A.; Grant, G. A.; Barton, D. H.; Jacobs, W. R., Jr.; Sacchettini, J. C. Modification of the NADH of the isoniazid target (InhA) from Mycobacterium tuberculosis. *Science* **1998**, *279* (5347), 98-102. DOI: 10.1126/science.279.5347.98 From 1998 Jan 2. Quemard, A.; Sacchettini, J. C.; Dessen, A.; Vilcheze, C.; Bittman, R.; Jacobs, W. R., Jr.; Blanchard, J. S. Enzymic Characterization of the Target for Isoniazid in Mycobacterium tuberculosis. *Biochemistry* **1995**, *34* (26), 8235-8241. DOI: 10.1021/bi00026a004.

(18) Wengenack, N. L.; Rusnak, F. Evidence for isoniazid-dependent free radical generation catalyzed by Mycobacterium tuberculosis KatG and the isoniazid-resistant mutant KatG(S315T). *Biochemistry* **2001**, *40* (30), 8990-8996. DOI: 10.1021/bi002614m.

(19) Desta, Z.; Soukhova, N. V.; Flockhart, D. A. Inhibition of cytochrome P450 (CYP450) isoforms by isoniazid: potent inhibition of CYP2C19 and CYP3A. *Antimicrob Agents Chemother* **2001**, *45* (2), 382-392. DOI: 10.1128/AAC.45.2.382-392.2001 From 2001 Feb. Wen, X.; Wang Js Fau - Kivistö, K. T.; Kivistö Kt Fau - Neuvonen, P. J.; Neuvonen Pj Fau - Backman, J. T.; Backman, J. T. In vitro evaluation of valproic acid as an inhibitor of human cytochrome P450 isoforms: preferential inhibition of cytochrome P450 2C9 (CYP2C9). *Br J Clin Pharmacol* **2001**, (0306-5251 (Print)), 547-553.

(20) Born JI Fau - Vaughn, D.; Vaughn, D. Binding of pyridine derivatives to cytochrome P-450. *J. Pharm Sci* **1977**, (0022-3549 (Print)), 1046-1047.

(21) Lama, A.; Pawaria, S.; Bidon-Chanal, A.; Anand, A.; Gelpi, J. L.; Swati, A.; Marti, M. A.; Estrin, D. A.; Luque, F. J.; Dikshit, K. L. Role of pre-A motif in nitric oxide scavenging by truncated hemoglobin, HbN of Mycobacterium tuberculosis. *J. Biol. Chem.* **2009**, *284*, 14457-14468. Singh, S.; Thakur, N.; Oliveira, A.; Petruk, A. A.; Hade, M. D.; Sethi, D.; Bidon-Chanal, A.; Marti, M. A.; Datta, H.; Parkesh, R.; et al. Mechanistic insight into the enzymatic reduction of truncated hemoglobin N of Mycobacterium tuberculosis. *J. Biol. Chem.* **2014**, *289*, 21573-21583. Koebke, K. J.; Waletzko, M. T.; Pacheco, A. A. Direct monitoring of the reaction between photochemically generated nitric oxide and Mycobacterium tuberculosis truncated hemoglobin N wild type and variant forms: an assessment of computational mechanistic predictions. *Biochemistry* **2016**, *55*, 686-696. Pesce, A.; Bustamante, J. P.; Bidon-Chanal, A.; Boechi, L.; Estrin, D. A.; Luque, F. J.; Sebilo, A.; Guertin, M.; Bolognesi, M.; Ascenzi, P.; et al. The N-terminal pre-A region of Mycobacterium tuberculosis 2/2HbN promotes NO-dioxygenase activity. *FEBS J.* **2016**, *283*, 305-322.

(22) Milani, M.; Pesce, A.; Ouellet, Y.; Ascenzi, P.; Guertin, M.; Bolognesi, M. Mycobacterium tuberculosis hemoglobin N displays a protein tunnel suited for O₂ diffusion to the heme. *EMBO J.* **2001**, *20*, 3902-3909.

(23) Savard, P.-Y.; Daigle, R.; Morin, S.; Sebilo, A.; Meindre, F.; Lague, P.; Guertin, M.; Gagne, S. M. Structure and dynamics of Mycobacterium tuberculosis truncated hemoglobin N: insights from NMR spectroscopy and molecular dynamics simulations. *Biochemistry* **2011**, *50*, 11121-11130.

(24) Charih, F.; Biggar, K. K.; Green, J. R. Assessing sequence-based protein-protein interaction predictors for use in therapeutic peptide engineering. *Sci Rep* **2022**, *12* (1), 9610. DOI: 10.1038/s41598-022-13227-9.

(25) Stagno, J. R.; Liu, Y.; Bhandari, Y.; Conrad, C.; Panja, S.; Swain, M.; Fan, L.; Nelson, G.; Li, C.; Wendel, D.; et al. Structures of riboswitch RNA reaction states by mix-and-inject XFEL serial crystallography. *Nature* **2017**, *541*, 242-246.

- (26) Dick, K.; Samanfar, B.; Barnes, B.; Cober, E. R.; Mimee, B.; Tan, L. H.; Molnar, S. J.; Biggar, K. K.; Golshani, A.; Dehne, F.; et al. PIPE4: Fast PPI Predictor for Comprehensive Inter- and Cross-Species Interactomes. *Sci Rep* **2020**, *10* (1), 1390. DOI: 10.1038/s41598-019-56895-w.
- (27) Hashemifar, S.; Neyshabur, B.; Khan, A. A.; Xu, J. Predicting protein-protein interactions through sequence-based deep learning. *Bioinformatics* **2018**, (1367-4811 (Electronic)), 802-810.
- (28) Arya, S.; Sethi D Fau - Singh, S.; Singh S Fau - Hade, M. D.; Hade Md Fau - Singh, V.; Singh V Fau - Raju, P.; Raju P Fau - Chodiseti, S. B.; Chodiseti Sb Fau - Verma, D.; Verma D Fau - Varshney, G. C.; Varshney Gc Fau - Agrewala, J. N.; Agrewala Jn Fau - Dikshit, K. L.; et al. Truncated hemoglobin, HbN, is post-translationally modified in Mycobacterium tuberculosis and modulates host-pathogen interactions during intracellular infection. *J. Biol Chem* **2013**, (1083-351X (Electronic)), 29987-29999.
- (29) Metallo, S. J. Intrinsically disordered proteins are potential drug targets. *Curr Opin Chem Biol* **2010**, *14* (4), 481-488. DOI: 10.1016/j.cbpa.2010.06.169.
- (30) Santofimia-Castano, P.; Rizzuti, B.; Xia, Y.; Abian, O.; Peng, L.; Velazquez-Campoy, A.; Neira, J. L.; Iovanna, J. Targeting intrinsically disordered proteins involved in cancer. *Cell Mol Life Sci* **2020**, *77* (9), 1695-1707. DOI: 10.1007/s00018-019-03347-3 From 2020 May.
- (31) Chong, B.; Li, M.; Li, T.; Yu, M.; Zhang, Y.; Liu, Z. Conservation of Potentially Druggable Cavities in Intrinsically Disordered Proteins. *ACS Omega* **2018**, *3* (11), 15643-15652. DOI: 10.1021/acsomega.8b02092 From 2018 Nov 30.
- (32) Dang, C. V. c-Myc target genes involved in cell growth, apoptosis, and metabolism. *Mol Cell Biol* **1999**, *19* (1), 1-11. DOI: 10.1128/MCB.19.1.1 From 1999 Jan. Ponzilli, R.; Katz, S.; Barsyte-Lovejoy, D.; Penn, L. Z. Cancer therapeutics: targeting the dark side of Myc. *Eur J Cancer* **2005**, *41* (16), 2485-2501. DOI: 10.1016/j.ejca.2005.08.017 From 2005 Nov. Nair, M.; McIntosh, P. B.; Frenkiel, T. A.; Kelly, G.; Taylor, I. A.; Smerdon, S. J.; Lane, A. N. NMR structure of the DNA-binding domain of the cell cycle protein Mbp1 from *Saccharomyces cerevisiae*. *Biochemistry* **2003**, *42* (5), 1266-1273. DOI: 10.1021/bi0205247 From 2003 Feb 11.
- (33) Berg, T.; Cohen, S. B.; Desharnais, J.; Sonderegger, C.; Maslyar, D. J.; Goldberg, J.; Boger, D. L.; Vogt, P. K. Small-molecule antagonists of Myc/Max dimerization inhibit Myc-induced transformation of chicken embryo fibroblasts. *Proc Natl Acad Sci U S A* **2002**, *99* (6), 3830-3835. DOI: 10.1073/pnas.062036999 From 2002 Mar 19. Ibrahim, M.; Xu, C.; Spiro, T. G. Differential sensing of protein influences by NO and CO vibrations in heme adducts. *J. Am. Chem. Soc.* **2006**, *128*, 16834-16845.
- (34) Pettinger, J.; Jones, K.; Cheeseman, M. D. Lysine-Targeting Covalent Inhibitors. *Angewandte Chemie International Edition* **2017**, *56* (48), 15200-15209, <https://doi.org/10.1002/anie.201707630>. DOI: <https://doi.org/10.1002/anie.201707630>.
- (35) Rosen, C. B.; Francis, M. B. Targeting the N terminus for site-selective protein modification. *Nat Chem Biol* **2017**, *13* (7), 697-705. DOI: 10.1038/nchembio.2416 From 2017 Jul.
- (36) Muhammed, M. T.; Aki-Yalcin, E. Homology modeling in drug discovery: Overview, current applications, and future perspectives. *Chemical Biology & Drug Design* **2019**, *93* (1), 12-20, <https://doi.org/10.1111/cbdd.13388>. DOI: <https://doi.org/10.1111/cbdd.13388>.

Chapter 7 Conclusions and suggestions for further study

The results of this thesis work show that the pre-A tail of trHbN affects every step of a putative NO dioxygenation catalytic cycle (Scheme 1.1) but it affects the rate of met-trHbN re-reduction most profoundly.

The Chapter 4 results showed that met-trHbN_{delN} was reduced about 40 times more slowly than met-trHbN_{WT} by the non-specific reductant Ru^{II}. On the other hand, met-trHbN_{DM} and met-trHbN_{TM} were both reduced about 5 times more rapidly than met-trHbN_{WT} by Ru^{II}. Both met-trHbN_{DM} and met-trHbN_{TM} lack the amino acids Tyr33 and Gln 58 which stabilize water coordination to the ferric heme. Thus, in the variants, the ferric heme exists as an equilibrium between 5- and 6-coordinate moieties, and even in the 6-coordinate form, the distal water ligand is likely weakly bound. The fact that ferriheme reduction is faster in variants that lack Tyr33 and Gln 58 suggests that water release from the heme after reduction (Scheme 4.1, step 2) is rate limiting, as it is in other heme proteins such as myoglobin.¹ In turn, the fact that pre-A tail deletion inhibits reduction only when Tyr33 and Gln 58 are present suggests that the pre-A tail's primary role is to influence active site residues Tyr33 and Gln 58 in ways that accelerate the rate-limiting release of water from the heme distal site upon heme reduction (Scheme 4.1, step 2). When the distal water ligand is absent or weakly held, as it is in both the met-trHbN_{DM} and met-trHbN_{TM} variants, loss of the pre-A tail has no effect on reduction rate.

The Chapter 3 results show that the pre-A tail also influences the rate at which oxy-trHbN dioxygenates NO and the rate at which red-trHbN is nitrosylated. Both reaction rates are diminished by a modest 50% in the trHbN_{delN} variant. The impact of pre-A tail deletion of red-trHbN nitrosylation may ultimately prove to be more profound than its impact on NO

dioxygenation by oxy-trHbN, but large scatter in the currently available data made it impossible to be sure of this; follow-up experiments with better instrumentation are planned for the near future. As with met-trHbN reduction, deletion of the pre-A tail had minimal effect on the rates of NO dioxygenation by oxy-trHbN or red-trHbN nitrosylation in the trHbN_{TM} variant that also lacked the distal pocket amino acids Tyr33 and Gln 58. Therefore, as with met-trHbN reduction, the pre-A tail's role appears to be to shift the conformational landscape of trHbN within the distal heme pocket in favor of more reactive conformers.

Future investigators should make it a top priority to determine the role that residual oxygen plays during reduction of met-trHbN_{WT} and its variants. As shown in Chapter 4, a transient species currently believed to be oxy-trHbN is the first to appear after mixing met-trHbN with Ru^{II}, but this species is subsequently reduced to red-trHbN. If the species is indeed oxy-trHbN though, then it is in a conformation that reacts with Ru^{II} much more rapidly than does bulk oxy-trHbN. An alternative hypothesis considered in Chapter 4 is that the transient species is mis-assigned and is instead a ferrous trHbN species with water still attached to the heme. Either outcome would be interesting, but to make further progress in understanding the mechanism of met-trHbN reduction, it is crucial to know which hypothesis is correct. To that end, strategies are already being explored for keeping oxygen concentrations well below 1 mM during the stopped-flow experiments. If the transient species no longer appears under such conditions, this will prove that it is in fact a fast-reducing form of oxy-trHbN. In that case, the rigorously anaerobic experiments could be followed up by ones in which oxygen is added in a controlled way so as to determine how much of the fast-reducing form of oxy-trHbN can form.

Once the nature of the transient species is conclusively established for the wild type, it will also be possible to do more quantitative studies of the pre-A tail's role on reduction kinetics.

Another top priority for future investigators should be to establish how the structure of the pre-A tail affects its function, which can be done with the variants described in Chapter 5 and possibly other variants. Based on the literature reviewed in Chapter 6,² our working hypothesis is that the tail exerts an entropic force that shifts the distribution of substates to favor water release from the distal heme pocket upon heme reduction. If this is the case, the pre-A tail's function should be minimally affected by changes in its composition, but it should depend on its length, as was observed with the C-terminal tail of UGDH.² One possible exception to the tail composition prediction might be trHbN_{DC} (Fig. 5.4), which could potentially form a disulfide bridge that would limit tail motion.

Initially, the tail variants listed in Chapter 5 could be tested for activity using the techniques described in Chapters 3 and 4. Though the reductive step is clearly rate limiting in the Scheme 1.1 catalytic cycle, the NO dioxygenation and red-trHbN nitrosylation steps report on motions occurring on the microsecond timescale, and such information would be fundamentally useful. Together, the three steps in the Scheme 1.1 catalytic cycle report on molecular motions that cover timescales from microseconds to seconds, and this provides a unique opportunity for testing molecular dynamics computational methods over this wide range of timescales. Variants that prove especially interesting could also be investigated via HDX mass spectrometry.

Once the mechanism by which the pre-A tail affects trHbN function is understood in more detail, then potential therapeutics that interfere with tail operation can be designed. Such

therapeutics could be Lys modifiers or peptide inhibitors as described in Chapter 6, or other compounds. Overall, the study of trHbN provides an exciting opportunity to obtain new knowledge from a rather well-studied group of proteins, with the added benefit that finding a way to inhibit trHbN in vivo could very well aid in the fight against TB.

7.1. References

- (1) Tsukahara, K. Kinetics and mechanisms of reduction of metmyoglobins. Importance of the geometry change at the heme iron site upon reduction. *J. Am. Chem. Soc.* **1989**, *111*, 2040-2044. Natan, M. J.; Kuila, D.; Baxter, W. W.; King, B. C.; Hawkrigde, F. M.; Hoffman, B. M. Modulation of interprotein electron transfer energetics by heme-ligand variation. *Journal of the American Chemical Society* **1990**, *112* (10), 4081-4082. DOI: 10.1021/ja00166a079. King, B. C.; Hawkrigde, F. M.; Hoffman, B. M. Electrochemical studies of cyanometmyoglobin and metmyoglobin: implications for long-range electron transfer in proteins. *Journal of the American Chemical Society* **1992**, *114* (26), 10603-10608. DOI: 10.1021/ja00052a066.
- (2) Keul, N. D.; Oruganty, K.; Schaper Bergman, E. T.; Beattie, N. R.; McDonald, W. E.; Kadirvelraj, R.; Gross, M. L.; Phillips, R. S.; Harvey, S. C.; Wood, Z. A. The entropic force generated by intrinsically disordered segments tunes protein function. *Nature* **2018**, *563* (7732), 584-588. DOI: 10.1038/s41586-018-0699-5.